



저작자표시-비영리-변경금지 2.0 대한민국

이용자는 아래의 조건을 따르는 경우에 한하여 자유롭게

- 이 저작물을 복제, 배포, 전송, 전시, 공연 및 방송할 수 있습니다.

다음과 같은 조건을 따라야 합니다:



저작자표시. 귀하는 원저작자를 표시하여야 합니다.



비영리. 귀하는 이 저작물을 영리 목적으로 이용할 수 없습니다.



변경금지. 귀하는 이 저작물을 개작, 변형 또는 가공할 수 없습니다.

- 귀하는, 이 저작물의 재이용이나 배포의 경우, 이 저작물에 적용된 이용허락조건을 명확하게 나타내어야 합니다.
- 저작권자로부터 별도의 허가를 받으면 이러한 조건들은 적용되지 않습니다.

저작권법에 따른 이용자의 권리는 위의 내용에 의하여 영향을 받지 않습니다.

이것은 [이용허락규약\(Legal Code\)](#)을 이해하기 쉽게 요약한 것입니다.

[Disclaimer](#)

공학박사 학위논문

**Prediction of tensile strength of
unidirectional fiber composites
considering interfacial shear strength**

계면전단강력을 고려한 일축 복합재료의
강력 예측

2016년 2월

서울대학교 대학원

재료공학부

나 원 진

**Prediction of tensile strength of
unidirectional fiber composites
considering interfacial shear strength**

Advisor: Woong-Ryeol Yu

by

Wonjin Na

2016

Department of Materials Science and Engineering
Graduated School
Seoul National University

Abstract

The tensile strength of unidirectional (UD) fiber composite is determined by the interfacial shear strength (IFSS). Usually it is expected to increase according to the improvement of interfacial shear strength due to higher load transfer capacity through matrix. In previous studies, however, it is reported that there can exist an optimum interfacial shear strength for maximum tensile strength, not making a monotonic enhancement. This can be explained by the dilemma of load transfer and multiple fracture. When a fiber is broken, it accompanies concurrent breakage of surrounding fibers due to increased fiber stress by local load concentration. Few theoretical researches have reported the effect of statistical multiple fracture, however a research which is linking the load transfer and multiple fracture in prediction of tensile strength was rare. That is, the simultaneous consideration of load transfer and multiple fracture is demanded.

This thesis proposes a strength prediction approach for UD composite and following fracture toughness. Differently from existing models, the new approach tries a coupling between interfacial shear loading and multiple fracture. First, the effect of local stress concentration is analyzed using finite element method, determining the stress concentration factor of each surrounding layer. Based on the stress concentration factor, the number of multiple fracture is predicted using stochastic fiber strength distribution. A statistical prediction model calculating the probability of multiple fracture occurrence and following expectation value was implemented using the material properties of materials and interface. The toughness was also predicted using

the multiple fracture.

Using the strength prediction approach, the validity of which is investigated using carbon fiber/epoxy composites with mechanical testing. UD fiber composite was fabricated by resin transfer molding process with specially designed metal mold. The tensile, bending, and fracture toughness test was operated. For the fracture toughness testing the composite was specially fabricated thicker than the specimens for tensile and bending test. In addition to that the internal multiple fracture was observed via X-ray computed tomography (X-ray CT) with micron-level high resolution. The testing results were compared with the simulations through the statistical approaches.

In the analysis of carbon fiber/epoxy composite the strength and toughness value were in reasonable agreement, showing a little higher value. Furthermore the proposed model was applied to the optimum design of composite, trying to find optimum interfacial shear strength. From the parametric study of interfacial shear strength it was found the optimum interfacial shear strength for maximum composite tensile strength exist at the region of 70-80 MPa of IFSS. Finally it was also tried to be applied to hierarchical fiber bundle composites (HFBCs) to see the practicality and potential of the model.

Keywords: carbon fiber composite, unidirectional composite, interfacial shear strength, multiple fracture, tensile strength, fracture toughness

Student number: 2010-20598

Contents

Abstract.....	i
List of figures	vi
List of tables.....	x
1. Introduction	1
1.1. Strength of unidirectional fiber-reinforced composite.....	1
1.1.1 Principle of composite fracture.....	1
1.1.2 Literature review.....	8
1.1.2.1 Effect of interfacial shear strength – experimental study	8
1.1.2.2 Stress concentration and multiple fracture phenomenon.....	15
1.1.2.3 Statistical approach to multiple fracture.....	17
1.1.2.4 Strength and fracture toughness	20
1.2. Research objectives	24
2. Theoretical strength prediction based on statistical model.....	26
2.1. Stress concentration analysis.....	26
2.1.1 Unit cell analysis condition	26
2.1.2 Analysis results and discussion	31
2.2. Statistical model	48

2.2.1	Overall scheme of statistical model	48
2.2.2	Probability of fiber breakage	51
2.2.3	Multiple fracture stress	57
2.3.	Determination of tensile strength	63
2.3.1	Analytic solution considering multiple fracture	63
2.3.2	Determination of tensile strength.....	66
2.4.	Prediction of fracture toughness	68
2.5.	Summary	69
3.	Experiments and analysis of carbon fiber/epoxy composite.....	71
3.1.	Experimental	71
3.1.1	Material preparation and specimen fabrication	71
3.1.2	Mechanical testing.....	76
3.1.3	Multiple fracture observation	87
3.2.	Analysis of tensile strength and toughness.....	93
3.2.1	Stress concentration analysis	93
3.2.2	Strength prediction based on statistical model	97
3.2.3	Optimum interfacial shear strength of composite.....	102
3.2.4	Toughness prediction.....	104
3.3.	Summary	107
4.	Application to hierarchical fiber bundle composites (HFBCs) model	108
4.1.	Overview of HFBCs model	108
4.2.	Simulation procedures	113
4.3.	Results and discussion	116

4.4. Summary	122
5. Concluding remarks	123
References	125
Korean abstract	131

List of figures

Fig. 1.1. Schematic diagram of failure mechanism in composite [1] (a) initial state; (b) matrix crack; (c) interfacial shear stress and debonding; (d) debonding and fiber breakage; (e) fiber friction and pull-out [1]

Fig. 1.2. Schematic diagram shear-lag theory in unidirectional composite.

Fig. 1.3. Schematic diagram of stress concentration [13]

Fig. 1.4. Schematic diagram of multiple fracture in composite material. The black dots mean broken fibers

Fig. 1.5. Typical micro-damage modes in single-fiber composite test with different IFSS showing different fracture mode. (a) Water-sized; (b) g-GPS-treated; (c) g-MPS-treated; (d)g-APS/urethane/paraffin-treated; and (e) urethane-sized [29].

Fig. 1.6. The three representative modes of fracture in a single-fiber composite (a) strong interface (high IFSS): a disk-shaped matrix crack; (b) intermediate interface (strong interface but with a matrix that has relatively lower shear than tensile strength capability): a double cone matrix crack; and (c) weak interface (low IFSS): interfacial debonding [27].

Fig. 1.7. Relationships between strength efficiency and IFSS [29]

Fig. 1.8. Three-dimensional model of Nedele and Wisnom [38]

Fig. 1.9. Tensile failure model for the cumulative fracture-propagation mode [7]

Fig. 1.10. Schematic representation of possible fracture behavior of a composite initiated by breakage of one fiber [44]

Fig. 1.11. Relationship between composite strength and total fracture toughness [54]

Fig. 2.1. A schematic view of unit cell which was used to finite element analysis (a)

a general view (b) a cross-section view

Fig. 2.2. A bilinear traction-separation law in physical cohesive zone and the numerical cohesive zone.

Fig. 2.3. An example of RVE of periodic boundary condition cell (2-dimensional)

Fig. 2.4. (a) The model of stress analysis of 6th layers, (b) the result of stress concentration factor

Fig. 2.5. Analysis result of stress concentration (a) graphical result (b) stress distribution of surrounding fibers according to the length direction

Fig. 2.6 Analysis of stress recovery and debonding (a) ineffective length (b) debonded length

Fig. 2.7. The effect of interfacial shear strength (IFSS) on stress concentration (a) 30 MPa of IFSS (b) 50 MPa of IFSS (c) 100 MPa of IFSS (d) the stress concentration factors

Fig. 2.8. The effect of volume fraction of composite on stress concentration (a) 40 vol% (b) 55 vol% (c) the stress concentration factors

Fig. 2.9. The effect of material properties on stress concentration (a) $E_f/E_m = 10$ (b) $E_f/E_m = 40$ (c) the stress concentration factors

Fig. 2.10. The effect of fracture energy

Fig. 2.11. The effect of fiber array

Fig. 2.12. Overall calculation scheme of statistical model

Fig. 2.13. Specific algorithm inside the main loop

Fig. 2.14. Schematic diagram of hexagonal fiber array including broken fiber

Fig. 2.15. Schematic diagram of occurrence of multiple fracture situation (a) overlapping of each effect from broken fiber (b) one-by-one fracture situation

Fig. 2.16. Example of three multiple fracture with existing two multiple fracture

group

Fig. 2.17. Probability of multiple fracture

Fig. 2.18. Determination of multiple fracture stress

Fig. 2.19. Comparison of model and experimental results

Fig. 2.20. The composite strength according to the multiple fracture number. Parameter values are from [30]

Fig. 2.21. The determination of composite strength via comparison of analytic solution and multiple fracture stress

Fig. 3.1. Schematic diagram of single fiber test

Fig. 3.2. Strength according to gauge length Weibull properties

Fig. 3.3. Formed micro-droplet of epoxy on the carbon fiber surface

Fig. 3.4. Schematic diagram of micro-droplet test for IFSS measurement

Fig. 3.5. Schematic diagram of manufacturing process using prepreg

Fig. 3.6. Tensile testing (a) testing specimen for tensile test (b) mechanical testing with tensile testing machine

Fig. 3.7. The result of tensile test (a) fractured specimen (b) stress-strain curve of tensile test

Fig. 3.8. Three point bending test (a) testing specimen for bending test (b) mechanical testing with universal testing machine

Fig. 3.9. The result of bending test (a) fractured specimen (b) stress-strain curve of bending test

Fig. 3.10. Specimen for fracture test (a) schematic diagram with the size (b) real specimen

Fig. 3.11. Fracture test (a) Schematic diagram of three point flexural test for fracture toughness adopting ASTM E1290-08 (b) demonstration of test

Fig. 3.12. Testing result of work of fracture

Fig. 3.13. Specimens for small-size tensile test for observation

Fig. 3.14 Image process (a) initial image (b) binary image (c) image treatment for multiple fracture cluster by deleting small-size particle

Fig. 3.15. Quantitative data of multiple fracture

Fig. 3.16. Stress concentration factor of tensile case

Fig. 3.17 Stress concentration factor of bending case (a) analysis model of bending analysis, including crack (b) stress concentration factors of cracked model (c) stress concentration factor of bending case

Fig. 3.18. The multiple fracture stress according to the stress level (a) 3 layer (b) 4 layer (c) 5 layer

Fig. 3.19. The tensile strength determination

Fig. 3.20. The flexural strength determination

Fig. 3.21. The composite strength determination in various IFSS condition (a) tensile strength (b) The tensile strength according to the IFSS, showing the optimum in relatively high IFSS

Fig. 3.22. The toughness of composite according to the multiple fracture number and comparison

Fig. 4. 1. The example of hierarchical structures

Fig. 4.2. Hierarchical structure in unidirectional composites (a) with inserting polymer (b) without inserting polymer

Fig. 4.3. Schematic diagram of HFBCs model

Fig. 4.4. SCF of HFBCs and comparison to homogeneous composite

Fig. 4.5. Composite properties of HFBCs (a) composite strength determination (b) fracture toughness prediction

List of tables

Table 2.1. The property of materials and interface in demonstration

Table 3.1. The material properties of carbon fiber/epoxy composite system

Table 3.2. Operation conditions of X-ray CT for CFRP observation

Table 4.1. Parameters of HFBCs

Table 4.2. Fracture energy of various materials

1. Introduction

Fiber-reinforced composites (FRC) are used in various engineering field. Unidirectional (UD) fiber composite, in which fibers are embedded in one direction, is the most popular one of FRC in various industrial applications. It is used for reinforcement or repair materials of building, pier beams, or columns. In addition to that, more importantly, the UD composites are used as a single laminar of laminated composite. Considering the usage, the failure strength is basically demanded to the UD composite for widespread applications.

The load in FRCs is mainly carried by the fibers. Even when a fiber is broken in composite, the load can be transferred through fiber/matrix interface, i.e., the composite is still able to carry the stress by load transfer through matrix. Thus in the design of fiber-reinforced composite, the interfacial shear strength (IFSS) should be considered to predict the strength of composite. To improve the interface between fibers and resin, surface treatments such as chemical oxidation or sizing agent treatment have been applied.

1.1. Strength of unidirectional fiber-reinforced composite

1.1.1 Principle of composite fracture

In most of design of composite the engineers are well aware that the macroscopic response of unidirectional (UD) fiber composite is highly dependent on the fiber-matrix interface and local matrix plasticity. The matrix and interface are often weak in shear loading as compared to the fiber strength so that debonding and fiber pull-

out can occur in most of case prior to the catastrophic failure, and importantly near the fiber fracture location. In previous experimental works it has been reported that interfacial statement which determine the debonding, frictional sliding and fiber pull-out largely affect the composite strength and toughness [1-5]. So the randomly-distributed cluster of such breaks and load transfer in shear deformation should be analyzed in a microstructural view to understand the failure mechanism, considering the stochastic property. Based on this we can consider the design of composite for synergistic interaction with the enhanced strength and toughness of composite. In other words, determination of the fracture properties (strength and toughness) requires an understanding of the single fiber fracture and stress distribution around the broken fiber, which means the stress concentration to neighboring fibers.

When a typical unidirectional fiber composite is loaded and fractured, the fracture mechanism follows few steps. The fibers have stochastic properties, so a weakest link exists [6-8]. Under tension the weakest link a fiber is broken first creating a crack and the crack propagation begins when the tensile stress in fibers close to the crack tip, i.e., fiber stress of right neighboring fibers and matrix, exceed their local strength. In the mechanism, however, the surrounding matrix makes deformation, yielding or interfacial debonding near the crack tip, reducing the stress concentration partially. Experimentally in many composite system including carbon fiber/epoxy composite we can expect interfacial debonding to be an important mechanism in failure and toughening. Especially in the composite with brittle matrix, when shear loading is applied the yielding and debonding process occurs since the interfacial shear strength (IFSS) and tensile strength of matrix are both weak. It is typically accepted that the failure mechanism following the fiber fracture is 1) matrix fracture

- 2) fiber-matrix interface debonding
- 3) post-debonding friction
- 4) stress redistribution
- 5) fiber pull-out (see Fig. 1.1).

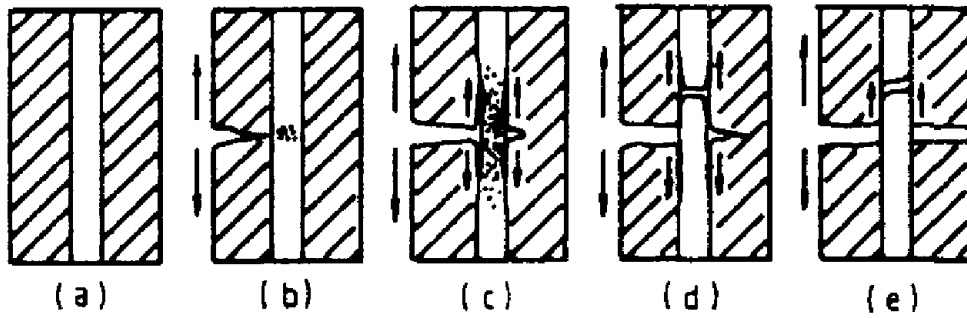


Fig. 1.1. Schematic diagram of failure mechanism in composite [1] (a) initial state; (b) matrix crack; (c) interfacial shear stress and debonding; (d) debonding and fiber breakage; (e) fiber friction and pull-out [1]

It is needed to the overview the essential concepts in this thesis in this chapter. The following concepts would be treated in detail in literature review, and only the short history is introduced next: shear loading in fiber-matrix interface, stress concentration factor and multiple fracture.

The foundation of debonding of interface and stress concentration is the shear-lag theory [9]. Though the detail would be treated in next section, the history of this shear-lag theory is enormous. The shear-lag model, which was established by Cox and developed by other researches, assumes that the following situations. The matrix is deformed in shear, and sustains no axial load. The axial load is carried by fibers only, and the fibers are deformed in simple tension and compression mode. These assumptions highly simplify the analysis so that the mechanics of the failure process

in a composite can be captured including complex random fiber break patterns, matrix plasticity in shear in between fibers, fiber-matrix debonding, matrix closing tractions near the crack tip, and fiber pull-out during crack formation and propagation. The one-dimensional equation for fiber composite can be presented as Equation (1).

$$\frac{d^2 \sigma_f}{dx^2} = \frac{n^2}{r^2} (\sigma_f - E_f \varepsilon_1) \quad (1)$$

in which σ_f is axial fiber stress, r is the radius of fiber, E_f is the elastic modulus of fiber and ε_1 is the fiber strain. Finally n is a dimension-less constant given by

$$n^2 = \frac{2E_m}{E_f (1 + \nu_m) \ln(1/f)} \quad (2)$$

in which the E_f is elastic modulus of matrix, ν_m is Poisson's ratio of matrix and f is volume fraction.

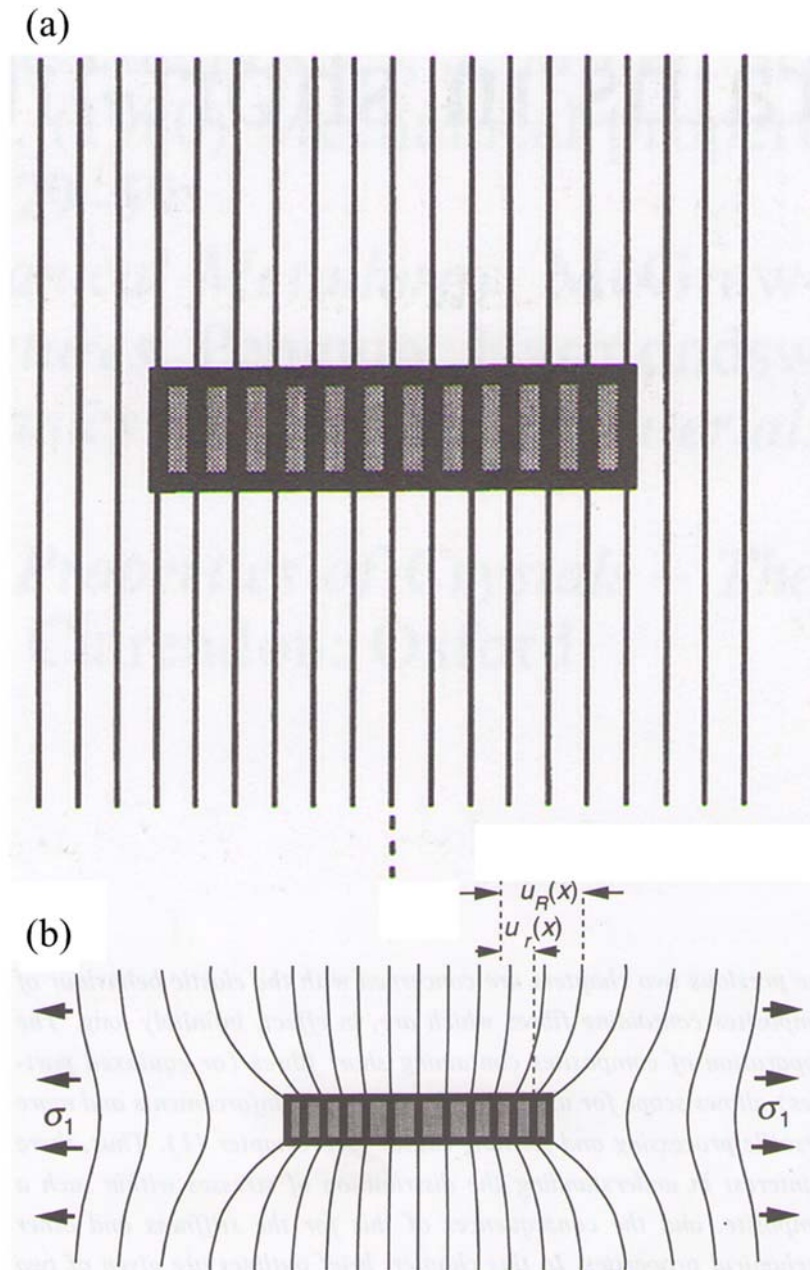


Fig. 1.2. Schematic diagram shear-lag theory in unidirectional composite (a) unloaded state (b) loaded state [10]

The stress concentration factor is the result of the shear-lag deformation and stress transfer. Stress concentration factor is defined as the ratio between the fiber stress of intact model and damaged model, which is having an isolated or coupled fiber fracture and deforming matrix. The basic principle of stress concentration is shown schematically in Fig. 1.3, showing the stress concentration of surrounding fibers in 2-dimensional array (in real it should be extended to the three-dimension). The initial concept of stress concentration factor concept was established by some pioneer including Rosen [6, 8], Zweben [7], Hedgepeth and van Dyke [11]. The researchers calculated differential equations using an influence function technique and the integration was carried out numerically. In the first stage the stress concentration was analyzed in linear elastic material and extended to the plastic material. Other researchers have studied the issue of stress concentration using the approach of analytic calculation [12-16] and finite element method [17-19], and most of the researches agree that the nearest fibers are influenced and the relation of adjacent fibers are important thing.

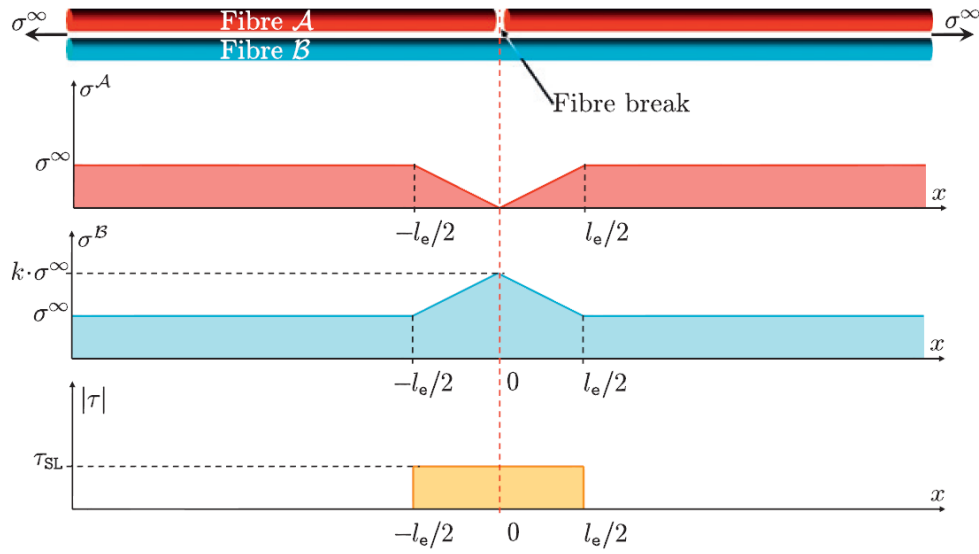


Fig. 1.3. Schematic diagram of stress concentration [14]

Aforementioned researchers also suggested the statistical analysis of the axial failure of a UD composite. The strength of each fiber is assumed to follow a statistical distribution such as Weibull distribution. Then the weak fiber is broken first at the lower stress level than expected average fiber strength. As explained in before it is expected that when a fiber breaks in the composite, a sudden stress concentration is induced on the surrounding fibers. Thus, surrounding several fibers break simultaneously. It is also assumed that the fiber fracture does not continue to propagate progressively at one event of the fiber fracture. That means, totally, k fibers are fractured at once. Then the important parameter k is defined as ‘multiple fracture number’ or ‘multiple fracture coefficient’ (see Fig. 1.4). In this thesis the former term would be used. Further assumptions would be derived next.

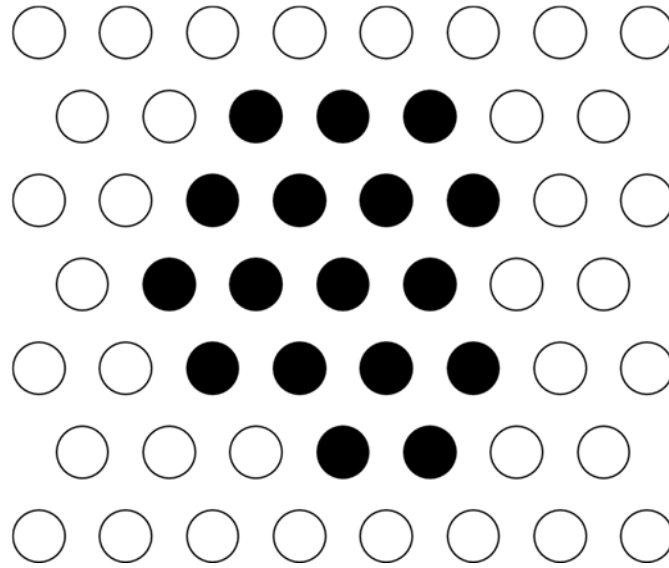


Fig. 1.4. Schematic diagram of multiple fracture in composite material. The black dots mean broken fibers

1.1.2 Literature review

In this chapter the overall history of the relation of strength prediction is introduced. Especially the effect of IFSS on the strength is summarized in the microscopic and macroscopic response. And the theoretical and empirical studies on stress concentration and multiple fracture is also presented.

1.1.2.1 Effect of interfacial shear strength – experimental study

Interfacial shear strength (IFSS) of composite, the strength of a material against the debonding or failure of interface, is the key factor in composite manufacturing process. Usually the interface is the weakest part of the composites. In order to achieve the best composite mechanical properties, many efforts have been tried to improve interfacial properties. In real process the IFSS is controlled by surface treatment, making the interface have a characteristics which is advantageous to the

interfacial bonding. There are many methods or treating agents for surface treatment for protecting fibers from micro-damage on process and proper adhesion. Generally the silane coupling agents are used to fiber surface[20-22]. A strong interface improves the tensile, compressive and flexural strength and the fatigue properties. Among that the effect of strong interface to the compression is clear however the effect to tensile strength have been argued because the interfacial bonding have been considered as unimportant factor in failure mechanism in relatively long time.

The effect of IFSS on the tensile properties of composite have been reported by several researches[23-26]. The common report is that as the IFSS increases, the tensile strength increases also even though it doesn't increase linearly. In addition to that the fracture surface was also observed and reported in same trend. Typically is accepted that a brittle failure is done with treated (i.e., high IFSS) fiber composites, and a broom-like small-bundle failure is done with untreated (i.e., low IFSS) fiber composites. The fracture mechanism have been studied systematically and the interfacial adhesion and micro-damage was observed by single fiber fragmentation test [27, 28]. The studies supplied the basic results for examination of the effect of IFSS on tensile property of UD composites. Especially the work by Drzal [29] has revealed that the improvement in tensile strength depends on the IFSS. The major conclusions from single fiber fragmentation test are following: the fracture modes are changed according to the IFSS. Thus, when the IFSS is low the interface is debonded only, and in opposite case the interfacial debonding is reduced. Furthermore in the high IFSS case the interfacial shear stress makes the matrix failure, inducing sharp disk-shaped failure. In the Fig. 1.5 [30] and 1.6 [28] the results are shown in microscopic image and schematic diagram

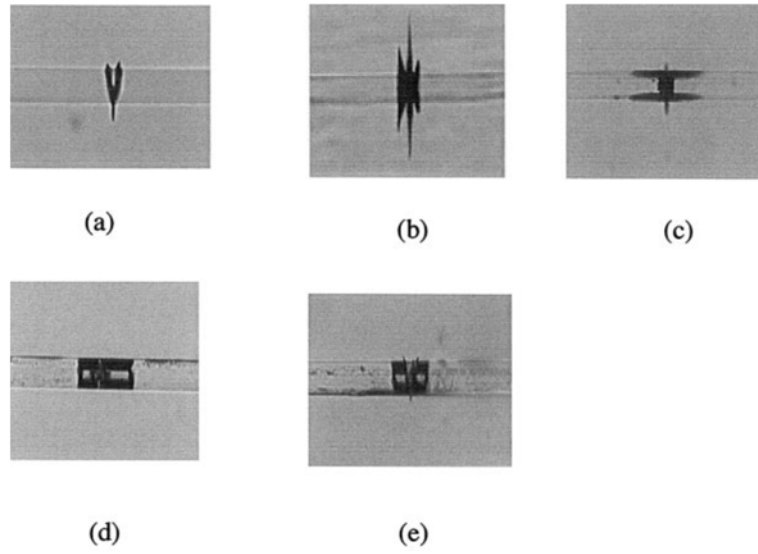


Fig. 1.5. Typical micro-damage modes in single-fiber composite test with different IFSS showing different fracture mode. (a) Water-sized; (b) g-GPS-treated; (c) g-MPS-treated; (d)g-APS/urethane/paraffin-treated; and (e) urethane-sized [30].

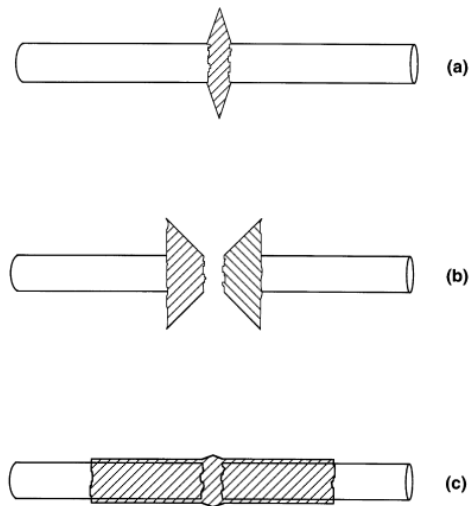


Fig. 1.6. The three representative modes of fracture in a single-fiber composite (a)

strong interface (high IFSS): a disk-shaped matrix crack; (b) intermediate interface (strong interface but with a matrix that has relatively lower shear than tensile strength capability): a double cone matrix crack; and (c) weak interface (low IFSS): interfacial debonding [28].

Based on the experimental studies the theoretical study also supported the relationships of IFSS and tensile strength. Most of that is based on the shear-lag theory by Cox, deriving a one-dimensional relationships (Equation (1) and (2)). The shear-lag theory firstly calculate the ineffective length, which means the distance from broken point to axial fiber stress recovery for certain stress level (in many researches it is determined as 90 % recovery zone). The stress distribution is calculated using the fiber radius R_f and surrounding cylindrical matrix radius R_m , where the matrix radius means the distance between nearest fibers. The volume fraction v_f is

$$v_f = \frac{2\pi R_f^2}{\sqrt{3} R_m^2} \quad (3)$$

and the force equilibrium equation is

$$\pi R_f^2 d\sigma + 2\pi R_f \tau dx = 0 \quad (4)$$

which means the tensile force on cross-section of fiber and the shear force on the side of cylindrical fiber surface make equilibrium (σ means tensile stress and τ means shear stress). The interfacial shear stress, calculated by solving the Equation (4) with

proper boundary condition, is

$$\tau = \begin{cases} -\tau_b & (0 \leq x \leq x_0) \\ -\frac{R_f E_f}{2\lambda^2} \left(u - \frac{\sigma_f}{E_f} x \right) & (x \geq x_0) \end{cases} \quad (5)$$

where τ_b is the IFSS, u is the displacement of fiber, x_0 is the debonded length, x is the distance from broken point, and λ is

$$\lambda^2 = \frac{R_f^2 \ln(R_m / R_f) E_f}{2G_m} \quad (6)$$

in which G_m is the matrix shear modulus. Then the tensile stress in matrix is calculated as

$$\sigma = \begin{cases} \frac{2\tau_b}{R_f} x & (0 \leq x \leq x_0) \\ -\frac{2\lambda\tau_b}{R_f} \exp\left(-\frac{x-x_0}{\lambda}\right) + \sigma_f & (x \geq x_0) \end{cases} \quad (7)$$

In this condition the critical length $l_c = (R_f \sigma_f) / \tau_b$ can be defined and the ineffective length is calculated as following Equation (8). The detailed derivation is in [31].

$$l_i = \begin{cases} 2(\ln 2)\lambda & (0 \leq l_c \leq 2\lambda) \\ -2\lambda \ln\left(\frac{el_c}{4\lambda}\right) + l_c & (2\lambda \leq l_c \leq 4\lambda) \\ \frac{l_c}{2} & (4\lambda \leq l_c) \end{cases} \quad (8)$$

The main interpretation of these theoretical studies can be summarized that as the IFSS increases: 1) the debonded length decreases 2) the shear stress increases 3) the tensile stress in fiber increases 4) the ineffective length decreases. In addition to that the material properties including yielding and failure supplemented the theory calculating the presence of matrix failure. In the theory to this, the IFSS should positive effect monotonically in tensile strength, enhancing the stress transfer capacity.

Even though the IFSS have positive relationships to the tensile strength as explained, however the interesting results have been reported in few experimental studies: there exists an optimum IFSS in tensile strength, not making continuous improvement (see Fig. 1.7 for the example of optimum IFSS. In the result the direct comparison of property was impossible due to the change of fiber property. The efficiency of strength was shown, which is normalized by the fiber property and volume fraction). The damage evolution via single fiber fragmentation test show that the different fracture mode. The longitudinal split in UD composite is the result of matrix crack and debonding, and it make the load drop in fiber direction [32, 33]. In high IFSS the matrix crack is easily created to the broken fiber and leads to the larger stress concentration in the neighboring fibers. Note that the stress concentration may

increase with increasing interface strength, which would be explained next. This increase of stress to surroundings increase the fiber failure probability of surrounding (the fiber failure follows an statistical trend, so it have a ‘probability’ of fracture in each stress level. When the fiber stress increases the probability of fiber fracture also increases). Consequently the sharp matrix crack which is induced under too high IFSS condition is not proper mechanism to the resistance to damage propagation, which is related to the tensile strength of composite. We already discussed about the weakness of debonding, not making the stress recovery. Then, the intermediate IFSS case, which is relatively strong IFSS, having debonding accompanied by matrix crack, is the most effective one. The breakage of multiple fibers also could be created with matrix crack, however the crack should propagate in the longitudinal direction in proper level. Finally the design of composite tensile strength is the optimization problem. The researches about stress concentration and propagation of multiple fracture emerged as important research issue related to that.

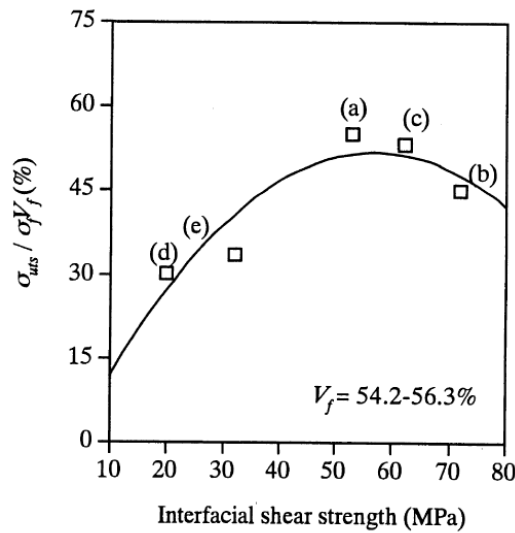


Fig. 1.7. Relationships between strength efficiency and IFSS [30]

1.1.2.2 Stress concentration and multiple fracture phenomenon

In this thesis the concept of stress concentration is limited to the ratio of stress that neighboring fibers carry. Stress concentration in this thesis stem from the crack or notch sensitivity of continuum material originally. Thus, in the composite, the isolated single fiber breaks is the basic unit. Thus the stress concentration and ineffective length analysis is basically starts from the single fiber composite. These stress concentration factor and ineffective length can be calculated analytically. It was originally calculated by Hedgepeth and van Dyke [11] for three-dimensional fiber-matrix arrays in the linear elastic material properties of the constituents first.

First, a calculation approach first developed for a one-dimensional packing, an array of parallel line [8]. In that case the SCF was predicted as 33 %. More monumental research was an approach of Hedgepeth and van Dyke, extending the shear-lag theory and stress concentration situation to two-dimensional fiber packing, the planar array of fibers. In that situation the stress concentration was calculated as 14.6 % and 10.4 % for square and hexagonal packings. The research suggested an analytic solution of stress concentration and opened initial way to the statistical model which would be described layer. The combination of shear-lag theory derived a solution, however the limitations were not solved perfectly. The remained problem is: anisotropic fiber property, plastic matrix property, matrix cracking and perfect bonding. Many following researchers [34-36] tried to solve the problem of complex situation, and the analysis of SCF in various situations have been done.

Another stream for stress concentration analysis is three-dimensional finite element method (FEM). Comparing to the analytic method, FEM is cost-intensive process, so that the limitations in models exists. Thus it is impossible to analysis the composite failure in full composite structure and FEM method developed supplementary analysis skills such as periodic boundary conditions [37, 38]. In spite of the limitations the main advantage of FEM in the analysis is the accuracy of calculation and consideration of various parameters even if it is complex model. The initial trial was done by Nedele and Wisnom [18, 39], predicting the SCF in the unidirectional composite (see Fig. 1.8). In that study hexagonal array is assumed and one-twelfth of the broken fiber and half of an adjacent fiber was assembled. The prediction of SCF was about 1.06 (5.8 %) for a hexagonal packing, which is lower value than the analytic solution. However further studies [34, 40, 41] founds that the lower SCF is more accurate to the experimental validation including micro-Raman spectroscopy, and the effect of shear deformation of carbon fiber itself can affect the stress redistribution making lower the SCF.

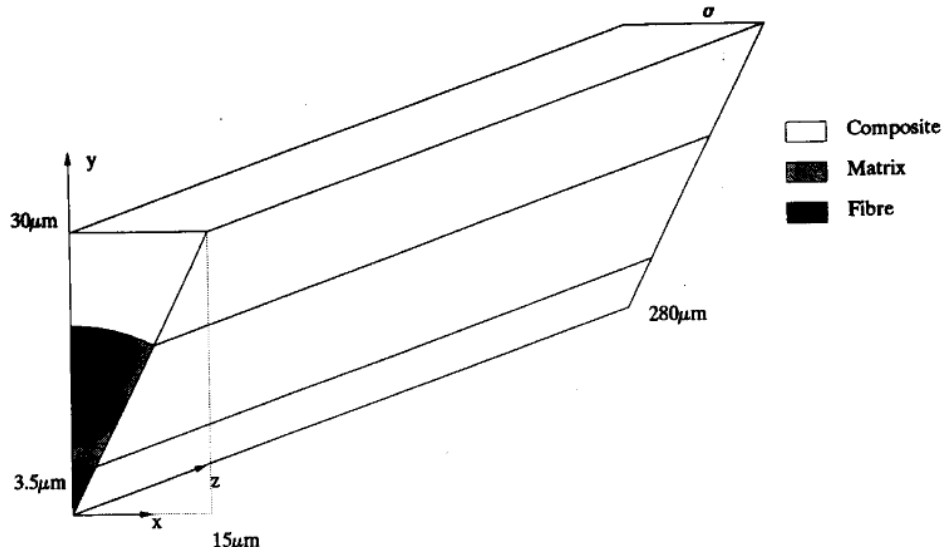


Fig. 1.8. Three-dimensional model of Nedele and Wisnom [39]

The relationship with SCF, multiple fracture and tensile strength was also studied [42-45]. Before the first Batdorf and Ghaffarian [42] studied the relationships of breakage bundle size and tensile strength by modeling. In the study the importance of fiber spacing was indicated, which is related to the SCF. The authors however, also summarized the limitations of the analytic modeling that the shear-lag model is limited to the random fiber packing and the application of interfacial property. Few studies have researched the SCF in complex situation [43, 46]. That researched tried to shorten the gaps of virtual space to real via FEM, many authors suggested the statistical approaches for higher accuracy.

1.1.2.3 Statistical approach to multiple fracture

Statistical analysis of a multiple fracture and axial failure of a UD composite was initially suggested by Zweben [6, 7] and Rosen [8]. A model that have parallel fibers

in a homogeneous matrix and statistical distribution of imperfections are established. The longitudinal region was separated as a link of ineffective length (see Fig. 1.9). The statistical distribution of link strength is obtained from the fiber stress distribution, so the associated cumulative distribution was used. The stress concentration factor calculated from the shear-lag analysis (analytic solution by Hedgepeth [11]) was used to the neighboring fibers. The concept of probability that an adjacent fiber of broken fiber will break due to the load concentration (later, it would be called as ‘transition probability’) is defined using the stress concentration factor and Weibull probability of fiber fracture. And the probability that a given element will break followed by the fracture of adjacent element, and the probability of having at least one such group is calculated. These probabilities would be adopted in this thesis in chapter 2.

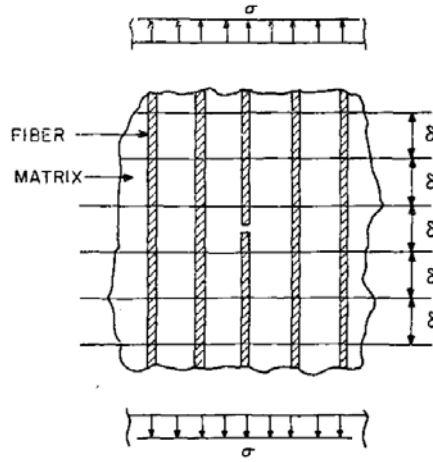


Fig. 1.9. Tensile failure model for the cumulative fracture-propagation mode [7]

Another approach using Weibull distribution and weakest link was done by Manders

[47]. A Monte-Carlo method was carried out for the process of failure in three-dimensional composites. Square fiber arrays are assumed and in the same cross-sectional plane the statistical failure and stress concentration concept was introduced. The result of the approach showed that when the small fracture bundle or cluster is created the composite strength degraded. Furthermore the simulation also showed the effect of ineffective length is critical to failure strength, which means the IFSS is the most critical factor. The effect of IFSS and debonding length in UD fibers was studied further by following researchers [25, 26, 48, 49] and they showed the statistical occurrence of multiple fracture can be matched to the strength prediction. Especially the research of Ochiai [50] tried the explanation of interfacial debonding and matrix failure via Monte Carlo method. As shown in Fig. 1.10 the possible form of fracture mechanism was simulated and following strength was derived. In addition to this the research of Goda [48] showed that if the interfacial properties have a variation, that means a distribution with the center of IFSS, the debonding is induced at weak interface and cluster of fibers are created to broken at once and pull-out. In this level the primitive relationships of multiple bundle size and the composite strength were studied.

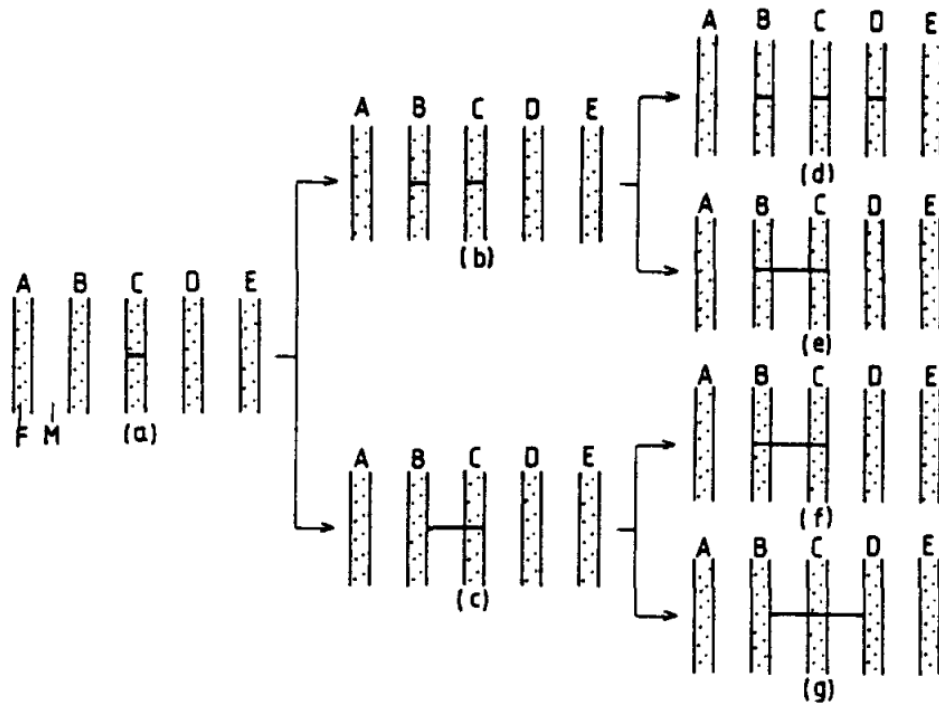


Fig. 1.10. Schematic representation of possible fracture behavior of a composite initiated by breakage of one fiber [50]

1.1.2.4 Strength and fracture toughness

The tensile strength have been discussed in this thesis, and another important property of a composite is a fracture toughness. A fracture toughness, which can be measured by specific work of fracture [51-53], is defined as the required energy for generating unit area of fracture surface of composite in this study (with units of kJ/m^2). The measurement method of work of fracture have been developed including the load-deflection curve of notched bend specimens (Tattersall and Tappin [54]), Charpy impact energy test (ASTM standard STP497 [55]) and it is now standardized as ASTM E1290-08 and E399. The resistance against fracture means the resistance

to crack propagation, so it is a phenomenon related to the fiber fracture (crack initiation) and multiple fracture (crack propagation). The relationships of fracture toughness is determined the maximum load and geometry as following equation referring ASTM E1290-08 standard (α is the ratio of notch depth and composite thickness).

$$K_I = \frac{4P}{B} \sqrt{\frac{\pi}{W}} \left[1.6\alpha^{1/2} - 2.6\alpha^{3/2} + 12.3\alpha^{5/2} - 21.2\alpha^{7/2} + 21.8\alpha^{9/2} \right] \quad (9)$$

The fracture toughness of a composite depends not only on the properties of fiber and matrix but also the efficiency of interfacial adhesion. Thus the local response of the interface in each step of failure mechanism should be identified for controlling the fracture toughness. There are some theoretical and experimental studies about fracture mechanism and the summary of each mechanism can be explained as following: matrix fracture, interface debonding, post-debonding friction, stress redistribution, fiber fracture and fiber pull-out. Note that the fiber fracture occurs progressively in the process of fracture, and it is quite not different to the single fiber failure aforementioned. Each failure mechanism creates new surface by external work, so the total multiple fracture is the summation of work of energy from each failure mechanism. The important point is that, the failure mechanism doesn't occur simultaneously for a given composite system, and even some mechanism cannot be done according to the interface system. In addition to that another important point is that some of these mechanisms contribute to the total toughness in dominance. By the research of Atkins [56, 57] the three major sources are dominant to the total toughness: stress redistribution, fiber pull-out, and generation of new surface (sum of the work of energies of fibers, matrix and interfaces which is absorbed in failure). The

work of energy on stress redistribution (Piggott [58] and Fitz-Randolph [59]) is

$$R_r = \frac{V_f \sigma_f^2 l_c}{3E_f} = \frac{V_f \sigma_f^3 d}{6E_f \tau_b} \quad (10)$$

when d is the diameter of fiber. And the toughness of fiber pull-out is (Kelly [60]) following as Equation (9). The pull-out length concept was introduced however the measurement of pull-out length was too hard so that the equation was modified [61].

$$R_{po} = \frac{2V_f \tau_b l_{po}^2}{d} \approx \frac{V_f \tau_b l^2}{6d} \quad (11)$$

Finally the toughness for surface generation is (note that it is based on rule of mixture and the interfacial toughness is approximated in matrix toughness)

$$R_s = V_f R_f + (1 - V_f) R_m + V_f \left(\frac{l_c}{d} \right) R_i \approx V_f \left(\frac{l_c}{d} - 1 \right) R_m \quad (12)$$

So the total toughness can be presented as

$$R_t = \frac{V_f \sigma_f}{\tau_b} \left[\frac{\sigma_f d}{6} \left(\frac{1}{4} + \frac{\sigma_f}{E_f} \right) \frac{R_m}{2} \right] + (1 - V_f) R_m \quad (11)$$

The relationships offers the results that the total toughness decreases according to the IFSS, showing a proportional relation to the reciprocal of IFSS.

In the prior section we discussed the enhancement of composite strength according to the IFSS (even if the opposite case was treated importantly). Thus we can identify the experimental knowledge mathematically, that is high strength and high toughness cannot be achieved in fiber-reinforced composite. We can call this as a ‘stress-toughness dilemma’. In previous research of Marston [56], the relationship between composite strength between toughness was reported. In the research, at high IFSS region the strength is determined by the small Griffith crack (so the toughness is proportional to the square of composite strength) and at low IFSS region the toughness is determined by the Equation (12). The relationship showed that the optimum IFSS and toughness can exist also exist (see Fig. 1.11).

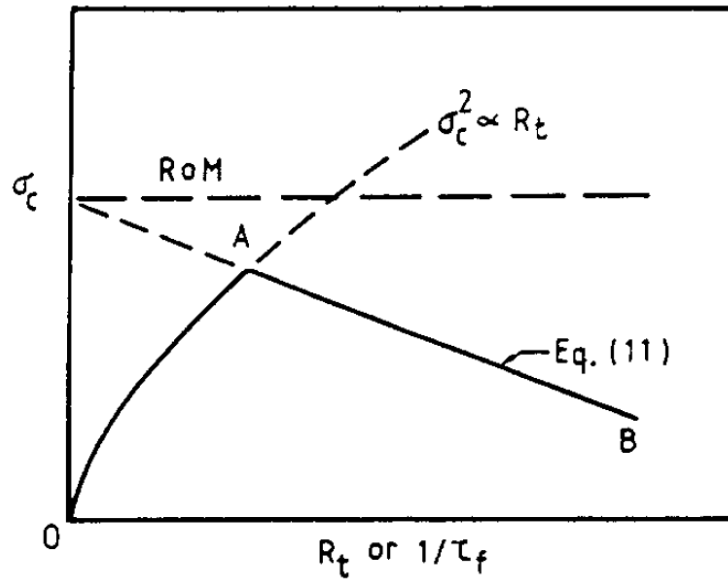


Fig. 1.11. Relationship between composite strength and fracture toughness [56]

1.2. Research objectives

As described in prior section, the prediction of tensile strength is an important issue and the interfacial shear strength is the most crucial factor to that. However the development of strength prediction scheme considering two interfacial effect in the same time has been rare. In this thesis an approach for considering the effect of interfacial shear strength was established in two-step. Analytic solution and statistical solution were calculated and compared.

In the chapter 2, the detailed scheme was described and validated in basic material system. For the analysis of stress concentration a finite element method was used. Tensile deformation was simulated in virtual space for intact and damaged, i.e. containing one broken fiber at the center. The stress distribution of surrounding fibers was analyzed and the stress concentration factor was calculated. The effect of each design parameter, including the interfacial shear strength, fiber volume fraction, and material property (property difference of constituents). Based on this stress concentration factor the multiple fracture stress was calculated. A statistical model was established and implemented via MATLAB program, considering the probability of multiple fracture and the occurrence of multiple fracture (expectation value of each multiple fracture). Finally the composite strength was determined by comparison. Referring to following section for further details, the composite strength in analytic solution decreases but the multiple fracture stress increases according to the multiple fracture number. The logic of final determination was proposed.

In the chapter 3, the model was applied to the unidirectional carbon fiber composite. Unidirectional composite was fabricated and tested in tensile and bending. Three-

point bending test was performed to consider the delamination mode and toughness calculation. The multiple fracture occurrence was observed through micro-CT operation. The cross-section of stressed composite was analyzed in some characteristic stress level. The result was compared to the multiple fracture in statistical model and composite strength determined in chapter 2. In addition to that the bending strength was predicted considering the delamination effect. In the bending situation the outer shell was fractured by tension first, however the effect of delamination create a difference of strength (usually lower). The delaminated condition, which have a crack near the broken fiber, was analyzed.

In the chapter 4, further consideration and applications were treated widely in the view of optimum design. First the strength-toughness dilemma, which means that high strength and toughness cannot be achieved in the same time, was considered. In the demanded strength and toughness condition at certain target material, a design parameter was proposed which can satisfy the demanded option in some applications. In the view of composite structure, hierarchical fiber bundle composites (HFBCs) was considered to avoid the effect of stress concentration. The strength prediction method of the HFBCs are considered utilizing the aforementioned prediction approach in chapter 2 and 3.

2. Theoretical strength prediction based on statistical model

In this chapter, a new strength prediction model of UD composite is proposed based on a statistical model and analytic solution. A stress concentration was analyzed through finite element method. The stress of surrounding fibers are analyzed so that the stress concentration factor was calculated. During the analysis the interfacial properties are treated with cohesive element. This stress concentration factor was utilized to describe the additional occurrence of multiple fracture. The probability of additional fiber breakage was calculated assuming hexagonal fiber packing and Weibull distribution, so the stress inducing certain multiple fracture (called ‘multiple fracture stress’) was derived. Finally the tensile strength of composite was determined.

2.1. Stress concentration analysis

2.1.1 Unit cell analysis condition

A square unit cell having a broken fiber at center was generated. The square shape was considered due to the boundary conditions (i.e., periodic boundary condition). Hexagonal fiber array was assumed and 3 layers of fibers are arranged in unit cell considering the effective stress concentration region (see Fig. 2.1 (a) for cross-section). In the main calculation the stress concentration was considered as 3 layers. Totally two broken fiber fragment (insisting of one central broken fiber), 11 surrounding full fibers, which were included in 1st surrounding layer and 2nd surrounding layer, 8 half-sized fibers (in the edge of unit cell), and 4 quarter-sized fibers (in

the corner of unit cell) were generated. Note that the effect of half and quarter-sized fibers are compensated by periodic boundary conditions. The fibers are assumed cylindrical and the length of unit cell was taken long enough considering the effective length, which means the axial fiber stress is recovered. The central fiber (which is broken) length was set as a half of the unit cell.

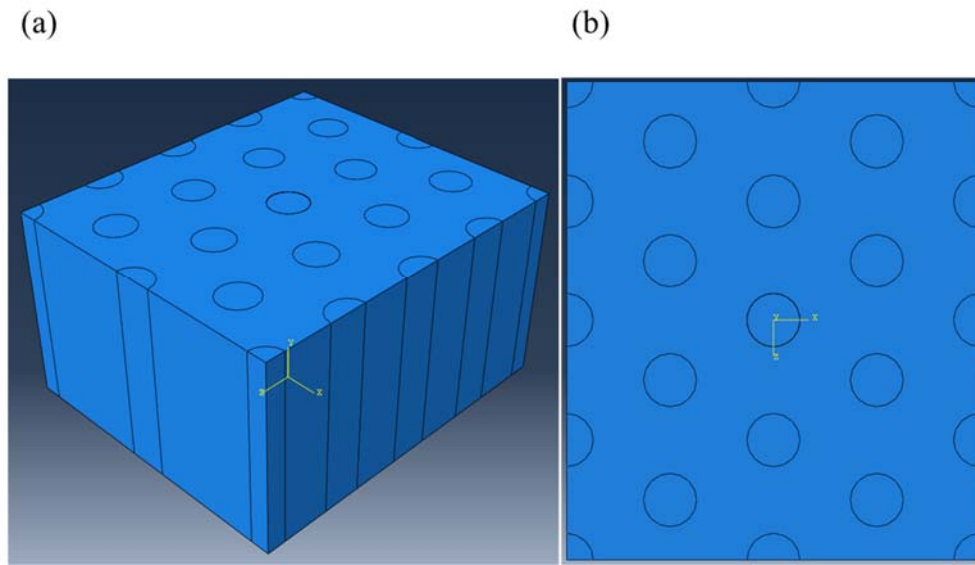


Fig. 2.1. A schematic view of unit cell which was used to finite element analysis (a) a general view (b) a cross-section view

The material properties are set as three parts. Transversely isotropic property was adopted to fiber element considering the characteristics of fiber. The properties in transverse direction was set about 1/10 of that of axial direction. The shear properties were calculated using Poisson's ratio. Isotropic elastic property was adopted to matrix element. Cohesive properties was adopted to interfacial element, which was set between the central broken fiber and surrounding matrix. Note that in this thesis the

cohesive zone is created using interface [62-64], but in another approaches the crack can extends between elements and re-meshing is done when the crack path is not known [65, 66]. Usually the approach is used in ductile materials and continuum so the cohesive zone approach was used. Traction-separate law was adopted using a bilinear constitutive equation. The onset criterion and propagation criterion followed Ye's criterion [67]. The governing equation is shown in Equation (12) and (13) The cohesive damage law was shown in Fig. 2.2., showing high stiffness for the equivalence between the physical cohesive model.

$$f_{initiation} = \left(\frac{\tau_1}{\tau_1^0} \right)^2 + \left(\frac{\tau_2}{\tau_2^0} \right)^2 + \left(\frac{\tau_3}{\tau_3^0} \right)^2 - 1 = 0 \quad (12)$$

$$f_{propagation} = \left(\frac{G_1}{G_1^0} \right)^2 + \left(\frac{G_2}{G_2^0} \right)^2 + \left(\frac{G_3}{G_3^0} \right)^2 - 1 = 0 \quad (13)$$

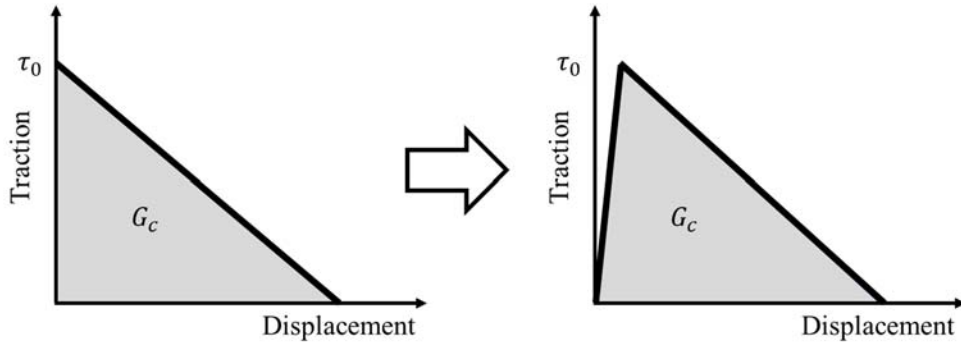


Fig. 2.2. A bilinear traction-separation law in physical cohesive zone and the numerical cohesive zone.

The interfacial bonding condition was applied to fiber/matrix interface. Firstly cohesive properties were applied between broken fiber and adjacent matrix. Cohesive layer which have less than 1/25 thickness of the fiber was generated, and the thickness of central broken fiber fragment was reduced following that thickness, assuming the interfacial bonding layer. The cohesive properties was same as aforementioned. The cohesive layer, fiber, and matrix element were constrained as tie. For accuracy of calculation the reduced integration technique, inducing an hourglass mode often, was not used. Element deletion mode, which means the element was deleted after propagation (i.e., more energies than toughness energy), was used.

Periodic boundary conditions (PBCs) was applied [68-70]. Periodic boundary conditions are mainly used to eliminate the existence of surface and downsize the amount of simulation. In composite material the number of lattice system is usually over thousands, so the whole system cannot be implemented in virtual space. A strain-controlled PBC may be specified for this RVE (see Fig. 2.3) by the following Equations (14)-(16) (one-directional deformation)

$$u(x+L) = u(x) + \varepsilon^0 x \quad (x \in B_1) \quad (14)$$

$$u(x+L) = u(x) \quad (x \in B_2) \quad (15)$$

$$t(x+L) = -t(x) \quad (x \in B_2) \quad (16)$$

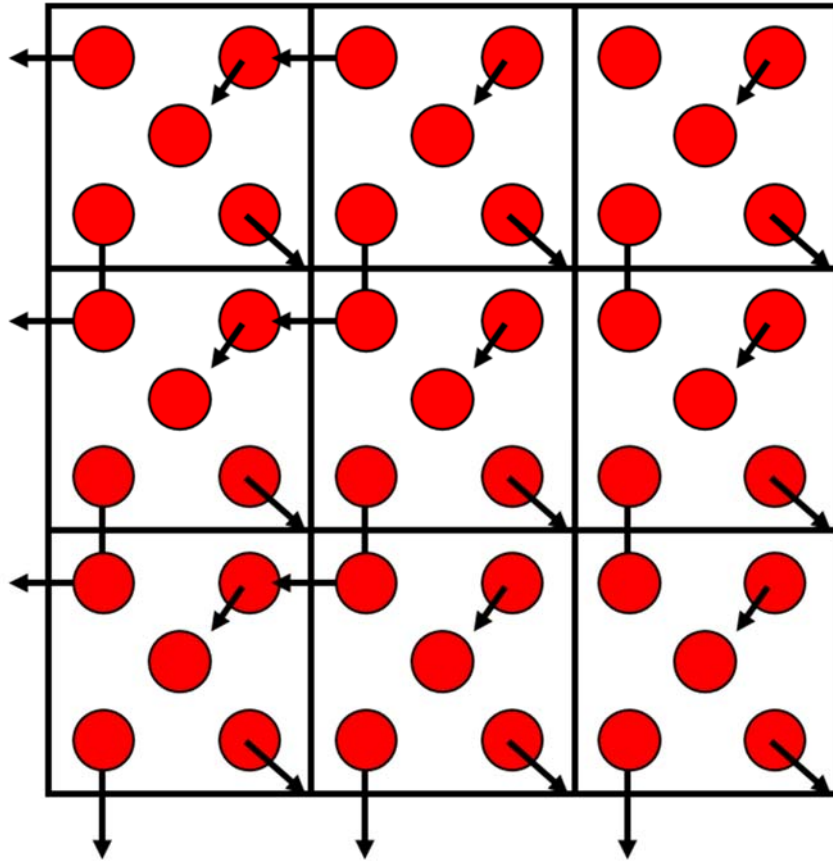


Fig. 2.3. A schematic view of periodic boundary condition cell (2-dimensional)

Where u is the displacement of x , ε is the applied strain, t is traction, and B_1 is the boundary that the deformation is applied and B_2 is the boundary the deformation is not applied.

In order to apply PBC, making constraint equations are essentially needed. For implementation, Package program ABAQUS was used. Aforementioned conditions were implemented in CAE virtual space. The unit cell was generated and following properties were applied to each section. The unit cell was stretched in fiber direction

inducing 1 % strain. In some interesting regions, that is the central region of central and surrounding fibers, sets are created. In the sets, the displacement and reaction force were measured from history output. The same calculation was done on intact (i.e., including the intact fiber at the center) unit cell. Note that in the intact unit cell the fiber stress was equal to all fibers. The fiber stress of intact unit cell is set as a reference, and concentrated fiber stress at surrounding fibers were compared. The ratio of fiber stress was defined as 'stress concentration factors (SCFs)'.

2.1.2 Analysis results and discussion

Analysis was carried out using properties in Table 1.1 which is the property of carbon fiber/nylon 6 composite system. Before that in other unit cell using larger unit cell, the effect of stress concentration was studied containing maximum 6th layer, however it was revealed that the effect of stress concentration was trivial after 4th layer Fig. 2.4. In the analysis the basic results were checked: the stress distribution in broken fiber and effective length, debonding length, stress distribution of surrounding fibers, and stress concentration factors. After the analysis the effect of each design parameter (IFSS, volume fraction, and material properties) was analyzed.

Table 2.1. The property of materials and interface in demonstration

Composite parameter	Fiber volume fraction	30-55 %
	Fiber diameter	6.8 μm
	Gauge length	0.1 m
Interfacial property	Interfacial shear strength	10-100 MPa
Young's modulus	Fiber - longitudinal	113 GPa
	Fiber - transverse	11.3 GPa
	Matrix	3 GPa
Failure strength	Fiber	5.56 GPa
	Matrix	80 MPa
Weibull Parameter	Weibull modulus	9
	Characteristic stress	5.56 GPa
	Reference length	1 m

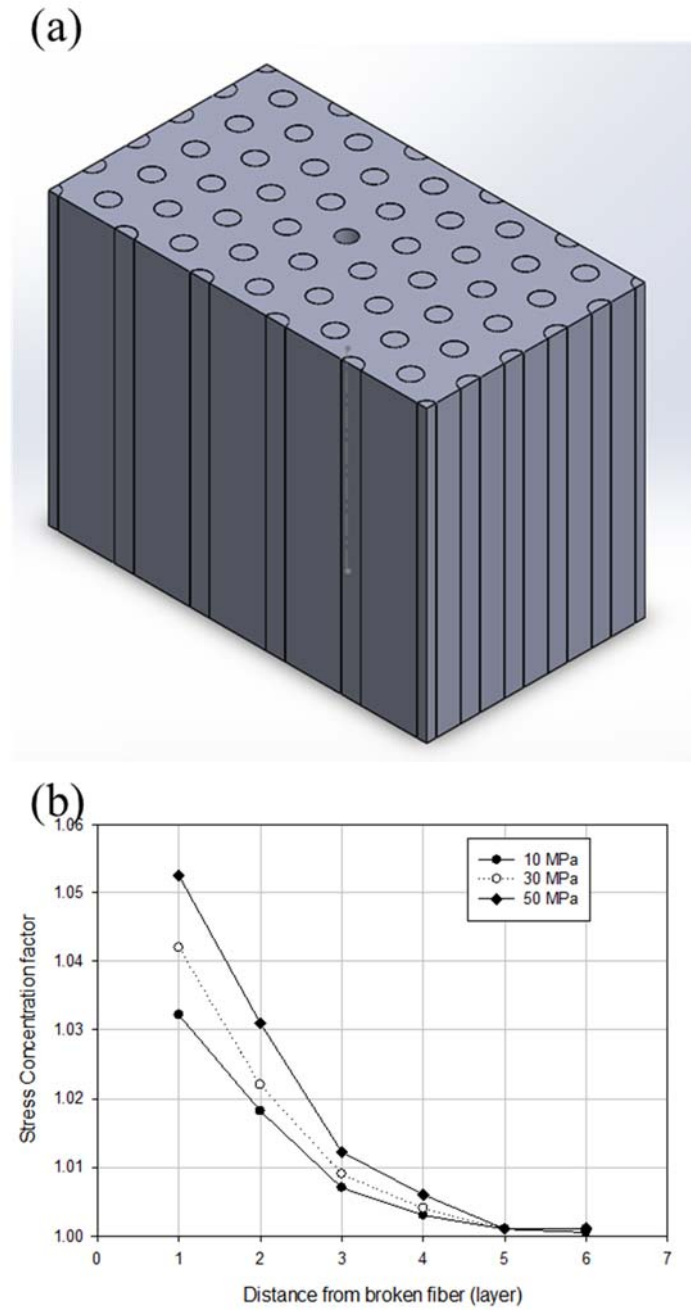
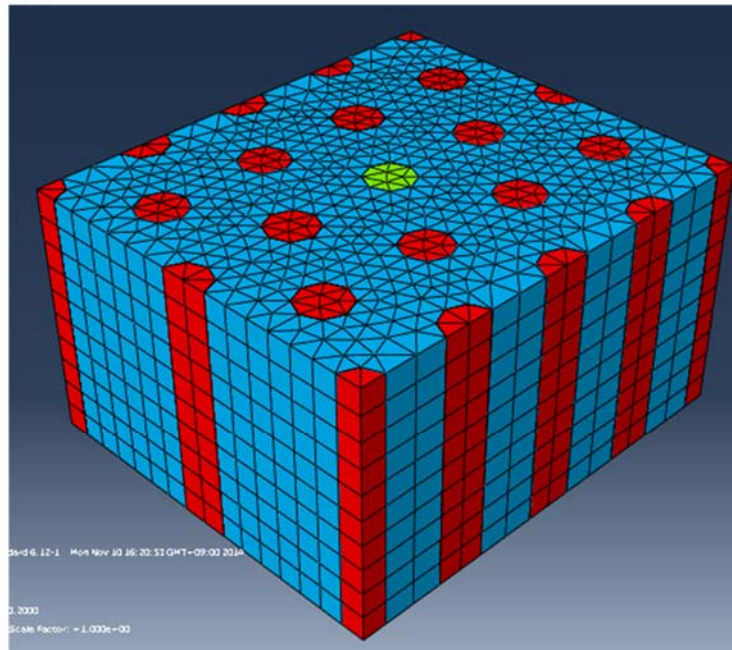


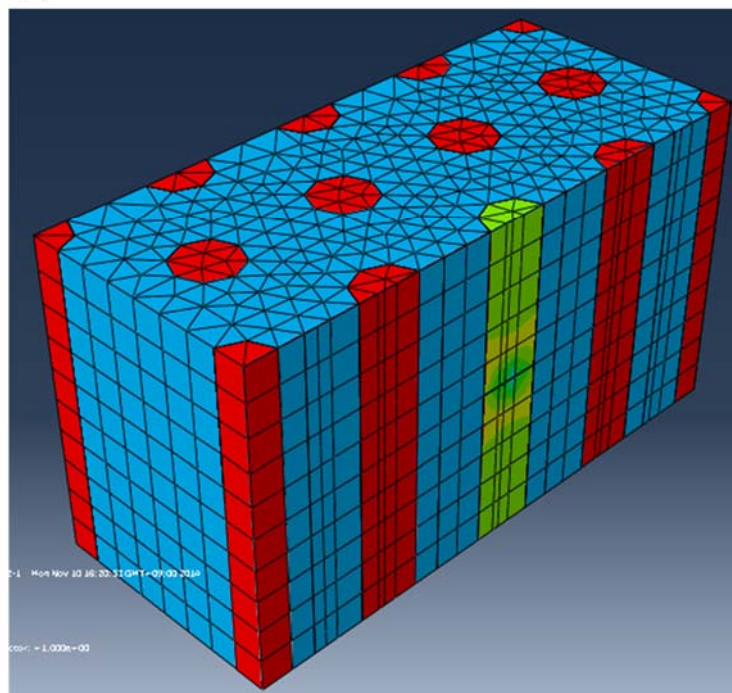
Fig. 2.4. The model of stress analysis of larger unit cell (a) The model of stress analysis of 6th layers, (b) the result of stress concentration factor

The stress recovery of broken fiber and stress distribution in surrounding fibers are seen in Fig. 2.5. The volume fraction was 40 % and the IFSS was 30 MPa as an example. Debonding also can be observed in same analysis, showing the element deletion of interfacial cohesive layer. The debonding was treated by initiation strength (which is matched to the IFSS) and final propagation, so the final displacement reaching to the element deletion was different to each IFSS case. Consequently more elements were deleted, that was interpreted as debonding, in higher IFSS case due to faster deletion of elements. The stress distribution shows the maximum value in broken point (referred as zero) and the value decreased drastically. The maximum value was defined as stress concentration factor. The ineffective length and debonded length was also plotted in Fig. 2.6. The effective length was defined as 90 % stress recovery in this thesis. The effective length shows decreasing trend according to the IFSS, same in the previous literatures [30, 31, 71]. The debonded length also decreased, being related to the interfacial failure. The analytic solution of ineffective length and debonded length was co-plotted considering the Equation (26) of reference [31]. The results show that the analytic values are much higher than the numerical value, which means the effect of ideal condition neglecting the distortion and geometry of interfacial element. In analytic solution when the IFSS is achieved the interface is debonded directly, however in FEM the interfacial element are only activated to fail by initiation theory and the propagation and deletion appears quite later step. Consequently the debonding length of FEM is much smaller and in this study the debonding length of analytic study would be replaced to the FEM value.

(a)



(b)



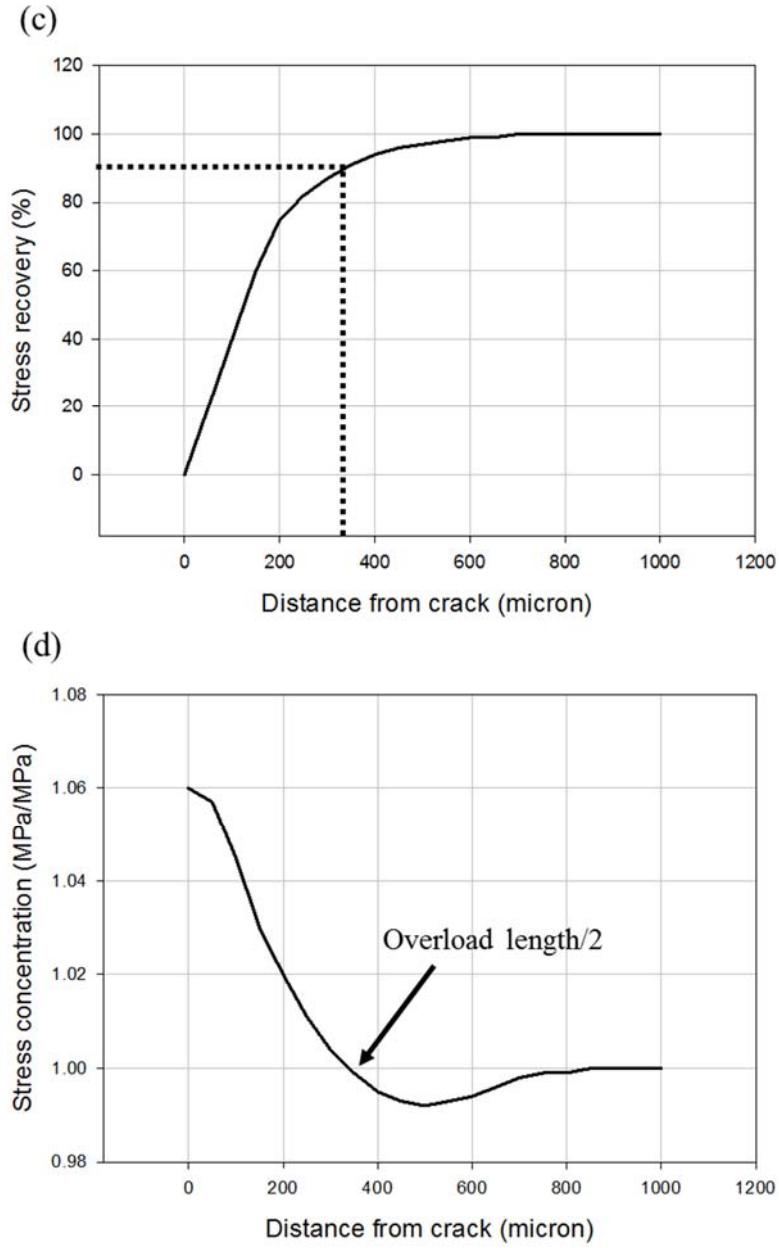


Fig. 2.5. Analysis result of stress concentration (a) graphical demonstration of analysis of full unit cell (b) cross-section of (a), a half cell (c) stress distribution of broken fibers (b) stress distribution of 1st surrounding fibers

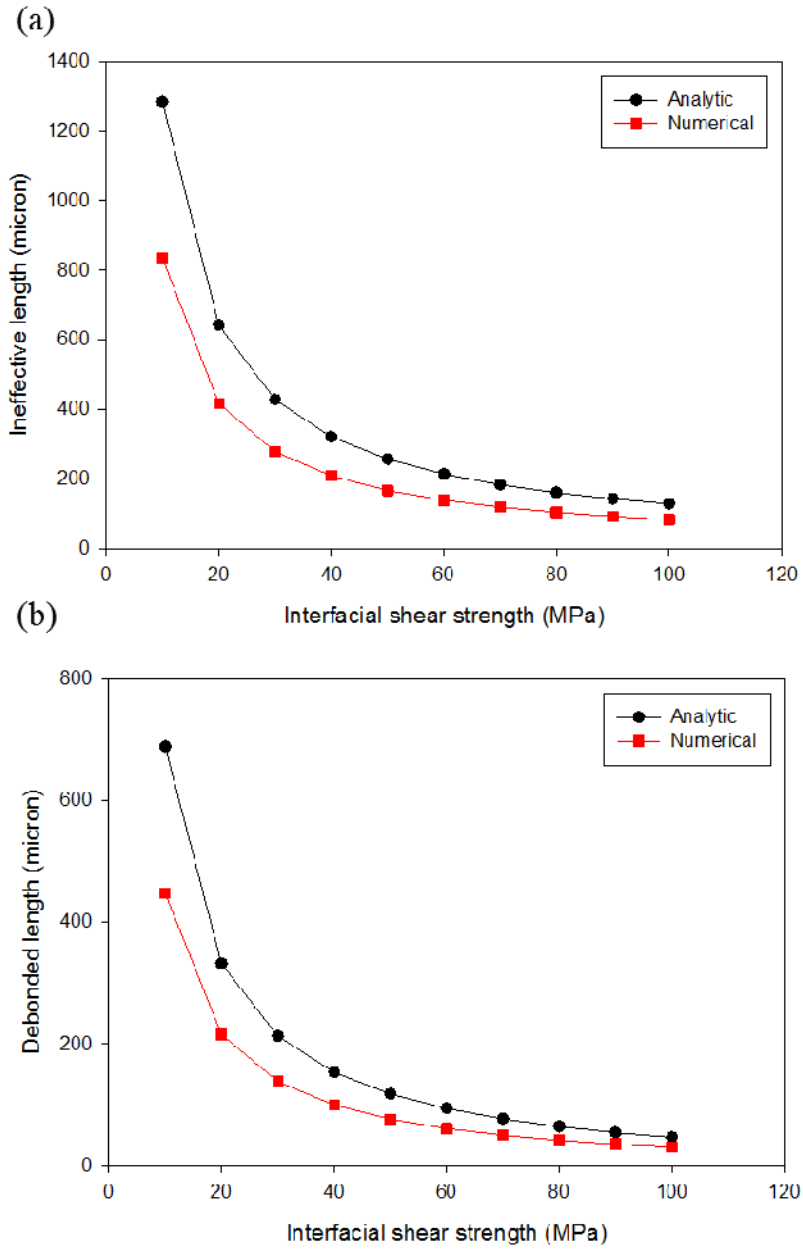
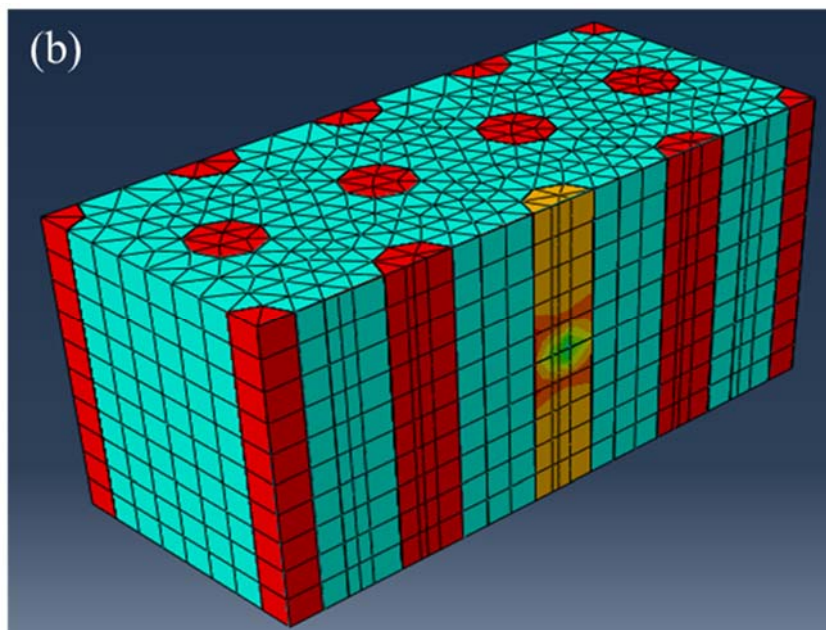
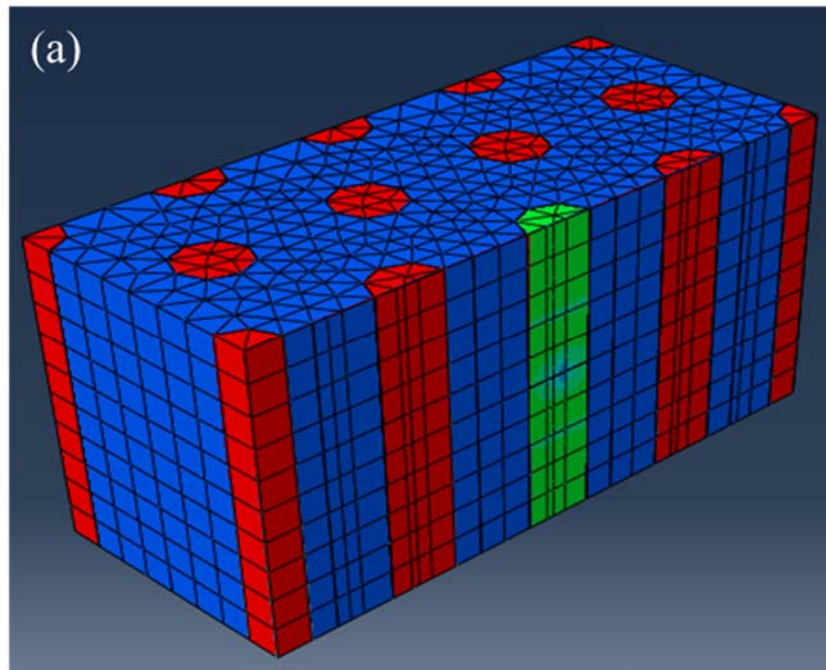


Fig. 2.6. Analysis of stress recovery and debonding (a) ineffective length (b) debonded length

Some parametric study was carried out. In the stress concentration analysis the IFSS, volume fraction, and the (relative) material properties are considered as important parameters. The importance of IFSS have been emphasized repeatedly in prior section. The volume fraction makes the distance between fibers closer, so that the load transfer has a tendency to increase according to the volume fraction. Finally the higher relative material properties, i.e. the stiffness difference, can affect the stress concentration, making more obvious difference in stress distribution. In this study the effect of three parameters are studied in some case. Basic material properties used in parametric study was shown in Table 2.1, and some values are varied upon each interesting parameter.

- 1) Effect of IFSS: A model with volume fraction of 30 % was generated and IFSS was controlled via the property of cohesive element. The cohesive element property was set by two criteria, i.e. the initiation of fracture by quadratic relation of stress and the propagation of fracture by quadratic relation of fracture energy. The result of SCF is shown in Fig. 2.7, showing the drastic increase according to the IFSS. In the previous research when the perfect bonding was assume the FEM analysis showed the 5.8 % addition [18, 19] and when the IFSS is high enough the value even exceeded the value.



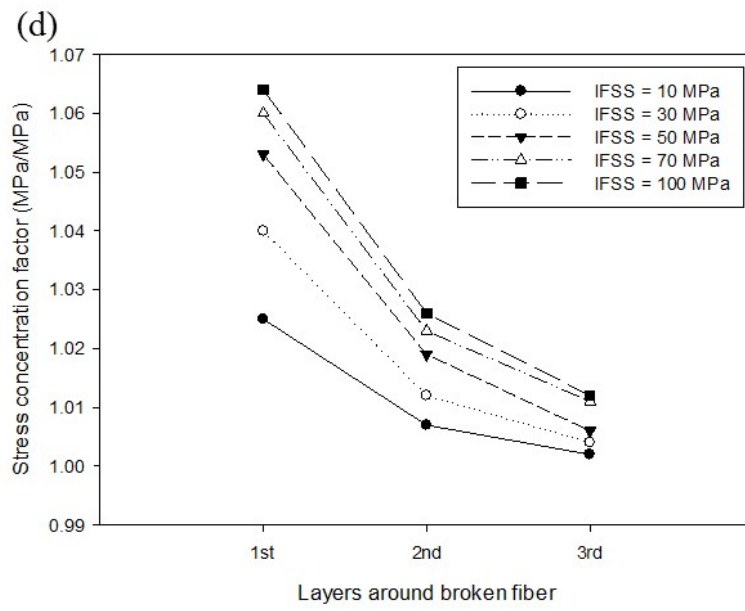
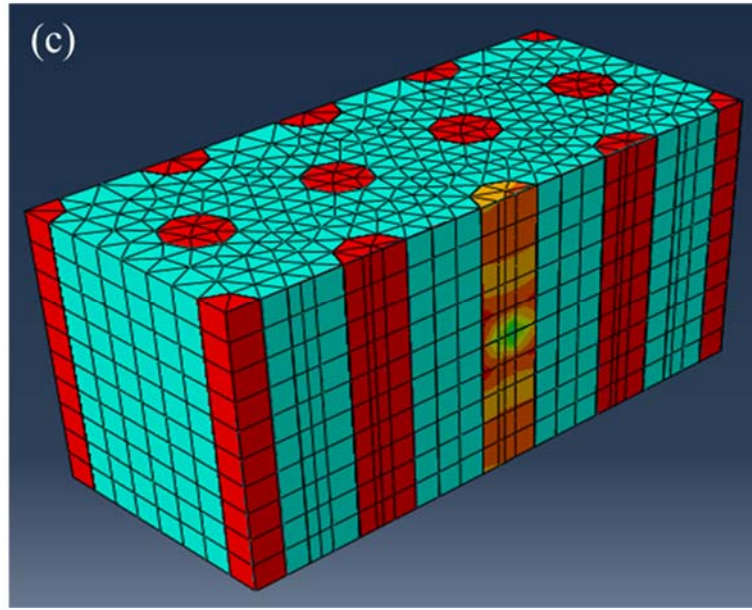
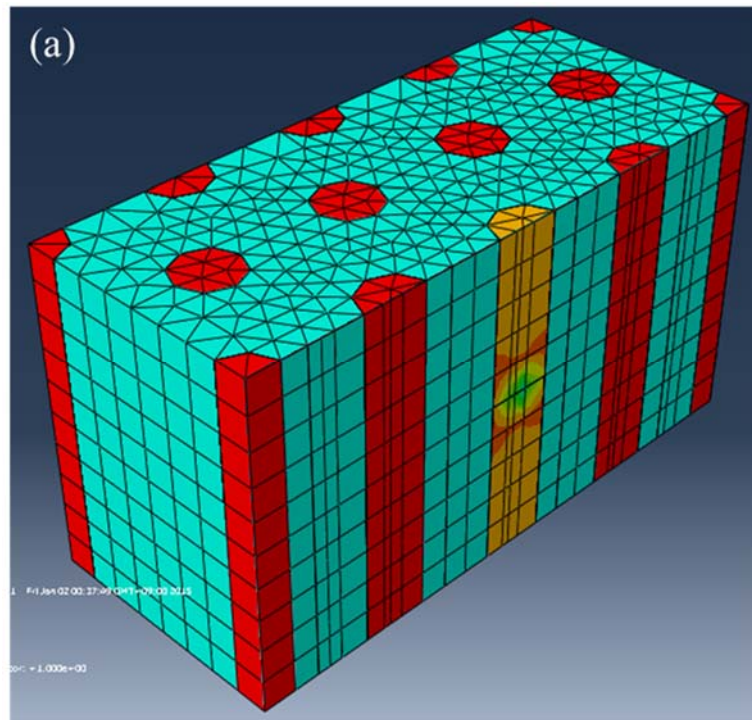


Fig. 2.7. The effect of interfacial shear strength (IFSS) on stress concentration (a) 30 MPa of IFSS (b) 50 MPa of IFSS (c) 100 MPa of IFSS (d) the stress concentration factors

- 2) Effect of volume fraction: The volume fraction was varied from 40 % up to 55 %. The result of SCF is shown in Fig. 2.8, showing the small increase according to the increase of volume fraction. It is seen that the effective region of stress transfer via surrounding matrix is fixed due to the IFSS however the distance of fiber got closer, making the stress transfer higher. Nevertheless the difference is not critical than that of IFSS.



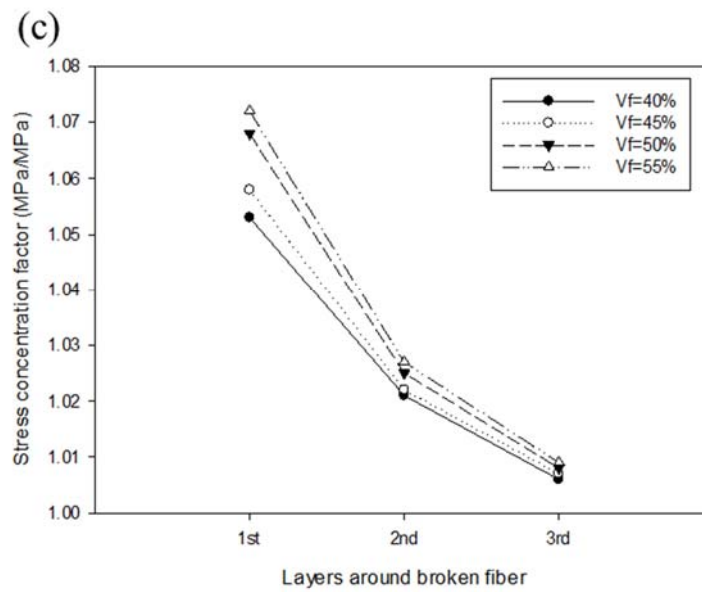
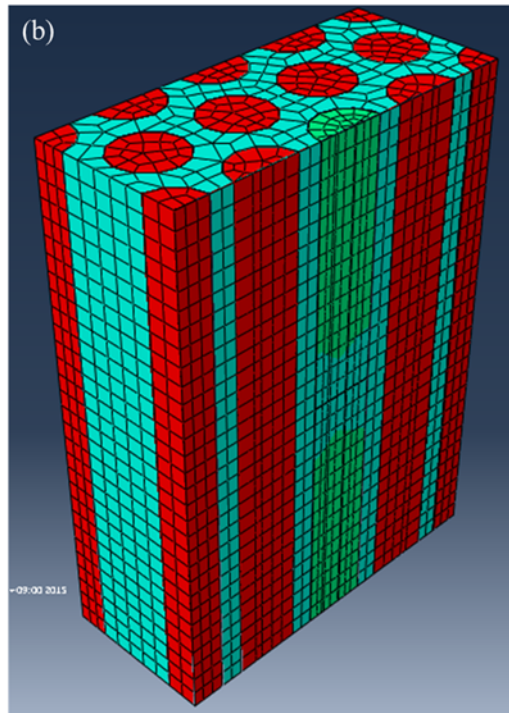
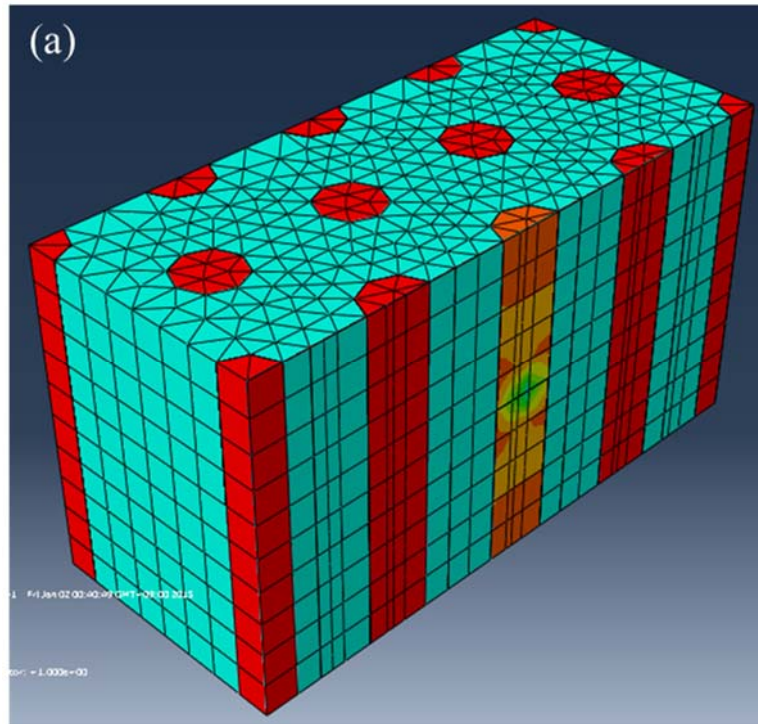


Fig. 2.8. The effect of volume fraction of composite on stress concentration (a) 40 vol% (b) 55 vol% (c) the stress concentration factors

- 3) Effect of material properties: Same model with 1) was utilized. The relative material properties, i.e. the ratio of fiber stiffness to matrix stiffness is varied from 10 to 80. The result of SCF is shown in Fig. 2.9, showing the small decrease according to the increase of relative material properties. It can be interpreted that the difference in stress distribution around the broken fiber decreased when the fiber property is lower. However the effect is the most trivial in the parameters.



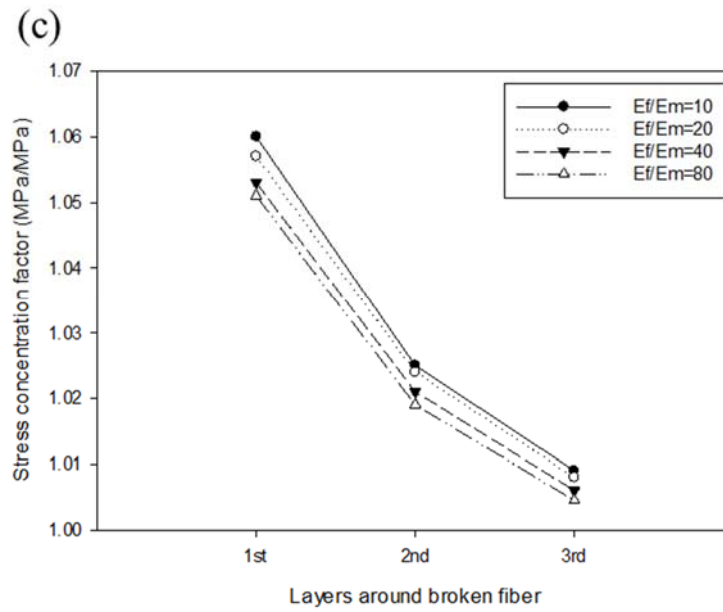
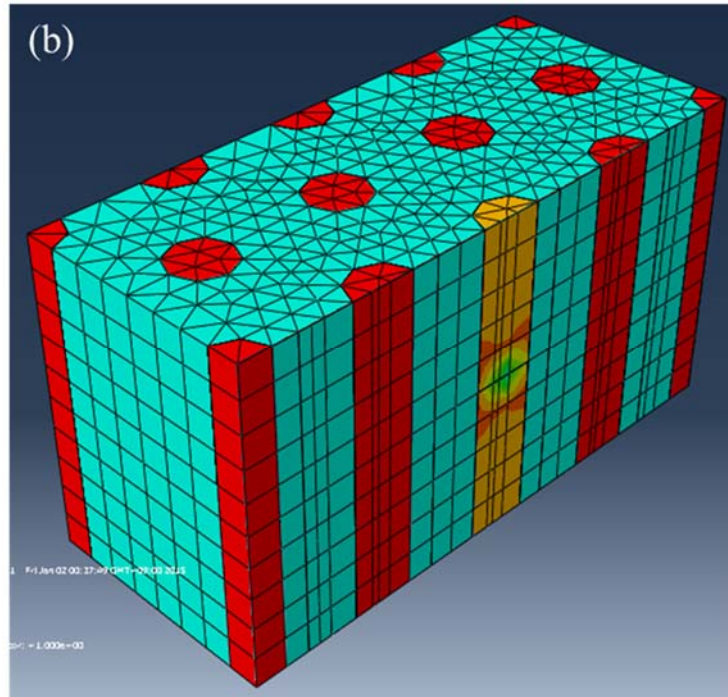


Fig. 2.9. The effect of material properties on stress concentration (a) $E_f/E_m = 10$ (b) $E_f/E_m = 40$ (c) the stress concentration factors

- 4) Effect of fracture energy: Same model with 1) was utilized. The fracture energy, a major parameter of cohesive element, was controlled from 10 kJ/m² (original interfacial property) and 50 kJ/m² (exaggerated property). The result of SCF is shown in Fig. 2.10 showing the large increase according to the fracture energy.

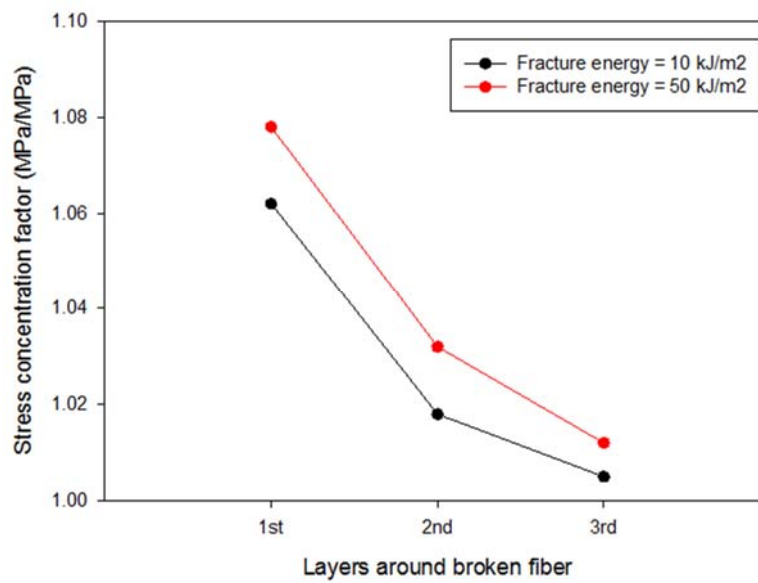


Fig. 2.10. The effect of fracture energy

- 5) Effect of fiber array: The fiber array was varied to three different case, maintaining the volume fraction to 50 %. Original hexagonal array was adopted as a reference and square array was adopted also. Finally random fiber array was analyzed. In the case of random fiber array the layers from broken fiber cannot be defined because the surrounding layers are not clear. To solve the problem the distance of hexagonal array was set as a reference length and

other distances of fibers were normalized by the reference length. The results are shown in Fig. 2.11. The clear point is that the effect of relative distance is important to the stress concentration factor. In very close case the SCF increased up to 14 %, that is a much higher value than the normal SCF expected in hexagonal and square array (up to 8 %).

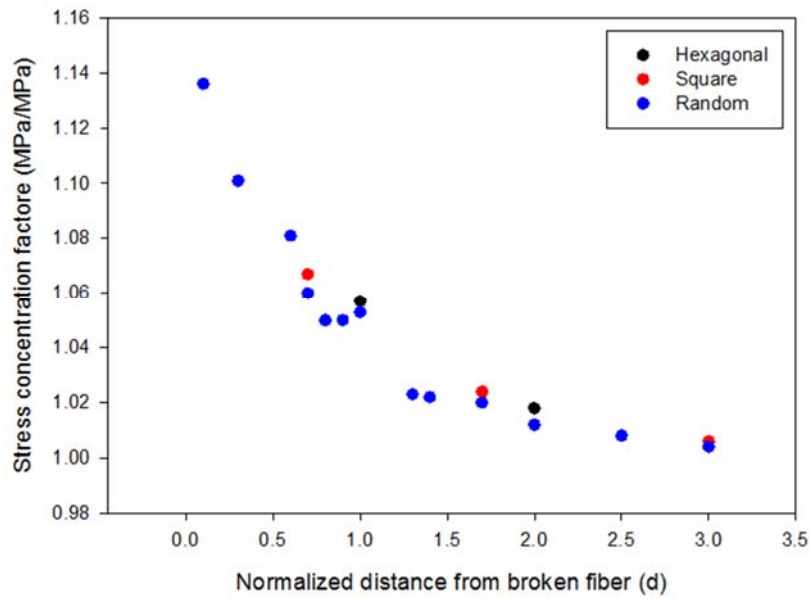


Fig. 2.11. The effect of fiber array

The parametric study showed the positive relationships, i.e. the increase of SCF, according to the ‘increase’ of IFSS, volume fraction, relative material properties and fracture energy. In all cases the SCF in the first nearest layer was highest and the value was up to 8 % addition. And from the second nearest layer the SCF value dropped drastically. More importantly, the effect of IFSS was critical to the SCF value and the effect of volume fraction and material properties are relatively lower

than that of SCF. In addition to that the importance of relative distance was revealed through random fiber array analysis. A fitting curve can be added to the SCF of random fiber array for utilizing to apply the SCF data to the statistical model without the analysis.

2.2. Statistical model

2.2.1 Overall scheme of statistical model

The overall calculation scheme is shown schematically in Fig. 2.10. First the basic information was input. The material properties of constituents, the elastic modulus and tensile strength, and the Poisson's ratio of fiber were taken from the materials. Interfacial properties, i.e., the IFSS, and the composite properties, the fiber volume fraction, fiber diameter, and stress concentration factor (which was calculated in prior section) were also input. Based on the information, preliminary calculation was done. Weibull property was calculated from the fiber strength according to the gauge length, and the inter-fiber distance was calculated from volume fraction. The information was used in main loop, calculating the probability of multiple fracture.

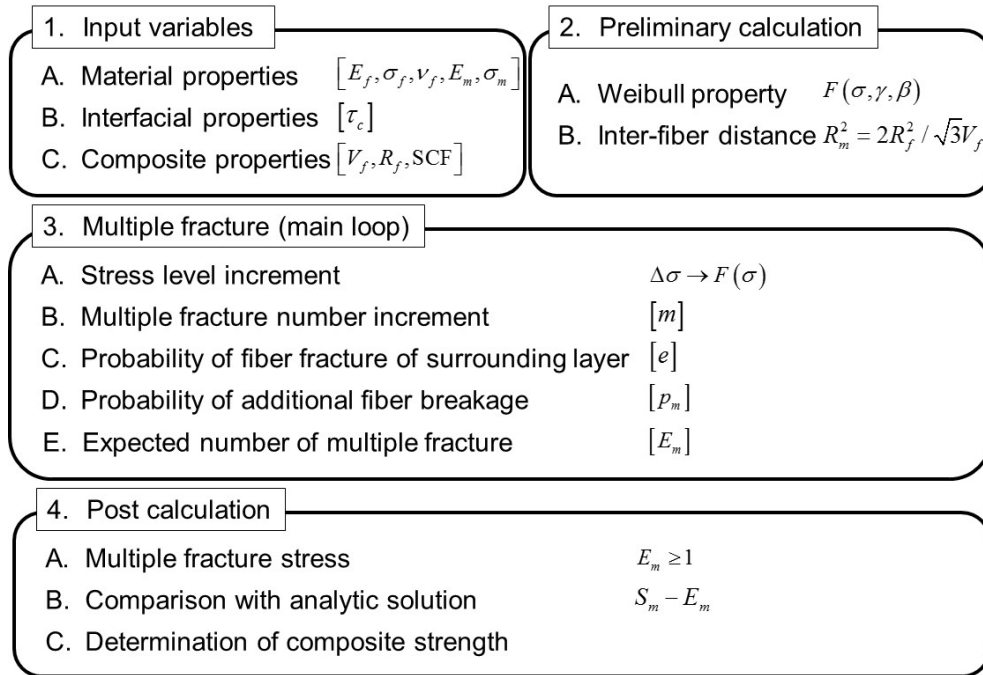


Fig. 2.12. Overall calculation scheme of statistical model

In the main loop, the probability of multiple fracture and expected number of multiple fracture were calculated (see Fig. 2.11). First the stress increment and multiple fracture increment was given. In this study the algorithm was implemented via MATLAB, the stress increment was 10 MPa, and the multiple fracture increment was 1. Then the probability of fiber fracture of surrounding layer, which was explained in introduction section and would be described in detail in following subsection, was calculated. Based on that the additional fiber breakage was calculated. After that same calculation was done on increasing multiple fracture number to enough multiple fracture number which was selected by research and material system. Note that the multiple fracture increment and calculation of probability were done in just one stress increment step, so in the following stress increment, the same calculation was done in the same manner, computing the same probability in certain stress level. If the stress also reaches to desired level, the probability of multiple fracture according to the stress level could be plotted. Finally the probability of multiple fracture was accumulated by trapezoidal rule, calculating the expected number of multiple fracture in composite. If the expected number reaches to unity in certain multiple number, the following stress level was defined as ‘multiple fracture stress’, inducing the multiple stress.

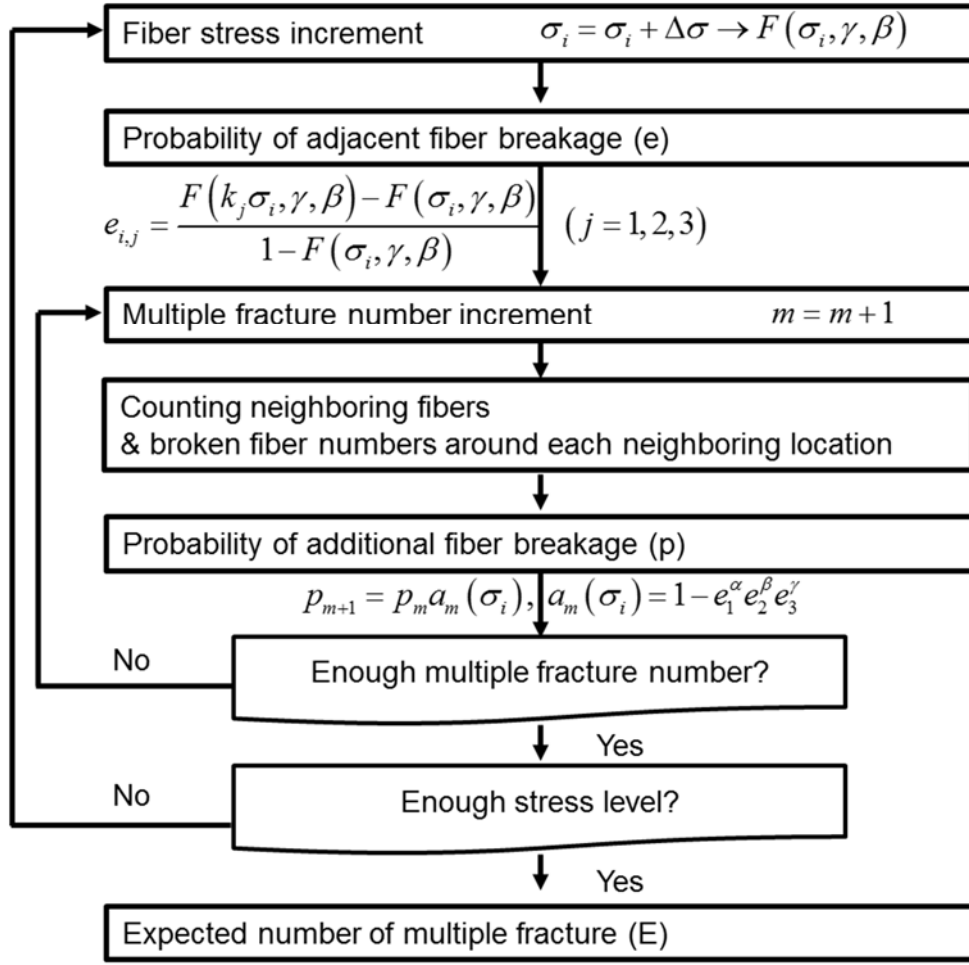


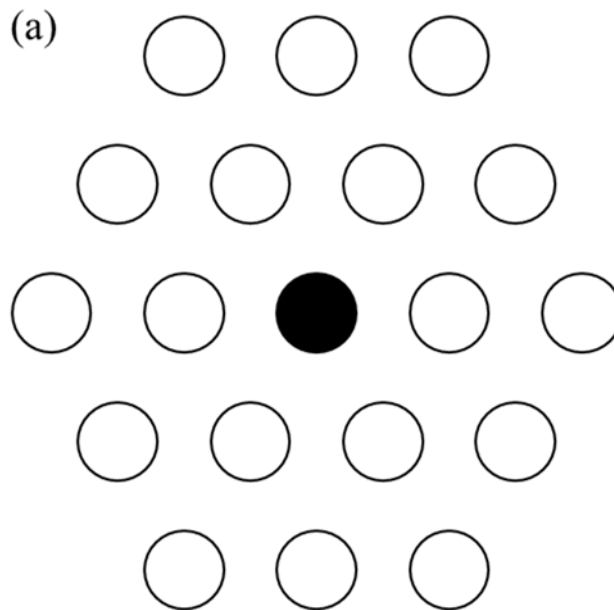
Fig. 2.13. Specific algorithm inside the main loop

Consequently the multiple fracture stress of each multiple fracture number is the final result. And the analytic solution (which would be explained in section 2.3.1) was also calculated in the multiple fracture number. So the analytic and numerical stress could be compared. The determination of tensile strength, i.e. the result of comparison, is the cross-point. In the implementation if the value (analytic solution) – (multiple fracture stress) changed from plus to minus, the value was defined as

composite strength.

2.2.2 *Probability of fiber breakage*

Fig. 2.12 shows the situation of fiber breakage and additional fiber breakage in hexagonal fiber packing. Central black fiber is broken fiber, and surrounding 3 layers which was distributed by colors are neighboring fibers. As I explained in prior chapter, the presence of a discontinuity cause a local stress concentration. Therefore according to this assumption there exist neighboring fibers under stress concentration. In the order of distance from broken fiber the stress concentration factors are given, which is decreasing. So in the average fiber stress level of σ , the fibers in first layer is subjected to the stress level of $C_1\sigma$, and in the same manner, $C_2\sigma$ and $C_3\sigma$ of stress level are subjected to surrounding second and third layer respectively.



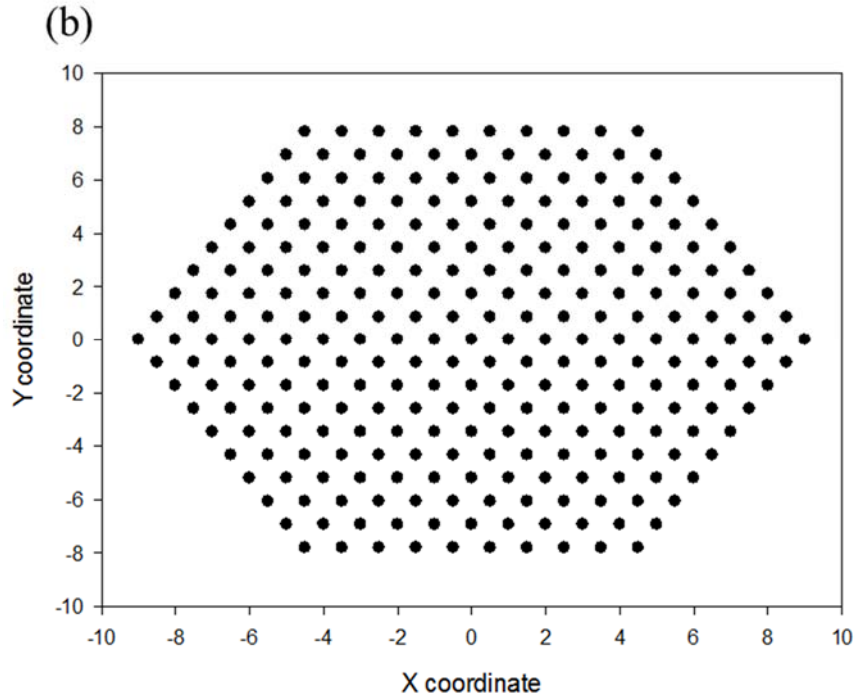


Fig. 2.14. Schematic diagram of hexagonal fiber array including broken fiber (a) schematic diagram. Central black dot represents the broken fiber in center (b) implemented hexagonal fiber array in MATLAB program, showing hexagonal array. The distance between dots was set as 1

The fractures can grow by breaking these neighboring fibers. It is necessary to compute the probability that a given element will fracture due to the increase in stress (from now we call this ‘transition probability’). If a fiber is intact in a certain stress level, however broken by overstress, and if the fiber breakage is following Weibull distribution the transition probability e is presented as following Equation (17).

$$e_n = \frac{F(C_n \sigma) - F(\sigma)}{1 - F(\sigma)} \quad (17)$$

where n means neighboring layer, F means Weibull distribution of fiber fracture. In the related research the denominator was often regarded unity because the Weibull probability of fiber fracture is relatively very small. However the denominator term is essential in this thesis, because when the stress level goes closer to the fiber strength the denominator get larger, affecting more influences in transition probability. In the view of mathematics, an event that a fiber is broken between the stress level of σ and $C_n\sigma$ is based on the event that the fibers are not broken under the stress level of σ . It is a conditional probability relation so Bayes' theorem can establish the relation between two events. The denominator term should be included like following scheme. The basic presentation of Bayes' theorem is presented in Equation (18). A and B represents an event respectively.

$$\therefore P(A|B) = P(B|A) \frac{P(A)}{P(B)} \quad (\text{Bayes' theorem}) \quad (18)$$

In this case the event A means the fiber fracture between two stress level ($F(C_n\sigma) - F(\sigma)$), and B means the not being break under certain stress level ($1 - F(\sigma)$). In addition to that the conditional probability $P(B|A)$, which means the fibers are unbroken under the stress level σ when the fiber is broken between the stress level σ and $C_n\sigma$, is 1. Finally the transition probability is defined.

The probability of multiple fracture p is the combination of this transition probabil-

ities. Fig. 2.13 shows the multiple fracture situation of some existing multiple fracture cluster. In this statistical model some assumptions were added for convenience in computation.

- 1) Only the nearest fibers, i.e. right the fibers adjacent to the broken fibers cluster, are broken.
- 2) The broken cluster is close-packed, not making a separated and oval shape.
- 3) The effect of each multiple fracture is overlapped independently to neighboring fiber.
- 4) One by one fracture is assumed. Actually the multiple fracture can occur in the same time, but this assumption

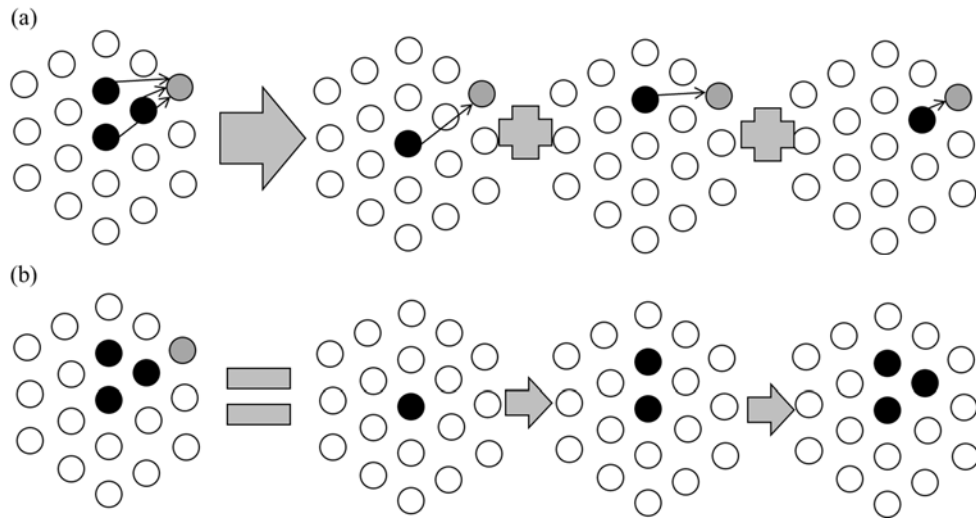
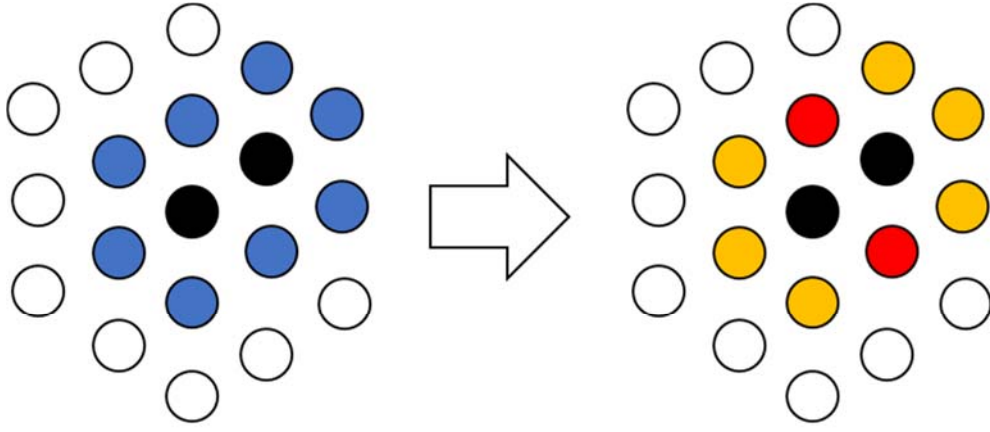


Fig. 2.15. Schematic diagram of occurrence of multiple fracture situation (a) overlapping of each effect from broken fiber (b) one-by-one fracture situation

In the implementation, the average of effect of nearest fibers are adopted. At a certain multiple fracture the adjacent fibers are found first. And in each adjacent fiber the

surrounding broken fiber circumstance is analyzed. And the each case was averaged in each case. Finally the probability of multiple fracture was calculated by the Equation (19). The transition probability was arranged in power law with the index of the average adjacent fiber in each layer up to third. The index α , β , and γ are the averaged adjacent fiber numbers. An example is shown in Fig. 2. . If there is a cluster of broken fibers which consists of two fibers, eight surrounding fibers are formed around the cluster. Then the broken fiber circumstance can be analyzed. The two fibers which is pointed by red color have two 1st nearest fibers so $\alpha = 2$ and $\beta, \gamma = 0$. And six fibers which is colored by orange have one 1st nearest fiber and one 2nd nearest fiber so $\alpha, \beta = 1$ and $\gamma = 0$. By averaging the average $\alpha = 10/8$ and average $\beta = 6/8$. So the multiple fracture of p_3 can be presented as Equation (20). Note that initial p follows the Weibull distribution of single fiber.

$$\begin{aligned}
 p_m &= p_{m-1} \left[1 - e_1^\alpha e_2^\beta e_3^\gamma \right] \\
 &= p_{m-1} \left[1 - \left(\frac{F(C_1 \sigma_f) - F(\sigma_f)}{1 - F(\sigma_f)} \right)^\alpha \left(\frac{F(C_2 \sigma_f) - F(\sigma_f)}{1 - F(\sigma_f)} \right)^\beta \right. \\
 &\quad \left. \left(\frac{F(C_3 \sigma_f) - F(\sigma_f)}{1 - F(\sigma_f)} \right)^\gamma \right]
 \end{aligned} \tag{19}$$




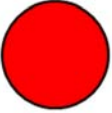
	$\text{Survive} = (1 - e_1)(1 - e_2)$ $\text{Breaking} = 1 - (1 - e_1)(1 - e_2)$
	$\text{Survive} = (1 - e_1)^2$ $\text{Breaking} = 1 - (1 - e_1)^2$

Fig. 2.16. Example of three multiple fracture with existing two multiple fracture group

$$\begin{aligned}
 p_3 &= p_2 (1 - e_1^{10/8} e_2^{6/8}) \\
 &= p_2 \left[1 - \left(\frac{F(C_1 \sigma_f) - F(\sigma_f)}{1 - F(\sigma_f)} \right)^{10/8} \left(\frac{F(C_2 \sigma_f) - F(\sigma_f)}{1 - F(\sigma_f)} \right)^{6/8} \right] \quad (20)
 \end{aligned}$$

The result of probability of multiple fracture p via MATLAB programming is shown

in Fig. 2.15, showing the drastic increase around the fiber strength (the typical trend of Weibull distribution). As the stress level increases the coefficient of recurrence formula also increases which is close to unity, so the gaps between multiple fractures become narrow.

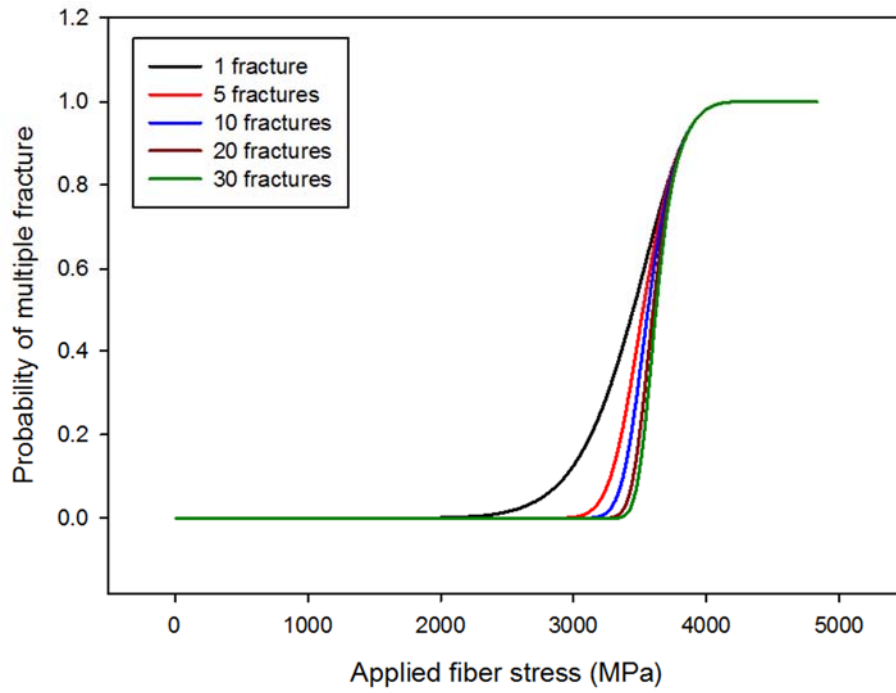


Fig. 2.17. Probability of multiple fracture

2.2.3 Multiple fracture stress

The probability of multiple fracture was calculated, however it isn't the expectation value itself. In previous literature [7, 8, 12, 72-74], the number of weak link in overall composite was calculated considering the dimension. The length of composite was divided by ineffective length and the number of fibers was considered and two values

are multiplied following the Equation (21) [7], drawing the number of places which can be damaged. The expectation value of multiple fracture cluster inside the composite is

$$E_m = p_m MN, \quad M = L / \delta, \quad N = (\text{number of fibers}) \quad (21)$$

where E is the expected number of cluster, M is the number of link and N is the number of fibers in composite. It have advantage that it can consider the dimension of composite, however in this model the infinite field of composite is considered ideally. The dimensionless approach is demanded and in this model the accumulation of probability is adopted. In the discrete data system, the multiplication of probability and value is the expected value, and it can be extended to the system. Finally the accumulation of this plot can draw the expected value. The result is shown in Fig. 2.16, showing the increasing trends. In Fig. 2. 16 (a) the multiple fracture stress determination is shown, same as the trend which is the gaps between multiple fractures get narrower according to the multiple fracture number. And in Fig. 2.16 (b) the multiple fracture stress was plotted, and note that it is a normalized stress by fiber volume fraction, meaning the ‘composite’ strength. If the expectation value reaches to unity, it is assumed that there exist at least one multiple fracture cluster in composite, and corresponding stress level is defined as ‘multiple fracture stress’ of each multiple fracture.

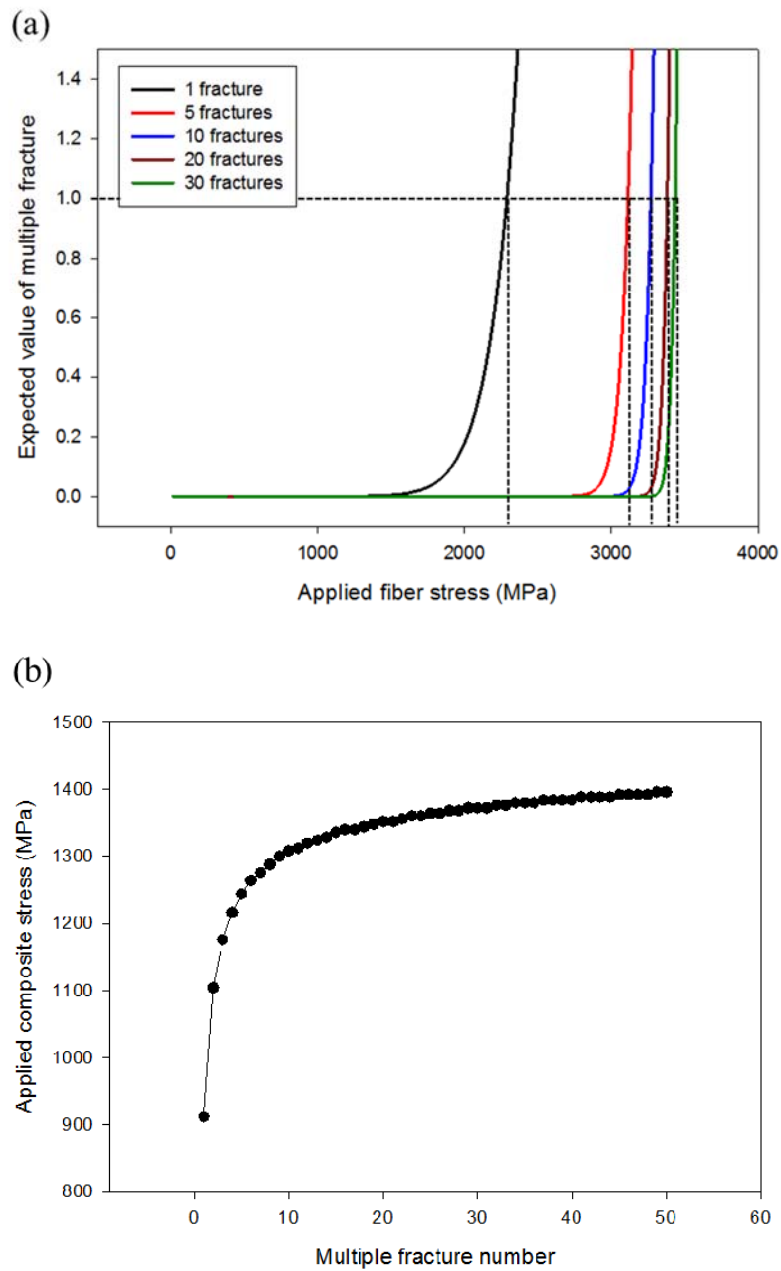
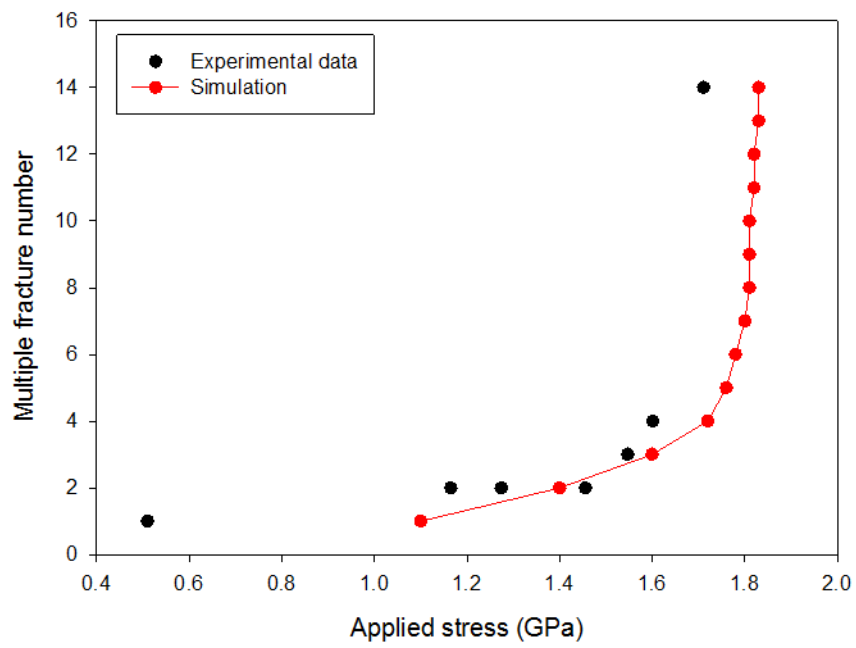


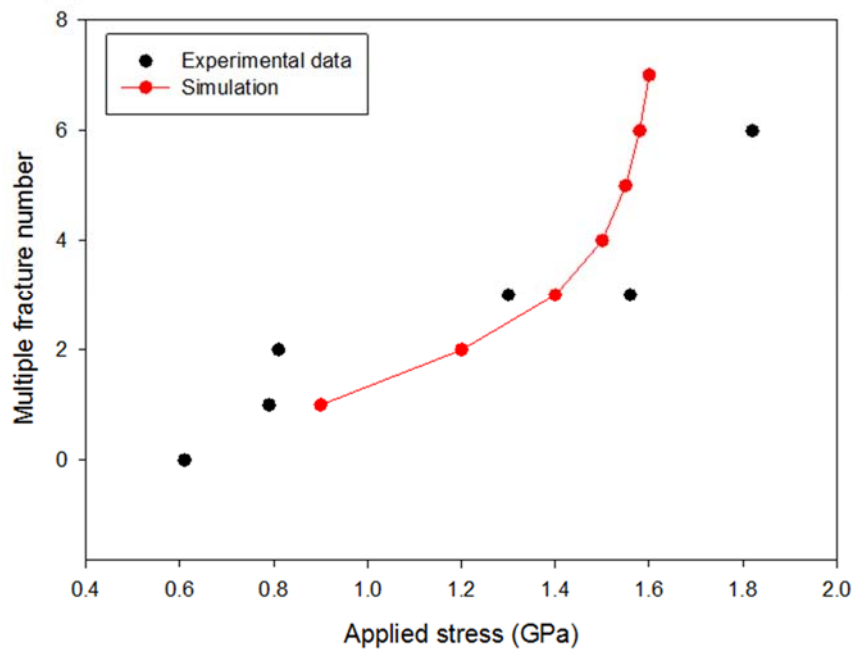
Fig. 2.18. Determination of multiple fracture stress (a) example of multiple fracture stress determination (b) multiple fracture stress according to the multiple fracture number

This calculation algorithms of multiple fracture should be validated with experimental results. Some previous literatures some literatures that have observation data and following Weibull properties were selected [8, 75-77]. The researched observed the fracture according to the stress level, finding the multiple ‘plets’ in the composites. The Weibull property and properties of constituents were input to the model and following multiple fracture stresses were calculated. The results are shown in Fig. 2.17, showing the similar increasing trend. The multiple fracture stress, however, is commonly larger in all cases. In other words, at the same stress level the real number of broken fiber is larger than the simulation. It can be interpreted as the composite is being damaged under the expected level, and it would be the gap between model and real composite. The considerable reason are: 1) imperfection of interface make a void in early-stage 2) local fiber alignment including the small waviness and twisting of fiber 3) connection of two or more multiple fracture cluster and 4) difference between progressive fracture model and simultaneous multiple fracture model. Even considering that the difference is within reasonable agreement, so the validity of this model can be concluded that it is valid in reasonable agreement to at least the brittle fiber composite system such as CFRP or GFRP, however it shows a little higher value than experiment.

(a)



(b)



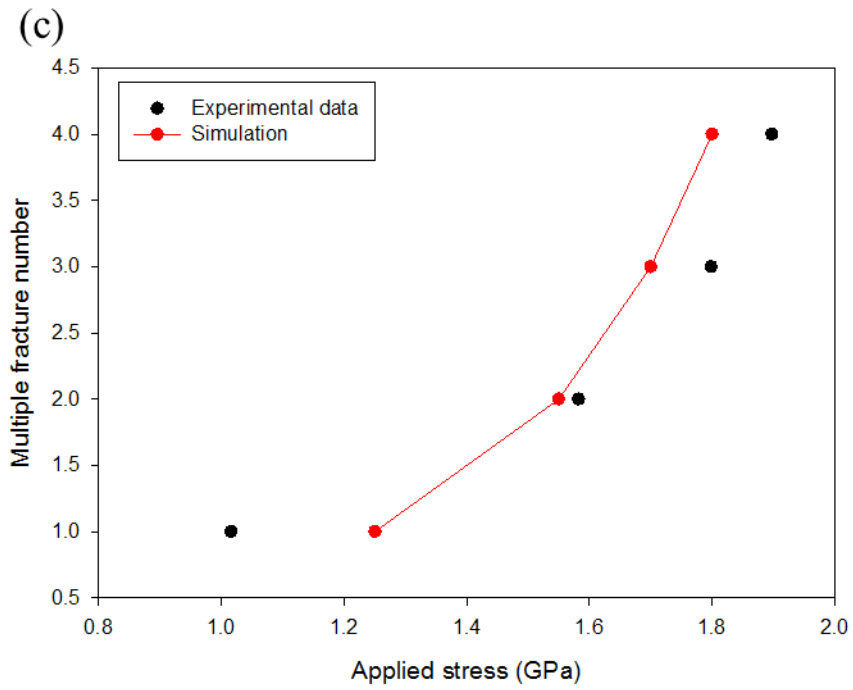


Fig. 2.19. Comparison of model and experimental results in previous literature (a) a comparison with [76] (b) comparison with [77] (c) comparison with [6]

2.3. Determination of tensile strength

2.3.1 Analytic solution considering multiple fracture

In this section the research of Shioya [31] was mainly referred. First the tensile strength of fiber was determined by 2-parameter Weibull distribution same as the statistical model. In reference the ineffective length was determined at 50 % stress recovery point as Equation (8). The basic concept is acceptable however in this research the standard of ineffective length determination was set as 90 % stress recovery. In addition to that in real circumstance the value of ineffective length can be approximately calculated by using either the equation of two condition only except the second row, thus the equation can be modified as

$$l_i = \text{Max} \left[2(\ln 10)\lambda, \frac{9l_c}{10} \right] \quad (22)$$

The tensile strength of composite was calculated by following scheme. The fraction of fibers which is carrying load was estimated first. A constant multiple fracture number was introduced and k fibers were treated as a package or bundle which can be broken simultaneously. The probability that a fiber doesn't break in an ineffective length at a certain stress level is given by $1 - F(\sigma_{\text{fiber}})$ (F is the Weibull probability of fracture. And note that the σ_{fiber} is different to the fiber strength, meaning the applied fiber stress). The fraction of fibers, which means the portion of tensile load in an arbitrary section of the composite is equivalent to the probability that k fibers (multiple fracture number of given composite) have not broken by themselves in the ineffective length. Note again that if the k fiber cluster exists inside the composite the

composite is fractured, and the k fibers are broken simultaneously, so the k fibers should not be broken under stress for load carry. The portion that the composite is intact at the certain fiber stress is

$$P = \left[1 - F(\sigma_{fiber}) \right]^k = \exp \left(- \frac{kl_i}{L_0} \left[\frac{\sigma_{fiber}}{\gamma} \right]^\beta \right) \quad (23)$$

Finally the tensile strength of composite material is determined by the multiply of the probability of load carrying and expected stress like

$$\sigma_s = P\sigma_{fiber} = \sigma_{fiber} \times \exp \left(- \frac{kl_i}{L_0} \left[\frac{\sigma_{fiber}}{\gamma} \right]^\beta \right) \quad (24)$$

As the fiber stress increases, the probability of load carrying decreases. At a low stress level the increase of fiber stress is dominant, and the dominance is transferred to the exponential term. So the composite strength value have an optimum at a certain point. Then at the maximum point the composite strength is determined. By putting the stress level corresponding to the maximum point into the Equation (25), the tensile strength of the composite material can be calculated as following.

$$\sigma_c = \text{Min} \left[\left(\frac{L_0}{2(\ln 10)e\beta\lambda k} \right)^{\frac{1}{\beta}} \gamma, \left(\frac{10L_0\tau_b}{9e(\beta+1)R_f k} \right)^{\frac{1}{\beta+1}} \gamma^{\frac{\beta}{\beta+1}} \right] \quad (24)$$

The example by the data of [31] is shown in Fig. 2.18. We can identify that as the multiple fracture number increases in the same composite, the composite strength decreases. In this stage, the multiple fracture number is only a constant, and which multiple fracture is the critical value and what is the composite strength are not known clearly. In the reference the multiple fracture number was calculated from the experiment inversely and the concept is used in this thesis, coupling with the statistical model.

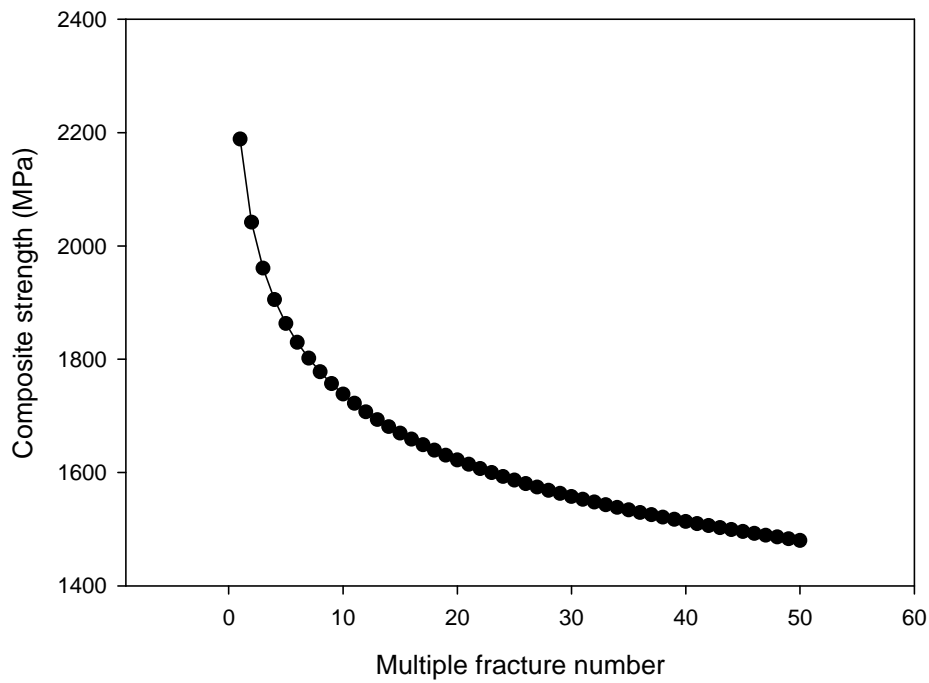


Fig. 2.20. The composite strength according to the multiple fracture number. Parameter values are from [31]

2.3.2 *Determination of tensile strength*

Now the relationship of multiple fracture and stress level, the multiple fracture stress, and the relationship of multiple fracture and composite strength, the analytic composite strength, were calculated by model. As the multiple fracture number increases, the multiple fracture stress increases (chapter 2.2) and the analytic composite strength with constant multiple fracture number (chapter 2.3.1) decreases. So we can plot the multiple fracture stress and composite strength against the multiple fracture number in the same plane. The result is shown in Fig. 2.19, showing a cross-point. Then we can discuss as

- 1) Before the cross point, the multiple fracture stress, i.e. the stress demanded to induce the multiple fracture, is lower than the corresponding composite strength. Consequently the composite still can carry the load under the multiple fracture condition.
- 2) After the cross point (now we call the cross point ‘critical multiple fracture number’), the multiple fracture cannot be occurred because the composite already reaches to the final failure. The multiple fracture after cross point can be treated as out of discussion.
- 3) Conclusion: When a composite is broken, the fiber breakage under the critical multiple number can exist, however the breakage group of critical multiple fracture number is the maximum value that the composite can possess.

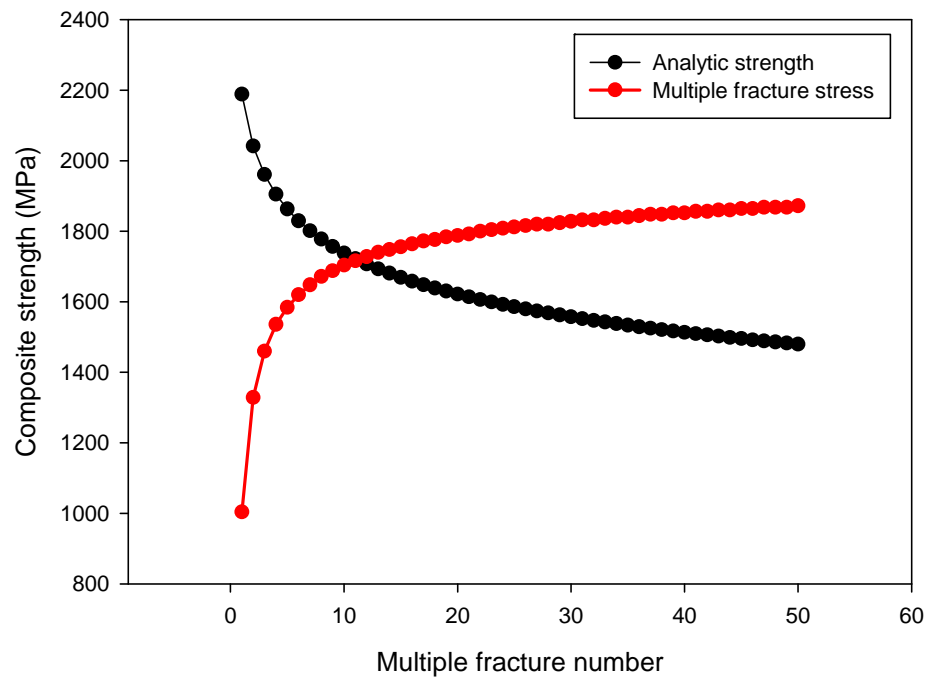


Fig. 2.21. The demonstration for determination of composite strength via comparison of analytic solution and multiple fracture stress (parameters from [31])

2.4. Prediction of fracture toughness

The fracture mechanism was reviewed in chapter 1. In the review the interfacial debonding and pull-out is the important mechanism in toughening. The equations of work of fracture in debonding and pull-out (W_{deb} and W_{po} respectively) are presented again as Equation (25).

$$W_{deb} = \frac{4\nu_f G_{SL} l_{deb}}{d}, \quad W_{po} = \frac{2\nu_f \tau_b l_{po}^2}{d}, \quad W_{total} = W_{deb} + W_{po} \quad (25)$$

in which G_{SL} is the mode-II interfacial toughness. Other properties are based on the material properties however, the debonded length and pull-out length should be determined. In the similar statistical approach by Pimenta [2], the debonded length and pull-out length was determined as a distribution via Weibull distribution. In this thesis the process is simplified largely. First the debonded length is adopted from analytic model in chapter 2.3.1. The pull-out length is hard to measure so calculated from another inherent property. And the debonded length was determined by material properties so the pull-out length was calculated by debonded length as Equation (26), following the scheme of ASTM STP452 standard and [61]. Following the scheme the toughness was also calculated.

$$l_{po} = \begin{cases} \frac{l_{deb}}{4} & (l_{deb} < l_c, \text{mean value}) \\ l_{deb} & (l_{deb} = l_c) \\ \frac{l_c}{l_{deb}} & (l_{deb} > l_c) \end{cases}, \quad l_c = \frac{R_f \sigma_f}{\tau_b} \quad (25)$$

2.5. Summary

In the chapter 2, a model was established about the composite strength determination model using the combination of analytic and statistical approaches. In addition to that the fracture toughness was also predicted using the critical multiple fracture determined by the strength prediction. Before the statistical model, the stress concentration analysis was done via finite element method. A square unit cell with hexagonal fiber array was generated and tensile deformation was simulated in 2 % tensile condition. The fiber stress of surrounding fibers were measured in virtual space for intact and damaged model. Especially the interface of broken fiber and matrix was treated by cohesive element, considering the IFSS. Periodic boundary condition was applied to the unit cell to assume an infinite fiber field. The debonding and pull-out were observed and the parametric study was done showing the positive effect of IFSS, volume fraction, and the relative material properties. Surely the calculation of stress concentration factor is the main purpose.

Based on this stress concentration factor the multiple fracture stress was calculated using implemented MATLAB program. The property of fiber, Weibull property of fiber, interfacial property, and the composite property were used to model. The probability of fiber breakage under stress concentration was calculated under Weibull distribution (the ‘transition probability’). Probability of multiple fracture was calculated via transition probability considering the number of adjacent fibers. Finally the expected value of multiple fracture was derived by accumulation, ignoring the effect of composite geometry. The final result of the statistical model is ‘multiple fracture stresses’, which is the certain stress that induce the multiple fracture in composite,

and making the expectation value over unity. Finally the composite strength was determined by comparison.

The critical multiple fracture number was also utilized to toughness prediction. The toughness of debonding and fiber pull-out was predicted. The debonded length was adopted from the analytic solution and the pull-out length was calculated from the debonded length. The toughness was calculated at the critical multiple fracture number. Aforementioned all prediction approaches would be applied to the certain unidirectional composite system.

3. Experiments and analysis of carbon fiber/epoxy composite

3.1. Experimental

3.1.1 Material preparation and specimen fabrication

Unidirectional carbon fiber prepreg (CU200NS, Hankuk Carbon Corporation, Korea) was prepared. The prepreg consists of Toray T700 fiber and epoxy resin. The basic properties of fiber and resin was provided in Table 3.1. Note that typical R/C contents, the ratio of resin in prepreg, was 33 % in CU200NS product, however a specially prepared prepreg with 38 % of R/C contents was used in this thesis. The density of fiber was measured by a laboratory scale based on Archimedes principle (Xs-204, Mettler Toledo, Switzerland). The weight was measured in air and in a cup of distilled water. The density was calculated using following equation.

$$\rho = \frac{W_1}{W_1 - W_2} \rho_w \quad (26)$$

W_1 is the weight without water, W_2 is the weight with water and ρ_w is the density of water. The density of fiber was measured as 1.70 g/cm³

The tensile property of carbon fiber material, i.e., the Young's modulus and tensile strength, was measured by single fiber tensile test of Toray T700 fiber. Single fiber was separated from carbon fiber tow and mounted on two paper tabs which have hole for hanging up to ring-type grips (see Fig. 3.1). The tabs were treated by glue

for making the tabs stiff. The arranged fiber was attached to tabs using commercial adhesive and dried for 1 hour. The gauge length was controlled as 10 and 20 mm for measurement of Weibull parameters (In this thesis 2-parameter Weibull distribution was used). The specimens were tested by universal testing machine (RB 302 ML, RNB, Korea) with the 2 mm/min of head speed. The above-mentioned fiber properties were measured. The single fiber tensile test showed lower tensile strength with longer gauge length, 30 mm, due to the stochastic properties of carbon fiber, and the tensile property of 10 mm was adopted as reference data. The tensile strength according to gauge length was plotted in Fig. 3.2 and the Weibull parameter was $\beta = 12.01$ and $\gamma = 3927$ MPa.

Table 3.1. The material properties of carbon fiber/epoxy composite system

Composite parameter	Fiber volume fraction	55 %
	Fiber diameter	7 μm
	Gauge length	0.05 m
Interfacial property	Interfacial shear strength	37 MPa
Young's modulus	Fiber - longitudinal	217 GPa
	Fiber - transverse	21.7 GPa
	Matrix	3 GPa
Failure strength	Fiber	3.912 GPa
	Matrix	80 MPa
Weibull Parameter	Weibull modulus	12.01
	Characteristic stress	3.927 GPa
	Reference length	0.01 m

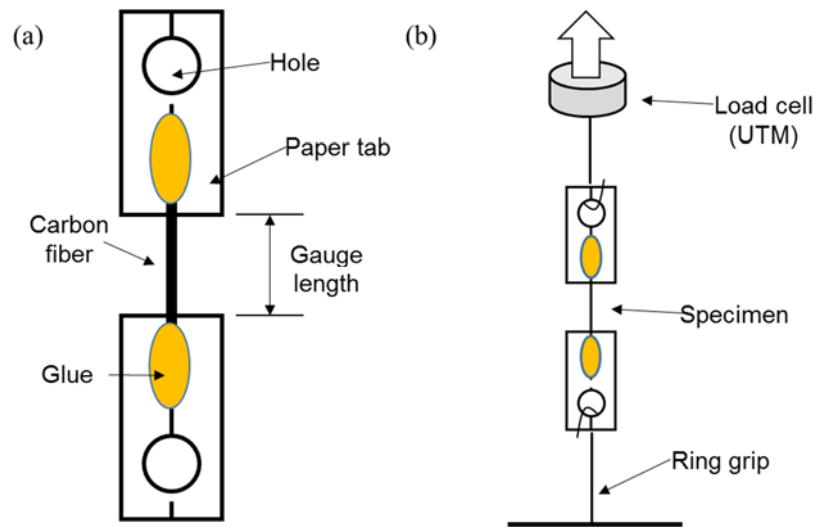


Fig. 3.1. Schematic diagram of single fiber test (a) specimen preparation (b)

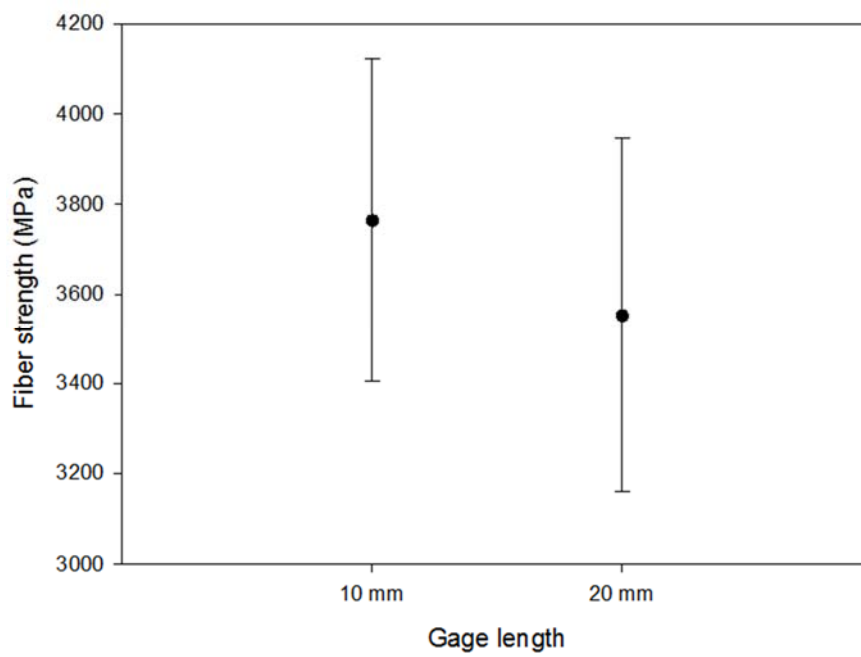


Fig. 3.2. Strength according to gauge length Weibull properties

IFSS was measured by micro-droplet test. Single fiber was separated from bundle and epoxy resin droplet was dropped on the fiber. Then micro-droplets were formed on the surface of carbon fiber due to surface tension. The specimen was cured on holder, making the droplet have a spherical shape. The droplet formed on surface was seen in Fig. 3.3. The carbon fiber having droplet resin interface was set between two blade collars with narrow slit, arranging the micro-droplet right below the collar (Fig. 3.4). The fiber was held by grip of universal testing machine (RB 302 ML, RNB, Korea) and the grip was moved with the speed of 1 mm/min. Then the micro-droplet was forced and finally the interface between fiber and matrix was failed. When the interface was finally failed the force was measured and IFSS was calculated by following Equation (27).

$$\tau_b = \frac{F_d}{\pi dL} \quad (27)$$

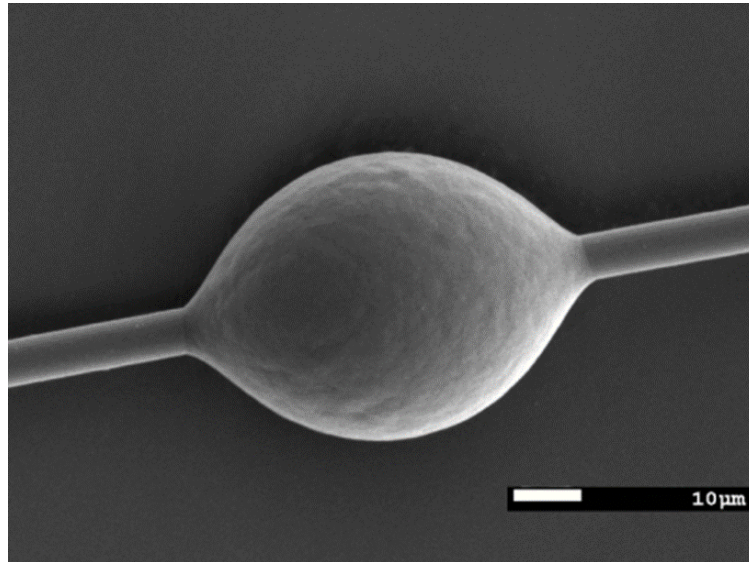


Fig. 3.3. Formed micro-droplet of epoxy on the carbon fiber surface

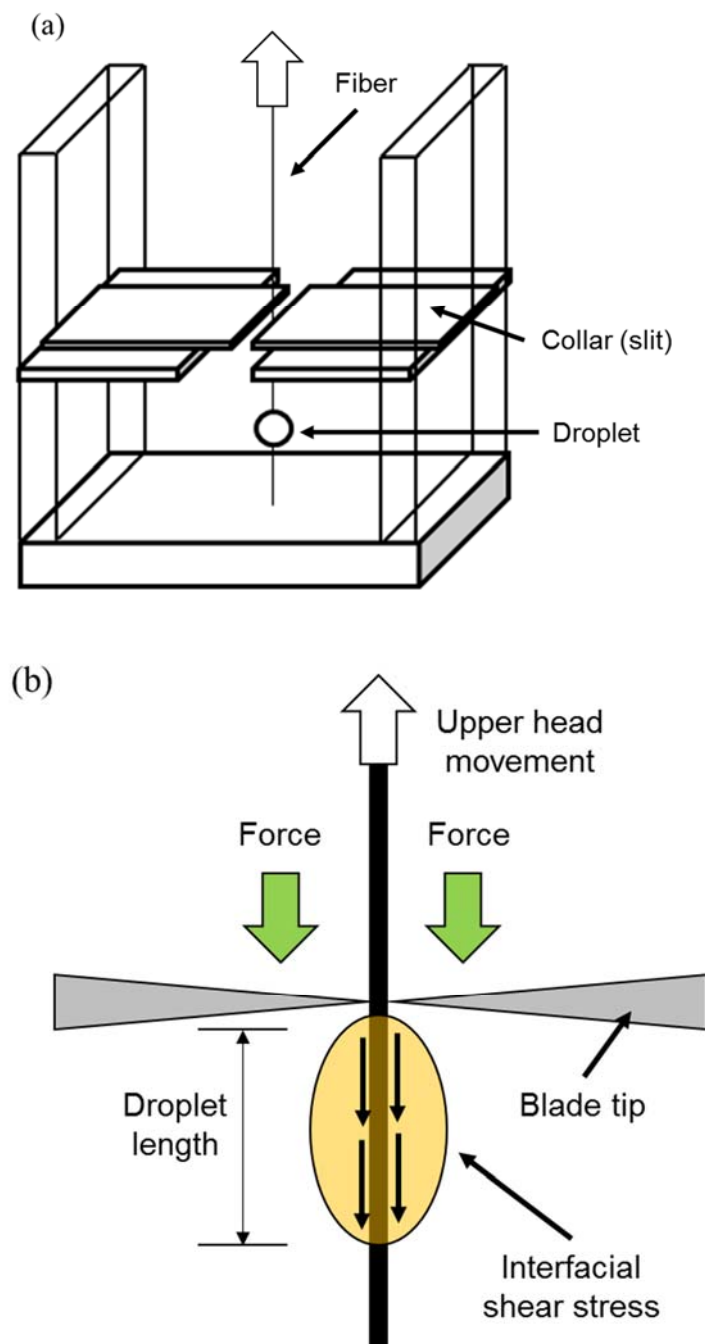


Fig. 3.4. Schematic diagram of micro-droplet test for IFSS measurement (a) apparatus consists of two blade collars (b)

Unidirectional composite was fabricated via prepreg laminating (supplied by T4L Corporation, Korea). Prepreg was laminated in mold on metal plate, making 1 mm of thickness (5 layers). The mold was cured for 30 minutes at 150 °C maintaining 0.8 atm. The process was shown in Fig. 3.5 schematically.

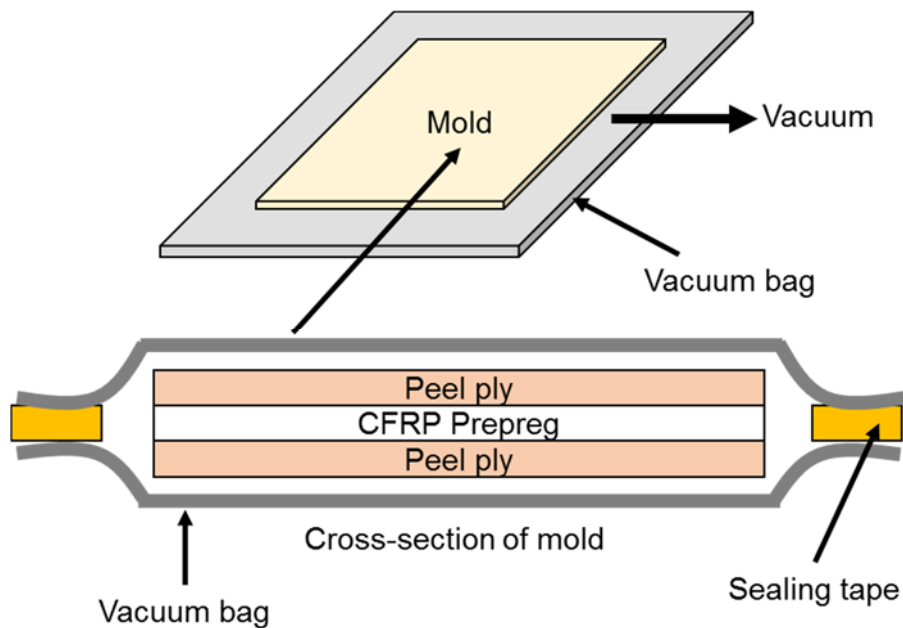


Fig. 3.5. Schematic diagram of manufacturing process using prepreg

3.1.2 Mechanical testing

Tensile test was operated following ASTM D3039 standard. The specimen was cut and grinded to 15 mm of width and 250 mm of length. Four end tabs, made of glass-fiber reinforced plastic, two tabs in each end, were attached using epoxy adhesive

(Plastic Welder, VersaChem, USA) which have 3,500 psi of lab shear strength. The tab length was 50 mm and thickness was 2 mm, making 150 mm of gauge length. The adhesive was used and cured in vacuum oven in 70 °C of temperature for 4 hours. The curing condition was set for the optimum adhesion, referring to the recommended specification by supplier (see Fig. 3.6 for specimen shape). The specimen was loaded using tensile testing machine (INSTRON 8801, INSTRON, USA) with the speed of 1.5 mm/min (1 % strain per minute). An extensometer with gauge length of 12.5 mm was attached for strain measurement. After the tensile test the modulus and strength of composite were measured as seen in the Fig. 3.7. During the test the specimens were broken in bundle (making a sound ‘ping’) and split in longitudinal direction occurred. This failure surface implies the multiple fracture phenomenon as reported in literature. The multiple fracture would be analyzed in next section. The following result seen in Fig. 3.7 shows the tensile behavior. The tensile strength was measured as 1506 MPa. The composite showed linear behavior and brittle fracture generally.

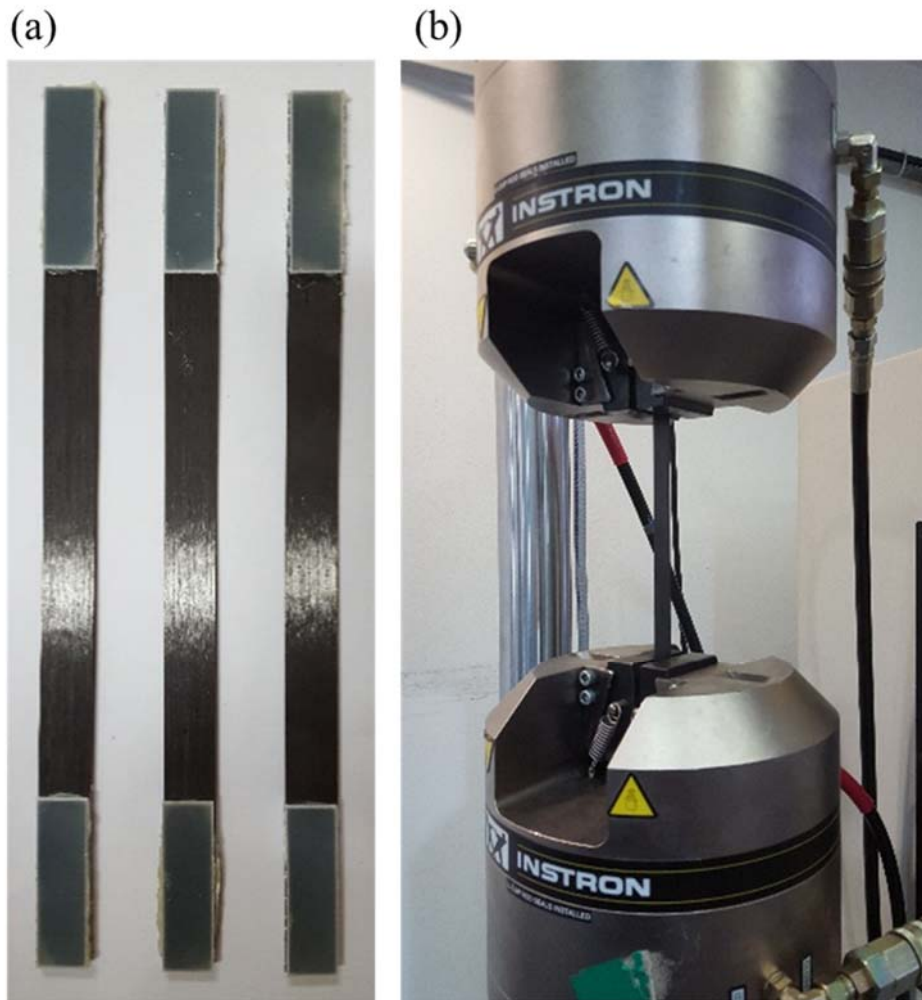


Fig. 3.6. Tensile test (a) testing specimen for tensile test (b) mechanical testing with tensile testing machine

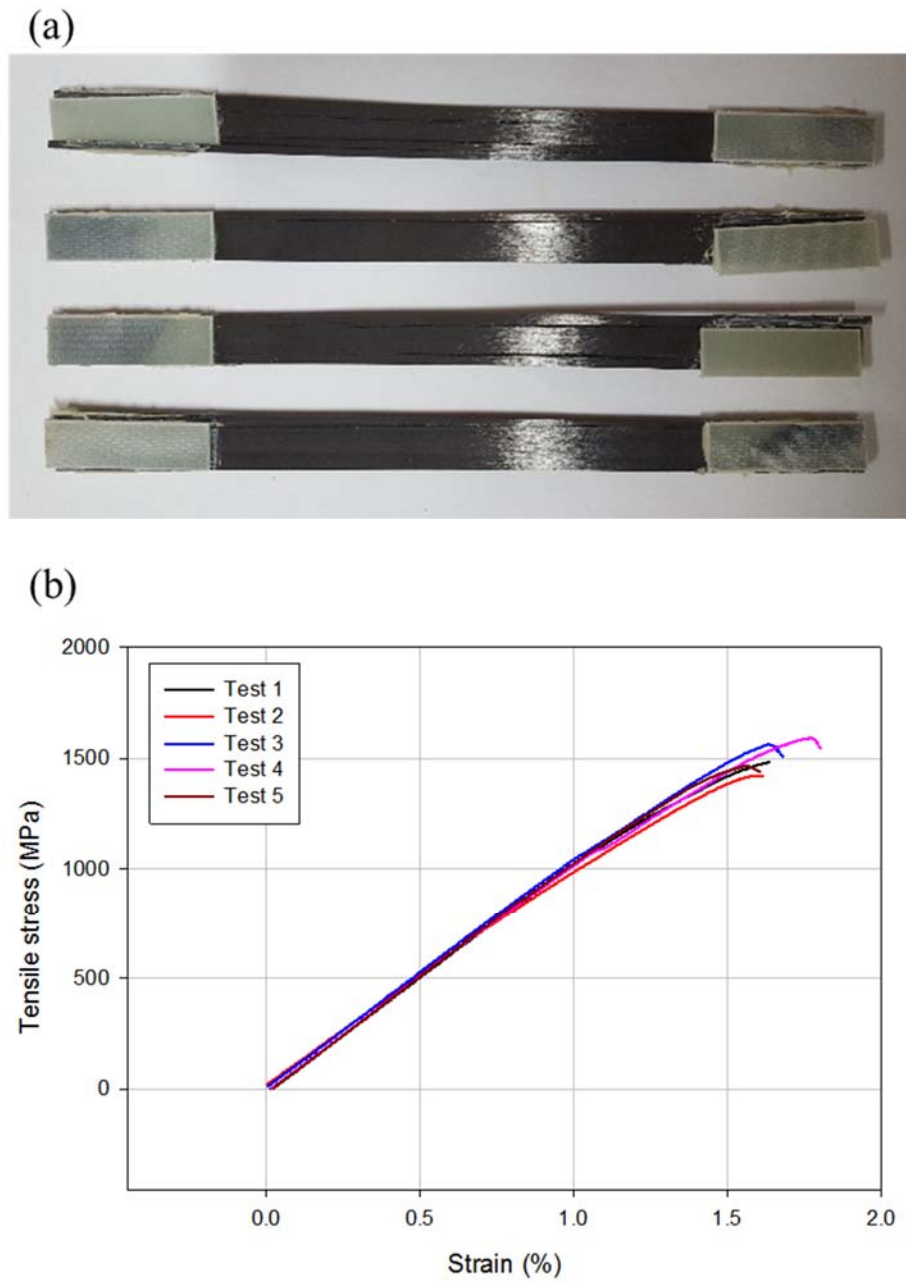


Fig. 3.7. The result of tensile test (a) fractured specimen (b) stress-strain curve of tensile test

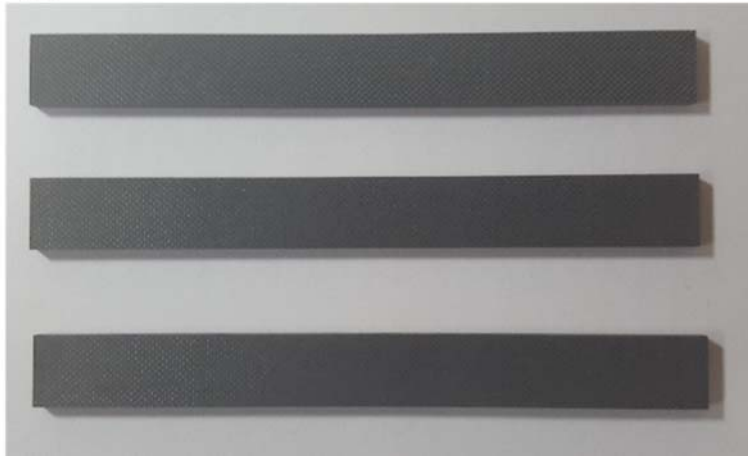
Three point bending test was operated also (Fig. 3.8). The specimen was cut and grinded to 13 mm of width and 120 mm of length in the same manner of tensile strength. The thickness of specimen was 3.2 mm, fabricating thick specimen (actually the specimen was fabricated in 3.2 mm thickness in original, however for tensile test the specimen was grinded to 1 mm thickness). The bending test was performed for comparison with tensile test, i.e., the effect of crack propagation and delamination, and for measurement of fracture toughness of composite. The specimen was loaded using universal testing machine (Quasar-5, Galdabini, Italy) in a span length of 51.2 mm at cross-head speed of 1.365 mm/min making 1 % strain per minute. The stress and strain were calculated by following Equations (28) and (29). The test referred ASTM D790 standard.

$$\sigma_f = \frac{3FL}{2bd^2} \quad (28)$$

$$\varepsilon_f = \frac{6Dd}{L^2} \quad (29)$$

where σ is flexural stress, ε is the flexural strain, F is the load, D is deflection, L is support span, b is the width and d is thickness.

(a)



(b)

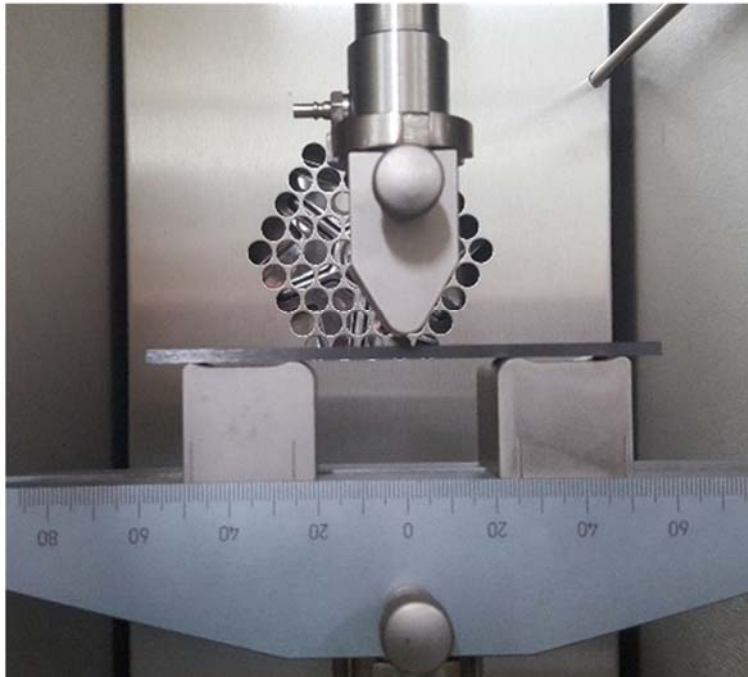


Fig. 3.8. Three point bending test (a) testing specimen (b) testing with universal testing machine

Fig. 3.9 shows the result of bending test. Similar to the tensile test the failed specimen showed stepped shape in failure surface, however the cracked part didn't separated perfectly. This failure surface implies the multiple fracture phenomenon as well as crack propagation in longitudinal direction, i.e. the delamination. The modulus and strength are seen in Fig 3.9 also. The composite showed linear behavior, however in large deformation nonlinear curve appeared implying the accumulation and propagation of micro-crack. In addition to that the strength measured by bending test showed lower value than that of tensile test. It is seen that the delamination effect. The measured strength was 1377 MPa.



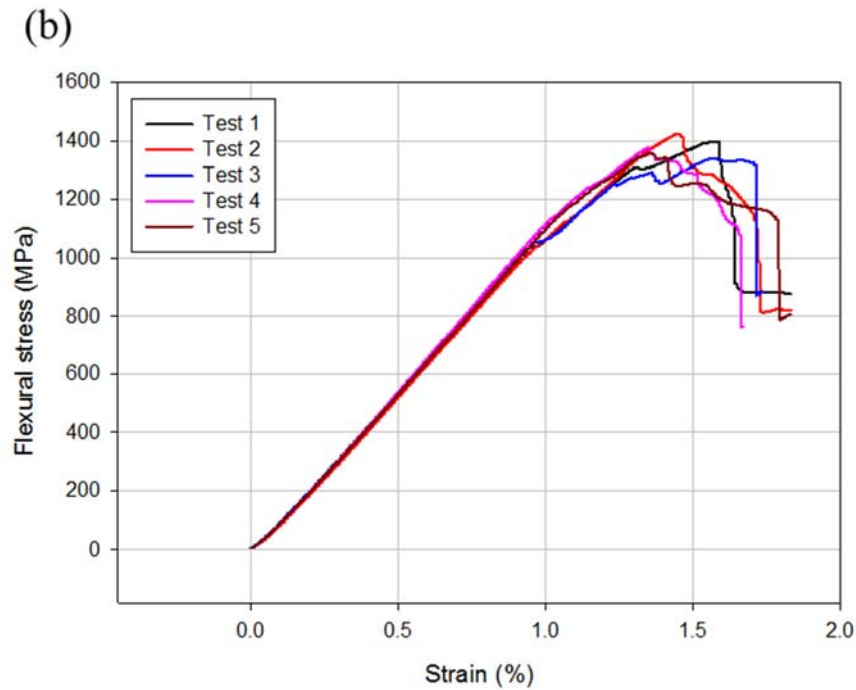
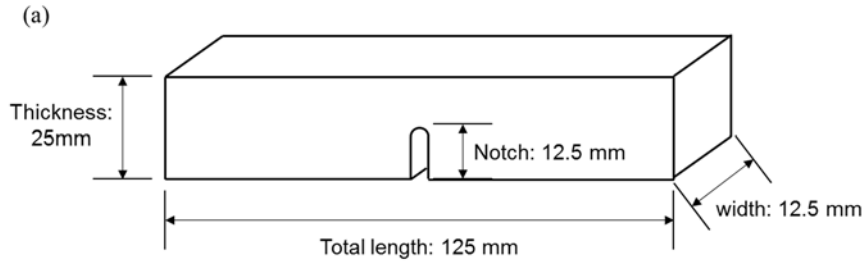


Fig. 3.9. The result of bending test (a) fractured specimen (b) stress-strain curve of bending test

With another universal testing machine (LR50K, Lloyd Instrument, UK) three-point test for fracture toughness was also carried out. For fracture toughness test notched specimens were prepared as shown in Fig. 3.10. Same prepreg material was laminated within metal mold having 25 mm thickness (140 layers). The material was cured for 30 minutes at 150 °C. The metal mold was loaded hydraulic pressure (kgf/cm²). This process was performed by T4L Corporation. Manufactured composite was cut by diamond blade and grinded to the specimen configuration shown in Fig. 3.10 (a). The central notch was made by diamond blade also, with 2 mm width

and 12.5 mm depth (that is, the ratio of notch depth to specimen thickness was controlled to 0.5). The configuration of testing specimen was from the ASTM E399, making the thickness of specimen as 25 mm. Note that the typical specimen thickness is 25 mm, i.e. 1 inch, following the ASTM standard. Following the ASTM standard the width and length of specimen were determined automatically as 12.5 mm, and 125 mm respectively. In the testing, the span length was set as four times of thickness, i.e. 100 mm. The testing was operated in load-control mode with 300 N/s following ASTM E399. The maximum load was used to calculate the fracture toughness and work of fracture following ASTM E399 and E1290-08. The specimen and testing process are shown in Fig. 3.10 and Fig. 3.11. Following testing results are shown in Fig. 3.12 and would be compared to the simulations. The maximum load was 9722 N (standard deviation of 585.4 N) and work of fracture was calculated as 26.23 kJ/m² (standard deviation of 94.95 J/m²). The fracture toughness was calculated by following equation.

$$K_I = \frac{6P}{BW} \alpha^{1/2} \left[\frac{1.99 - \alpha(1 - \alpha)(2.15 - 3.93\alpha + 2.7\alpha^2)}{(1 + 2\alpha)(1 - \alpha)^{3/2}} \right], \quad W = \frac{K_I^2}{E / (1 - \nu^2)} \quad (30)$$

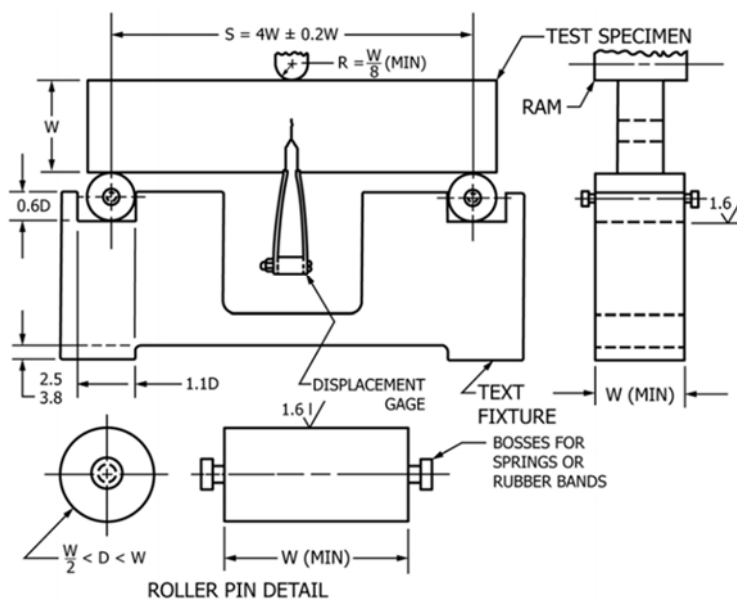


(b)



Fig. 3.10. Specimen for fracture test (a) schematic diagram with the size (b) real specimen

(a)



(b)



Fig. 3.11. Fracture test (a) Schematic diagram of three point flexural test for fracture toughness (from ASTM E1290-08 and E399) (b) demonstration of test

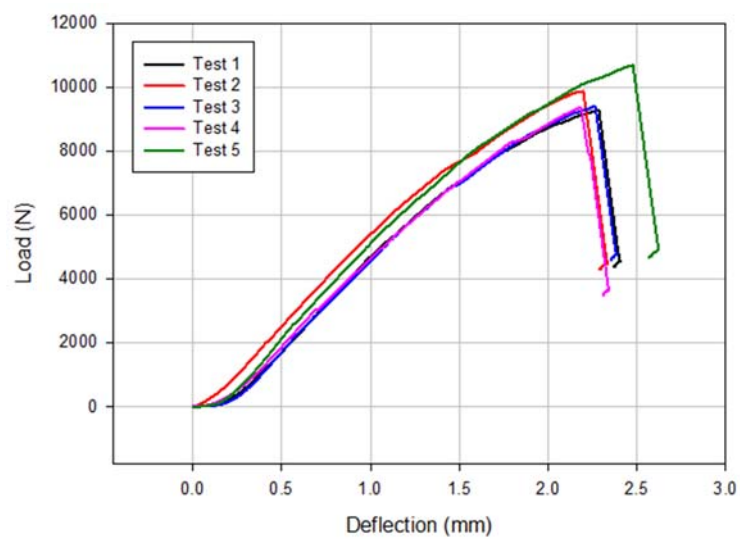


Fig. 3.12. Load-displacement curve of fracture test

3.1.3 *Multiple fracture observation*

Special specimen was fabricated and loaded. A mold having 4 mm of width was designed and carbon fiber tows which have been separated from fabric were mounted in mold, 4 tows for each mold space making 4 layer composite. through this process composite specimens having demanded geometry could be fabricated directly without cutting and grinding process. Same VARTM process was used for fabrication. The specimens were separated from mold and end tabs were attached to both ends in the same manner (see Fig. 3.13).

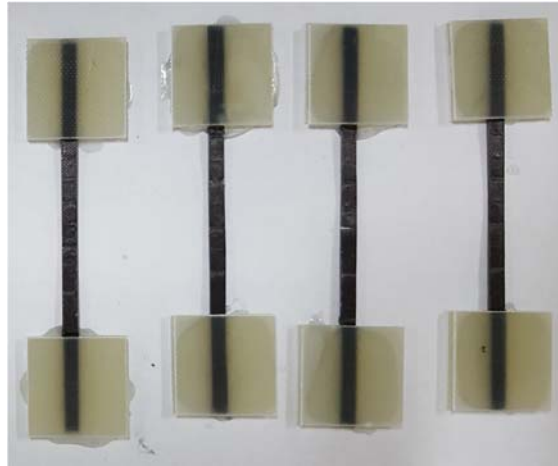


Fig. 3.13. Specimens for small-size tensile test for observation

In the testing 4 specimens was loaded to final fracture, and the load for fracture was measured. Next the 30, 50 and 70 % of the failure load was applied to 4 specimens in each case. The tested specimens were analyzed by employed X-ray CT (Skyscan 1172, Bruker, Belgium). End tabs were removed and specimen was mounted on holder vertically using wax. The scanning process was carried out in the condition of Table 3.3. Before the main scanning the preview image was investigated and

micro-crack during specimen preparation was detected. The medium part of specimen was scanned avoiding the effect of micro-crack. The X-ray beam was emitted and made a TIFF image, followed by a slight specimen rotation and operation again. Consequently a series of TIFF images were generated for image reconstruction and analysis. Average scan time was about 100 minutes.

Table 3.2. Operation conditions of X-ray CT for CFRP observation

Parameters	Values
Source voltage	40 kV
Source Current	200 μ A
Number of rows	2096
Number of columns	4000
Image pixel size	0.95 μ m
Object to source	28.46 mm
Camera to source	345.215 mm
Image format	TIFF (16 bit)
Exposure	589 ms
Rotation step	0.4 deg
Frame averaging	15 frames
Random movement correction	30 frames

Image analysis was performed in following steps.

- 1) The reconstruction of images : The image reconstruction, which is making cross-sectional images from raw data, was performed through the package program Nrecon (Bruker, Belgium). The reconstruction range (in frontal

section) was decided. In this analysis the range was usually about 2000 pixels in fiber length direction, i.e., 2 mm length in real. Specific options to image correction were carried out in same program. The specimen usually could be moved slightly during operation. So the alignment of images was essential (the post-alignment operation was different to each specimen). Following that, the image was rotated properly making the cross-sectional image horizontal, and the conversion range of image was set (in all cases 0.02~0.3).

- 2) Region of interest : Reconstructed images were loaded to another package program CTAn (Bruker, Belgium). In the reconstructed range the multiple fracture of fiber was detected in cross-section. Ruling out the edge effect of small sized specimen the square shaped inner region of specimen was set as a region of interest, which means all of graphical and statistical analysis were conducted in the region.
- 3) Binary image : The reconstructed images have grayscale spectrum from 0 to 255. Usually as the material is harder and denser it is detected in low grayscale level, i.e., the fiber material is in low grayscale, matrix is medium, and the voids created by fiber fracture is in high grayscale level. The level was separated from the analysis program (CTAn) and binary images, showing the location of voids clearly and excluding others, was made.
- 4) Stereological decision : From the binary image the area of voids could be measured in CTAn program, in pixels unit. The fiber and matrix have a certain area in average considering the fiber volume fraction. In this analysis the resolution (i.e. the size of one pixel) is 1 micron, so a pixel space per one fiber or one unit cell of fiber (see Fig. 3.14) can be calculated using the

volume fraction information. For example in the case of 43 % volume fraction, the space that a fiber and surrounding matrix can maintain is 100 pixels.

The results are shown in Fig. 3.14. As shown in graphical results in Fig. 3.14, the cluster of fiber fracture and cracks are found in specimen. The multiple fracture was counted by stereological approach, counting the pixels. At the most of the cases the shape of multiple fracture was close to round shape. Only in some cases the shape was oval or jagged, which is analyzed that some close clusters are connected by the concentration of two or more clusters. In the cases the multiple fracture was much more than expectation. The quantitative data was shown in Fig. 3.15. The multiple fracture number was plotted according to the applied composite stress. In the same trend in literature review and expectation the multiple fracture increases when the applied stress increases. The increasing trend showed an dramatic rise after certain stress level. The result would be compared to the analysis results.

(a)





Fig. 3.14. Image process (a) initial image (b) binary image (c) image treatment for multiple fracture cluster by deleting small-size particle

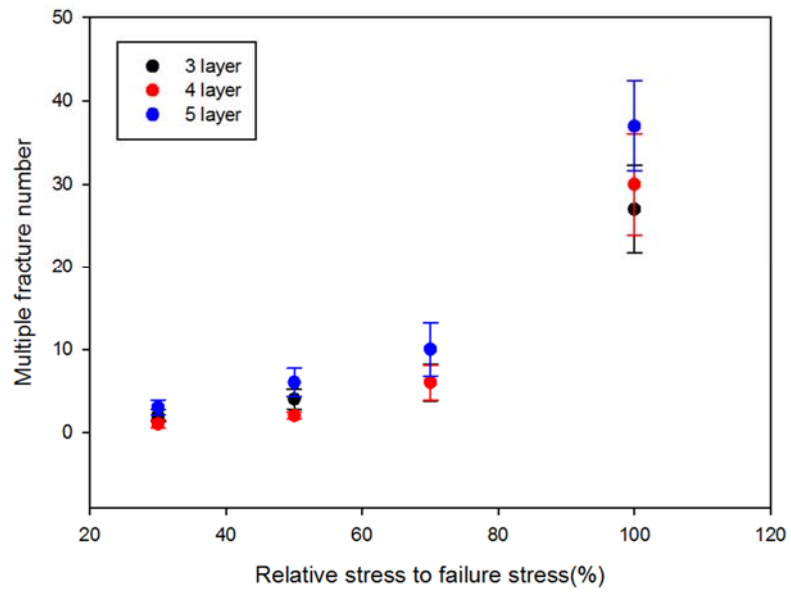


Fig. 3.15. Quantitative data of multiple fracture observation

3.2. Analysis of tensile strength and toughness

3.2.1 Stress concentration analysis

The volume fraction was calculated using the R/C contents provided by supplier. The analysis model was generated with the inter-fiber distance of $8.98\text{ }\mu\text{m}$. The hexagonal fiber array with given inter-fiber distance was arranged in a unit cell up to third layer. The length of analysis model was set as $200\text{ }\mu\text{m}$, considering the limitation of computational virtual memory and the debonded length in this situation at the 37 MPa of IFSS. Cohesive element was inserted around the broken fiber and periodic boundary condition was applied to whole unit cell. The unit cell was deformed in fiber direction as $2\text{ }\mu\text{m}$, the 1% deformation. The analyzed model and stress concentration factor is shown in Fig. 3.16. As discussed in chapter 2.1 the effect of volume fraction is not critical than that of IFSS however the difference could be seen, showing 6.2% stress addition in maximum.

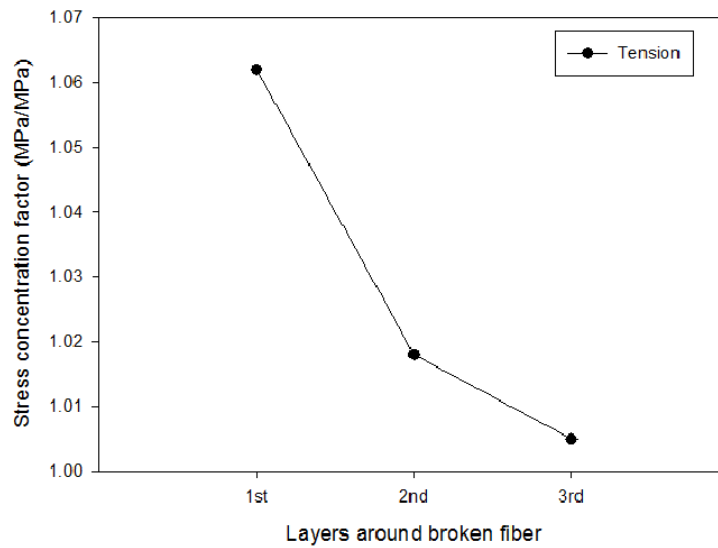
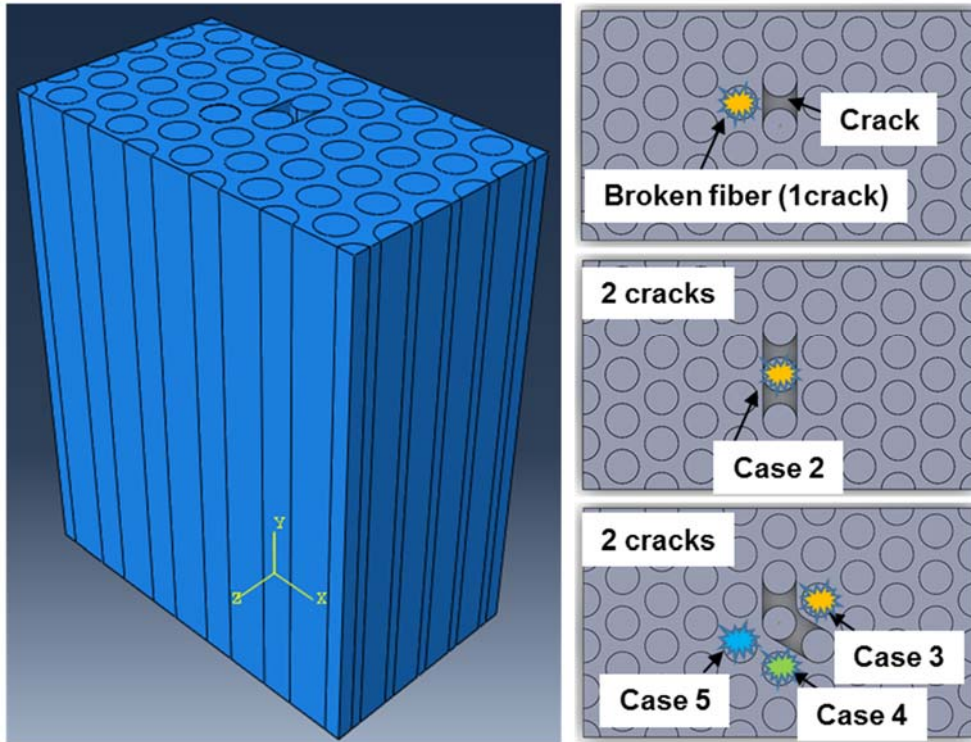


Fig. 3.16. Stress concentration factor of tensile case

Same SCF analysis was done for bending situation. In the bending situation the tension and compression is combined in a materials, however the failure is determined by the tensile failure of outer surface. In addition to that the most critical difference between the tensile and bending situation is the presence of delamination in transverse direction. The delamination consumes the energy itself and make more severe the stress transfer to neighboring fibers in the case of right before the crack. So the bending stress can be interpreted as a special case of tensile, which possess a long crack in model. A model having a continuous long crack around the broken fiber was made and the same analysis of tension was done. The results of analysis is shown in Fig. 3.17. In the Fig. 3.17 (a) the analyzed model and crack type was represented, from case 1 to 5. In each case the marked fiber was broken fiber and the stress concentration factor was measured. The main purpose of this case study is to understand the effect of the crack state related to the broken fiber. And the result shows, the position of crack enhances the stress concentration factor however the presence near the broken fiber is only important and the effect of crack shape is not important (see Fig. 3.17 (b)). So the stress concentration factor can be simplified in the situation of simple crack, the case 1, and the SCF result is shown in the Fig. 3. 17 (c). Due to the effect of matrix cracking the load transfer via matrix was distorted and the stress concentration made higher in the neighboring fibers.

(a)



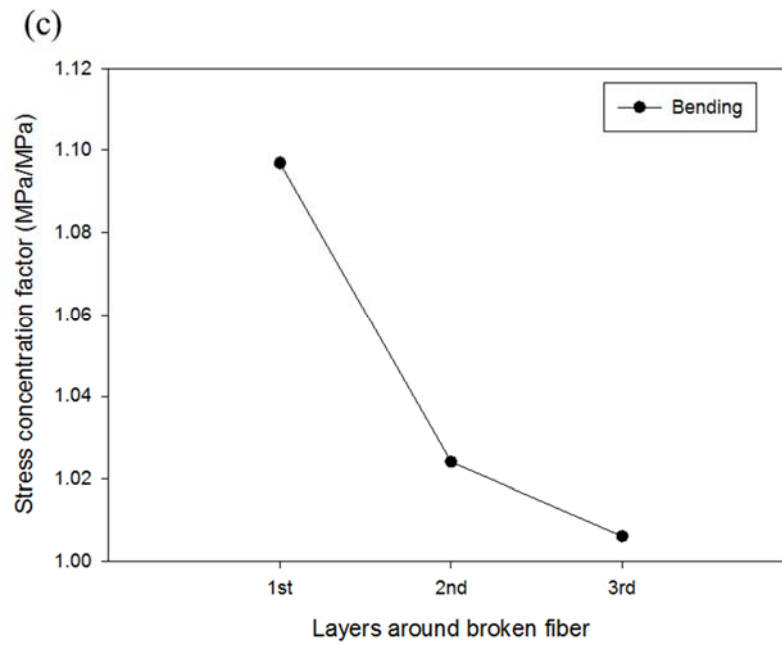
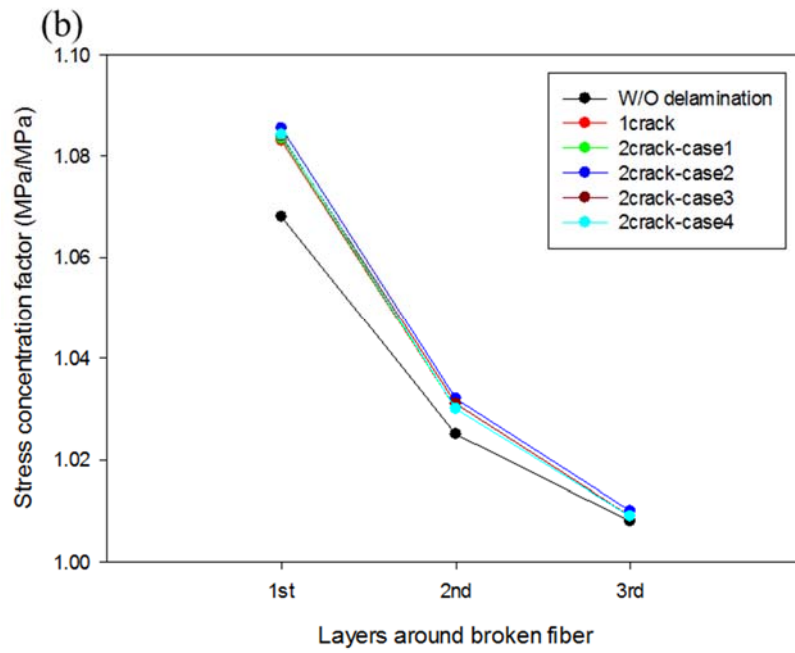
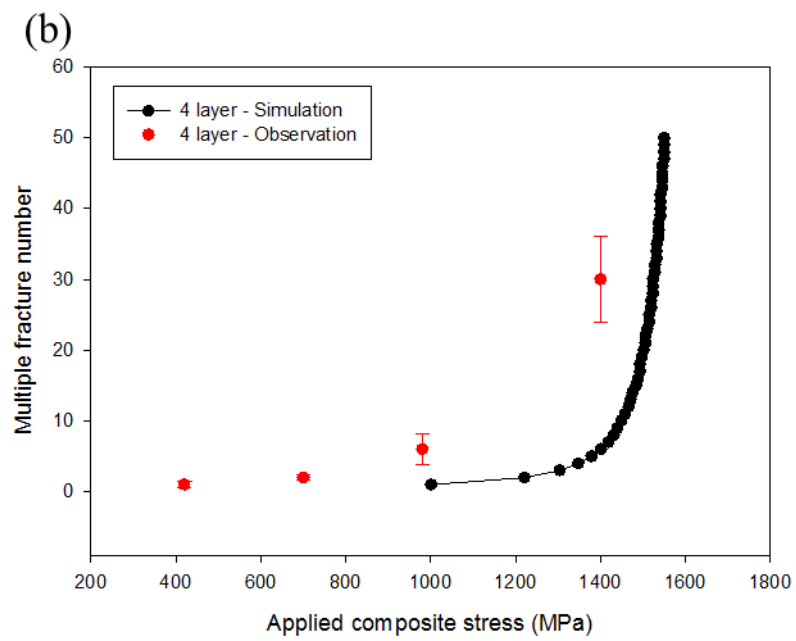
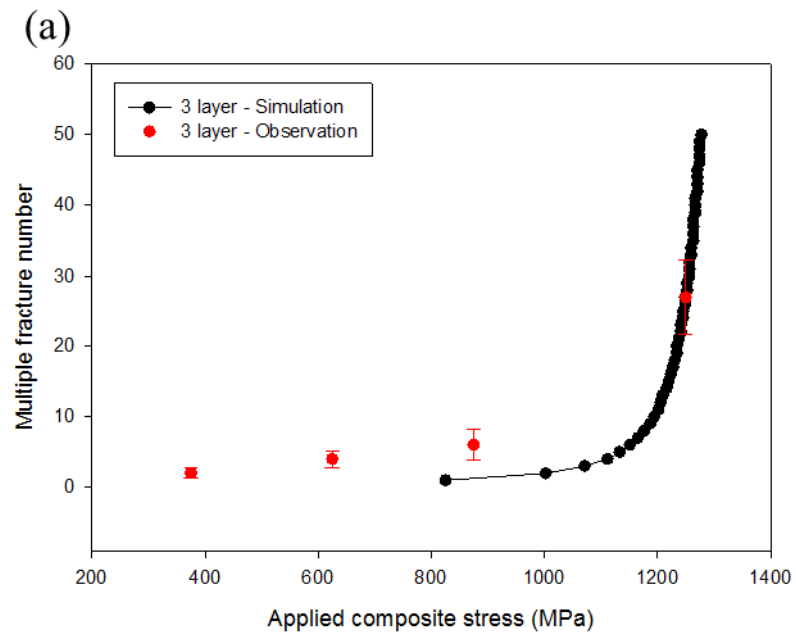


Fig. 3.17. Stress concentration factor of bending case (a) analysis model of bending analysis, including crack (b) stress concentration factors of cracked model (c) stress

concentration factor of bending case

3.2.2 *Strength prediction based on statistical model*

The statistical model was implemented via MATLAB program. The probability of multiple fracture and expected value of multiple fracture were calculated. The predictions of the statistical model was compared with experimental data. First the multiple fracture number observation via X-ray CT was compared to the simulations in the same stress level. The quantitative data was shown in Fig. 3.18. The data shows the increasing trend according to the stress level, and the increasing trend is close to exponential. The multiple fracture in certain stress level was calculated by the SCF, so the multiple fracture of 5 layered composite was highest due to high SCF. The experimental results was co-plotted and the data was in error range with the simulation. The most interesting difference is in the low stress level such as 30 % stress level and 50 % stress level, which is much higher than the simulation. It is seen that in the simulation the ideal case was assumed but the local statistical randomness including the twist of fiber or existing void affect the initial state fiber breaks. Consequently the multiple fracture of experiments are higher than that of simulation, but within the reasonable range. The progressive weakening also affects the difference.



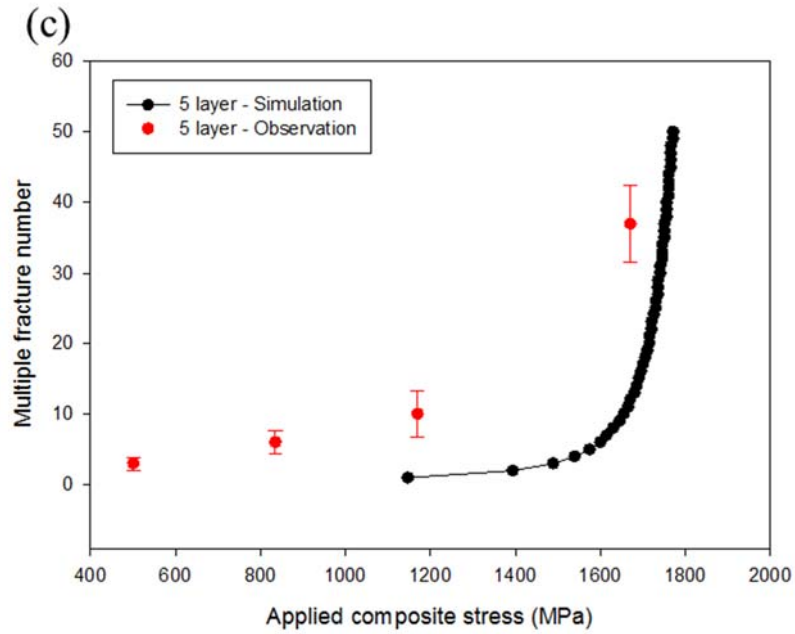


Fig. 3.18. The multiple fracture stress according to the stress level (a) 3 layer (b) 4 layer (c) 5 layer

The tensile strength was determined using analytic solution as shown in Fig. 3.19. In Fig. 3.19, the analytic solution and multiple fracture stress according to the multiple fracture are plotted. The multiple fractures are presented in straight lines and analytic composite strength are presented in dashed lines. Same as expectation and validations in chapter 2, the analytic solution decreases and multiple fracture stress increases (the multiple fracture stress increase was already shown in Fig. 3.19.). The cross point, that is the critical multiple fracture number was determined and following stress level was determined as composite strength. And the predicted result was 1564 MPa, which is higher than the experiments but in the reasonable agreement

showing only 3.8 % difference. In addition to that the critical multiple fracture number was 21, within the range of observation.

In the same manner with different SCF the flexural strength was determined (Fig. 3.20). As explained, the SCF only varied so the trend should be same. But due to the effect of higher SCF the composite strength decreased much more in the same condition and it is the same result in experiment. In the tensile and flexural condition the simulation results shows somewhat higher value than the experiment and the reason is due to the initial evolution of multiple fracture and following larger multiple fracture number somewhat. In the analytic solution and FEM analysis the ideal state is assumed so the local randomness is not reflected, only making some increase in results. The predicted result was 1476 MPa, which is higher than the experiments but in the reasonable agreement showing 7.1 % difference. The critical multiple fracture number was 45, which is higher than that of tensile case.

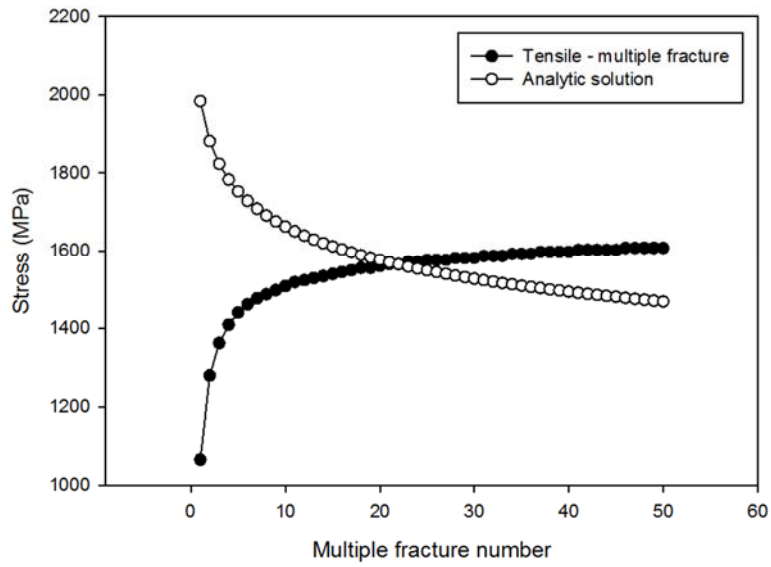


Fig. 3.19. The tensile strength determination

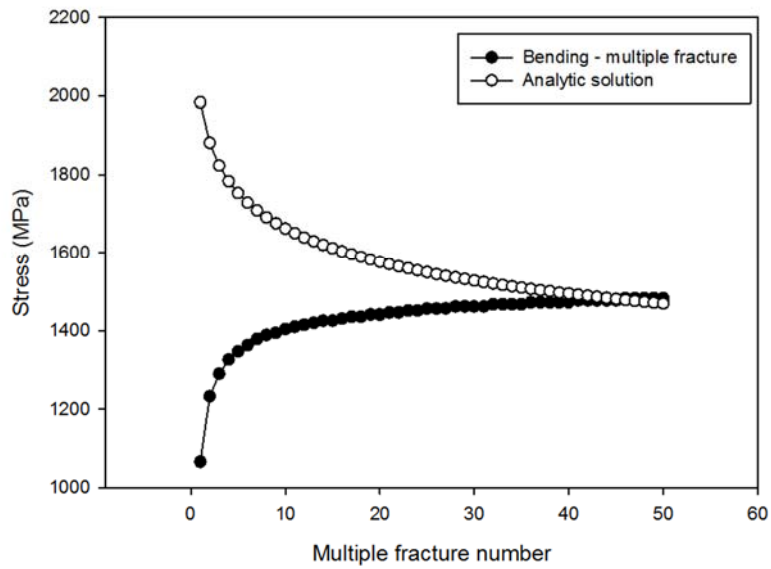


Fig. 3.20. The flexural strength determination

3.2.3 *Optimum interfacial shear strength of composite*

When the IFSS increase, the trend of curve movement is identified. From the result the higher multiple fracture number according to the volume fraction seems to be inevitable, however the upward movement is relatively smaller, so the monotonic increase of composite strength is not clear. If this model can verify the optimum IFSS that is experimentally shown in some previous researches [28, 30, 56, 77] it would be further value of this model. From the tensile results, the design of IFSS for optimum tensile and flexural strength was done. From 10 MPa to 100 MPa the IFSS was varied and following SCF data were calculated. The results are shown in Fig. 3.21. When the IFSS rise to 100 MPa, the critical multiple fracture number is predicted over 50 fiber cluster, which is very high. And the initially found interesting result is, the strength forms an optimum around the 70 MPa of IFSS, same in both or tensile and flexural strength condition. .

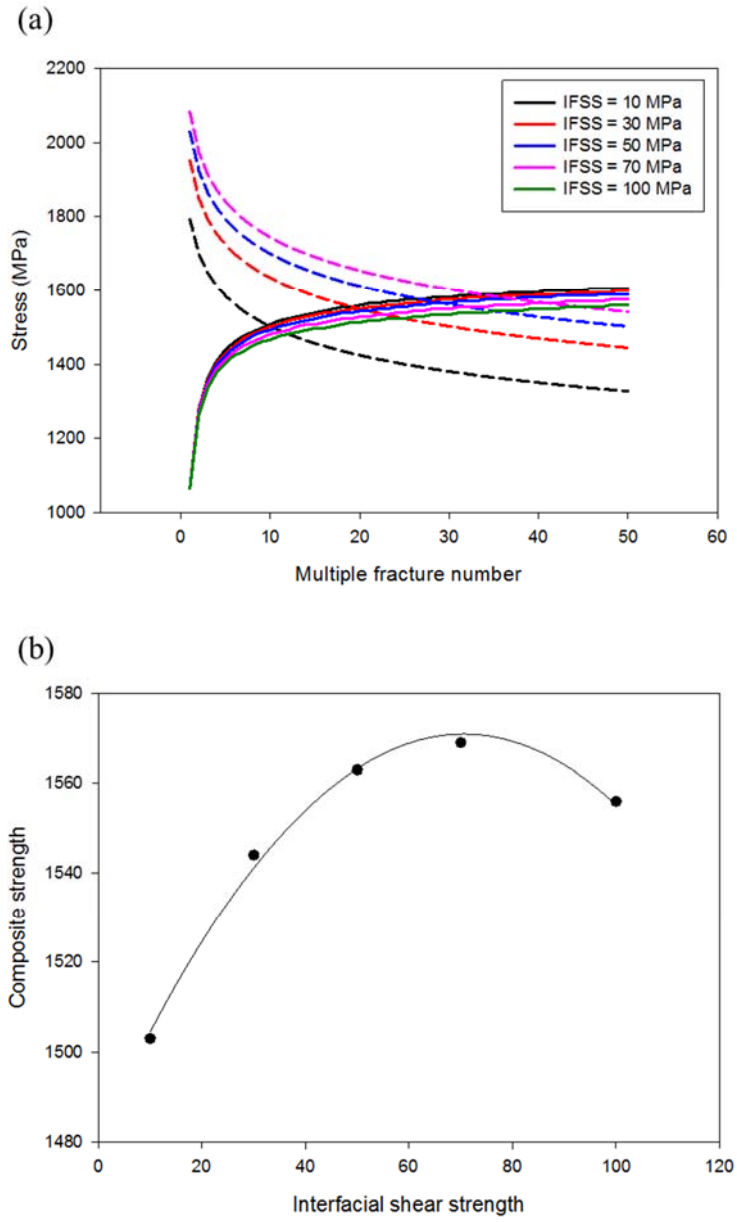


Fig. 3.21. The composite strength determination in various IFSS condition (a) tensile strength (b) The tensile strength according to the IFSS, showing the optimum in relatively high IFSS

3.2.4 Toughness prediction

The critical multiple fracture number in each tensile case was investigated first, and the value was 21 in tensile case. The toughness of debonding and pull-out was calculated in each multiple fracture number. For the multiple fracture situation the equation of fracture toughness was modified considering the multiple fracture. First the relationship of fracture toughness is

$$g_{total} = g_{deb} + g_{po} = \frac{W_{deb}}{m \times A / v_f} + \frac{W_{po}}{m \times A / v_f} = \frac{C \cdot g_{SL} \cdot l_{deb}}{m \times A / v_f} + \frac{C \cdot \tau_b \cdot l_{po}^2}{m \times A / v_f} \quad (31)$$

where k is the multiple fracture number and A is the area of multiple fracture cluster which is used to calculate the volume fraction (the product of area of fiber and multiple fracture number). And C is the perimeter of broken fiber group, considering the group as a unit. In this thesis however, the multiple fracture occurs cumulatively so the debonding and pull-out should be treated in each fiber. So the surface area of debonded region is calculated and adopted. Finally the equation is modified to

$$\begin{aligned} g_{total} &= \frac{(2R_f \pi) \cdot m \cdot g_{SL} \cdot l_{deb}}{m \times A / v_f} + \frac{(2R_f \pi) \cdot m \cdot \tau_b \cdot l_{po}^2}{m \times A / v_f} \\ &= \frac{(2R_f \pi) \cdot g_{SL} \cdot l_{deb}}{A / v_f} + \frac{(2R_f \pi) \cdot \tau_b \cdot l_{po}^2}{A / v_f} \end{aligned} \quad (32)$$

When the multiple fracture number increases, other factors are fixed however the region of interest, i.e. the area A , only increases so the toughness decreases. The toughness calculated is shown in Fig. 3.22, and the following experimental data is

co-plotted with the corresponding critical multiple fracture number. The results show good agreement in the error range. In a number, 21.73 kJ/m² of work of fracture was predicted.

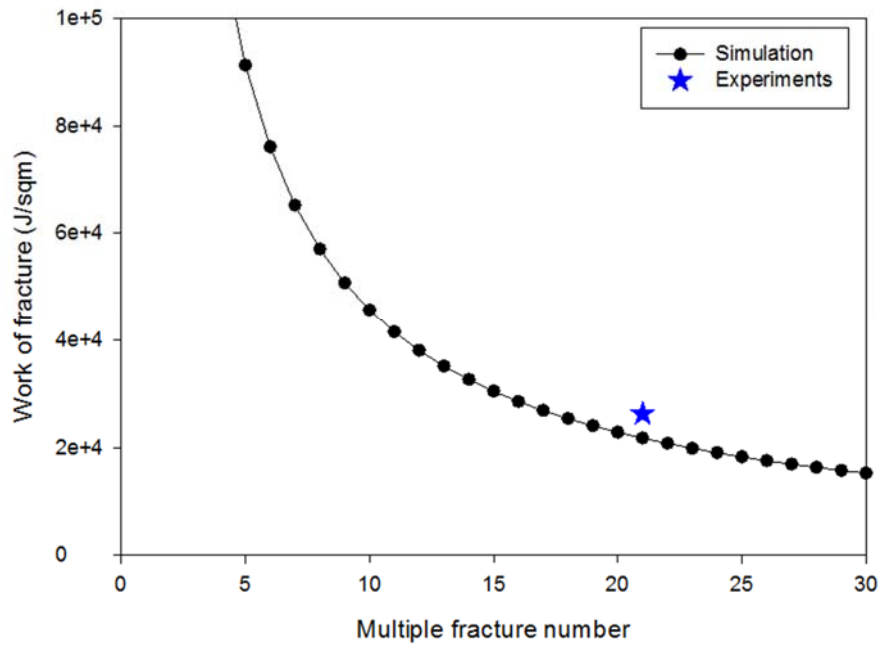


Fig. 3.22. The fracture toughness of composite according to the multiple fracture number and comparison

Finally we can discuss shortly the relationship between the strength and toughness. If it can be controlled, the single multiple fracture of composite, in other word the isolation of each fiber breakage is ideal for both of strength and toughness. On the other hand, in real composite if the same composite system is same (same materials and volume fraction), as the IFSS increases the strength increases under critical level but the toughness definitely decreases according to the IFSS. It means the important

conclusion: in unidirectional composite system, the simultaneous achievement of high strength and toughness is impossible by controlling the IFSS only. It is called ‘strength-toughness dilemma’ in this thesis. More structural consideration should be demanded and it would be discussed next.

3.3. Summary

A UD composite system, that is the carbon fiber reinforced polymer (CFRP) with epoxy resin, was analyzed in the view of fracture using the statistical model. For the validation of analysis UD composite was fabricated using UD prepreg laminate and cut and grinded for experiment. UD composites were prepared and tensile, bending, and fracture test were carried out to each specimen. The results showed good consistency and some basic properties were utilized to analysis. Separately some specimens in some stress level, 30, 50 and 70 % of failure stress, were prepared and observed via X-ray CT operation. The multiple fracture occurrence was observed especially.

The strength prediction approach suggested in chapter 2 was applied to the aforementioned UD CFRP. The stress concentration analysis was done to each volume fraction up to 60 % and SCF values were calculated. Especially for bending situation the delaminated circumstance was considered using a crack, identifying the uprising SCF value. The multiple fracture stresses were calculated from MATLAB program. First the multiple fracture stress was compared to the multiple fracture observations and the results showed reasonable agreement, only a little higher multiple fracture in experimental case. On the other hand, the comparison of the tensile and flexural strength showed the lower strength values in experiments. The main reason of this difference is the randomness of composite inducing the complex fracture in early stage of deformation.

4. Application to hierarchical fiber bundle composites (HFBCs) model

In the chapter 3, the validity of strength prediction approach was identified through carbon fiber/epoxy composite. The main purpose of chapter 3 was prediction method itself, however in this section one optimization issue was considered and studied. The most important factor for the failure of composite was stress concentration factor, which is right the result of IFSS. The change of IFSS of other factor was not reflected directly in statistical model, only the stress concentration factor can affect that. So the control of stress concentration factor in the same IFSS is possible, it can enhance the strength or toughness of composite significantly to the applications. Through this consideration, a breakthrough for the strength-toughness dilemma can be suggested.

4.1. Overview of HFBCs model

The brittle behavior of conventional unidirectional CFRP under tensile load in the fiber direction is widely reported in the literature and industrial data. The brittle composite materials are enough to tensile strength, however, in the view of applications such as automotive body higher toughness is demanded even though the tensile strength are degraded to a reasonable level. It is related to the strength-toughness dilemma in chapter 3. Looking at the fracture mechanism again, the single fiber fracture is uncontrollable because it is the fiber property. We can control SCF by controlling the IFSS, volume fraction and material property. If the material system is same the IFSS and material properties are given and only the volume fraction varies, affecting the SCF. In previous studies, the experiments and modeling show

that broken fibers make the cluster of about 8~30 fibers [14, 76], inducing such stress concentrations in neighboring fibers. And in the prior chapter the trend of multiple fracture cluster was shown to about 10~40 clusters matching to the previous studies. This tendency would be fixed if the materials system is fixed and the hexagonal packing system is assumed, however we can consider the fracture of local cluster and isolation of that depending on the non-homogeneous internal structure.

The hierarchical fiber bundle composites (HFBCs) are one promising structure which have been inspired by bio-materials. Hierarchy in a material system is reflected by some features. First hierarchy lies in the form of multiscale, so the system consists of structures in some level. Furthermore this multiscale often generates multiple phases, making a unique structure in each gradual level. The aim of hierarchical structure, making even complex the internal structure is to achieve the outstanding properties comparing to the base materials. Usually the significant scaling-effect is controlled by local fibrous structure [78-80], high elastic modulus of local reinforcement [81], and interfacial effect [82, 83]. The good examples of this bio-inspired materials are tissue, bone, wood, and bird beak. In Fig. 4.1, the representative structure of this hierarchical structure, a structure of bone is shown.

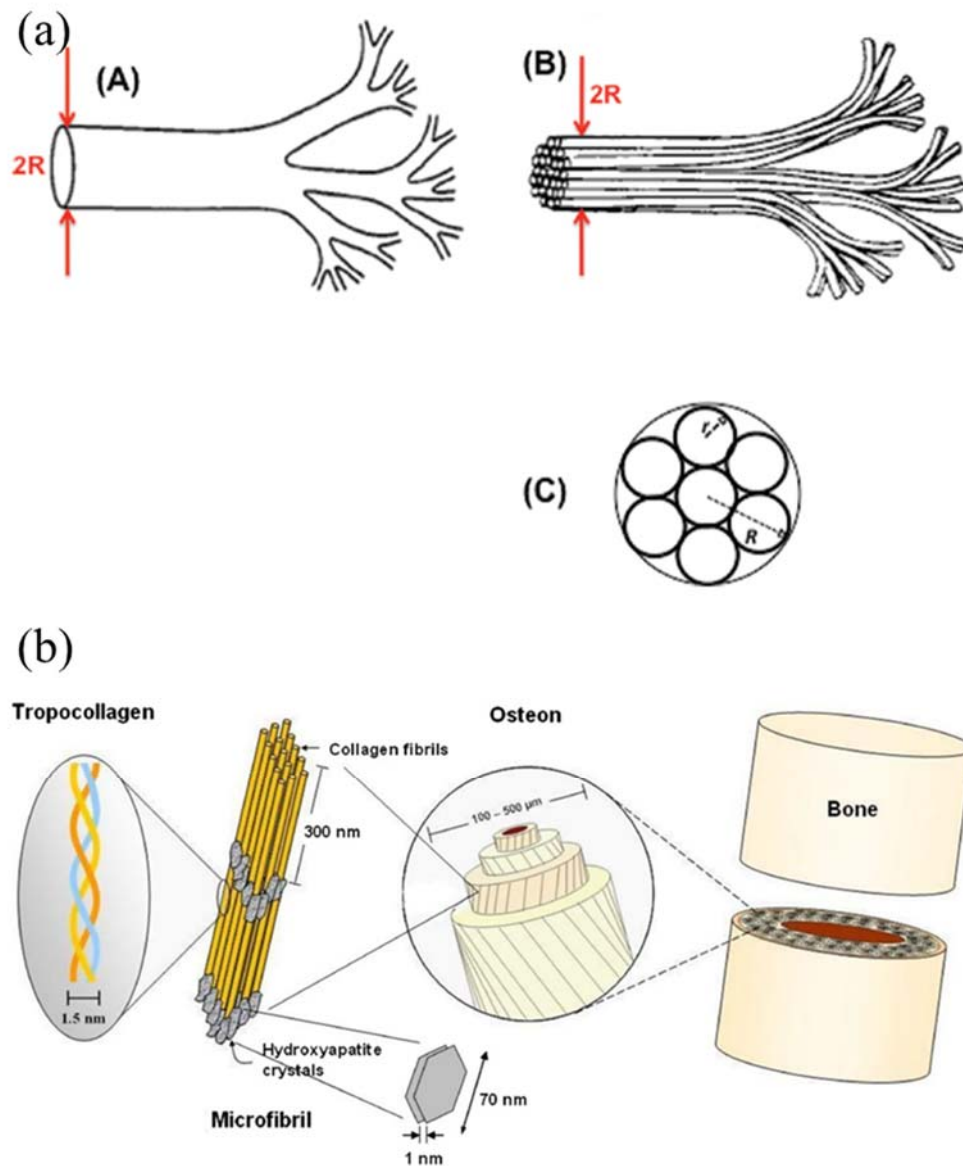
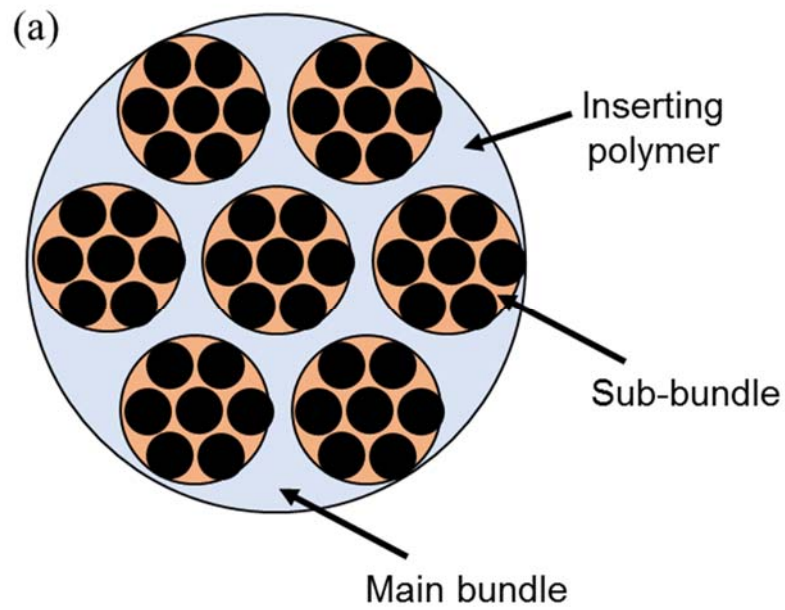


Fig. 4.1. The example of hierarchical structures (a) Mammalian circulatory and respiratory system from [84] (b) Bone structure from [85]

In this study the term hierarchy means that the fibers are arranged according to

relative level of size (or inclusiveness). Inspired by bio-materials, the isolation of local fiber bundle structure from whole composite structure is needed, and it can be achieved by inserting an interface or a polymer material between the bundle (see Fig. 4.2). In this chapter, the same material with matrix was assumed. In addition to that the volume fraction and IFSS should be maintained according to the system.



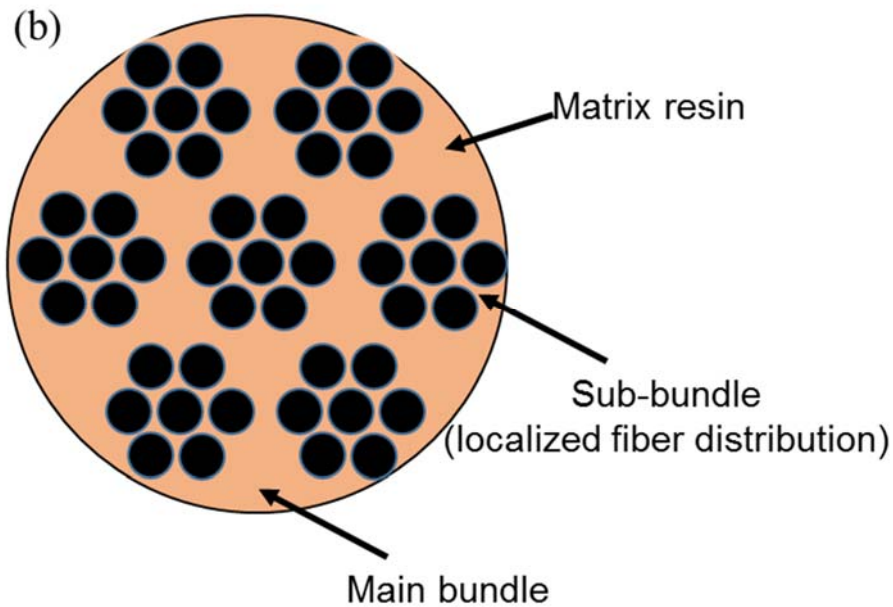


Fig. 4.2. Hierarchical structure in unidirectional composites (a) with inserting polymer (b) without inserting polymer

Through hierarchical structure, this chapter intends to understand whether it is possible to enhance a fracture toughness under tensile failure process in a UD composite, inducing less stress concentration and more gradual tensile failure in the same time. By building the sub-bundle microstructure and making a UD composite maintaining the same volume fraction, clusters of broken fibres are isolated from one another to reduce stress concentrations in the material. So the research objectives are set as following: (i) to understand the failure mechanism and the stress concentration of hierarchical structure, (ii) to understand the reason why the HFBCs structure can reduce the stress concentration, (iii) to try to overcome the strength-toughness dilemma in specific application. For the analysis, some assumption for the HFBC

model were added and finite element method which is same to chapter 2 was used to predict the stress distributions in the neighboring fiber bundle.

4.2. Simulation procedures

Schematic diagram of HFBC was shown in Fig. 4.2. The basic structure of composite is same with UD composites and the major difference is the bundle consists of another bundle of fiber. So the inter-fiber distance and inter-bundle distance is different, the latter is significantly larger than the former. In the system the following assumption is applied.

- 1) Composite geometry: A bundle is treated as an unit, so a bundle is replaced to a cylindrical fiber-like structure in analysis. Based on this assumption we can make a continuum model representing a fiber bundle. Although a situation that each fiber is represented in unit cell is the most realistic case, but it is too cost-consuming process. In addition to that, the geometry and property of bundle are able to be calculated from the basic material. First the perimeter of bundle is calculated by the following Equation (32), considering the number of fibers in bundle. In this thesis it is assumed that each bundle contains 100 fibers. In the Equation (32) and (33) C means the perimeter, m is multiple fracture number, d is fiber diameter, v_f is fiber volume fraction.

$$C = 3 \left(\sqrt[3]{m} - 1 \right) \cdot s + \left(3 \cdot \sqrt[3]{m} - 1 \right) \frac{\pi d}{2} \quad (33)$$

$$s = \left(\sqrt{\frac{\pi}{2\sqrt{3} \times v_f}} - 1 \right) d \quad (34)$$

2) Fiber bundle property : The modulus and strength of bundle are calculated from the aforementioned prediction approach in chapter 2, using the parameter of fiber property, matrix property, IFSS, and volume fraction of local fiber bundle. In this thesis the parameters of chapter 3 was taken. Following previous studies and the empirical standard, the volume fraction of local bundle is assume as 60 % and same analysis through stress concentration analysis, statistical multiple fracture should be processed. The material property and geometric parameter of fiber bundle were shown in Table 4.1.

Table 4.1. Parameters of HFBCs analysis

Parameters	Values
Fibers per bundle	100 fibers
Bundle diameter	285 μm
Volume fraction in bundle	60 %
Volume fraction in composite	30 %
Inter-fiber distance	1.56 μm
Inter-bundle distance	100 μm
Young's modulus of bundle	102 GPa
Strength of bundle	1907 MPa (from prediction)
Interfacial shear strength	30 MPa

The greatest characteristics of this model is, relatively larger elements are arranged in unit cell, even though it have the right similarity with the fiber composite model in chapter 3. The shape of bundle is assumed as circle considering the typical fabrication process of bundle and yarn composite. The diameter was calculated via Equation (32), dividing by circular constant. But we can expect that there exist significant difference in stress concentration between two models due to the larger inter-bundle distance, and the reduced modulus and strength via the assumption 2). To separate the effect of large-scale unit cell and reduced property, the comparison should be operated. In the prediction process larger unit cell was generated (see Fig. 4.3) and stress concentration factor was analyzed first in the same manner. The statistical model was implemented using the property of HFBCs, only the Weibull property was re-calculated. It is quite hard assumption because the Weibull property of single fiber and bundle is clearly different. Generally the evaluation of Weibull property of fiber bundles is impossible due to high twist and resulting friction between the fibers. In this thesis the Weibull modulus (in this thesis, β) was adopted in same, and the characteristic stress value (in this thesis, γ) was used as the bundle strength.

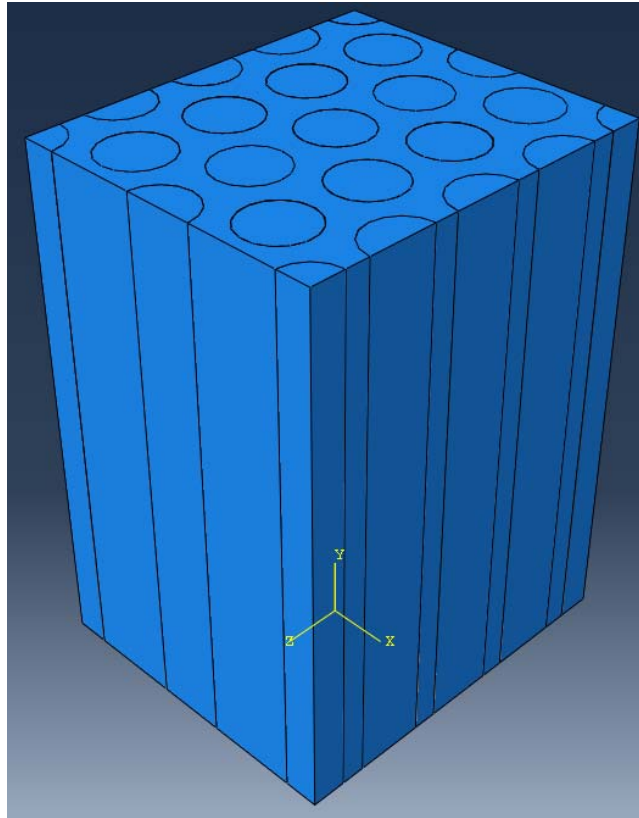


Fig. 4.3. A generated geometry for analysis of HFBCs

4.3. Results and discussion

The SCF is calculated and compared to the some other cases. First the previous model in chapter 2 and 3 (the fiber diameter is $7\text{ }\mu\text{m}$) is analyzed in the same total volume fraction 30 % (it is used as a reference). In this homogeneous UD composite the parametric values in chapter 3 were input for comparison (actually the results are already shown in chapter 3). The generated hierarchical model was also analyzed. And for comparison of mesh size effect one additional models were tried, the combination of homogeneous model of 50 % volume fraction and degraded property.

Note that the generated geometry is much larger but the volume fraction of the composite made by the bundle is much higher, up to 50 %. The results are presented in Fig. 4.4. Much smaller SCF is taken from the hierarchical model in three cases. Interestingly the SCF of hierarchical model is even smaller than the same analysis result of homogeneous model and 50 % volume fraction model. Ideally it can be seen that the stress concentration effect is same due to the relation of similarity, but a little difference are observed. It is thought even the geometry got enlarged maintaining the relative ratio the debonded length is right same due to the same IFSS so that the overload length and ineffective length was same in two model. That affect induce the rapid stress recovery and less stress transfer.

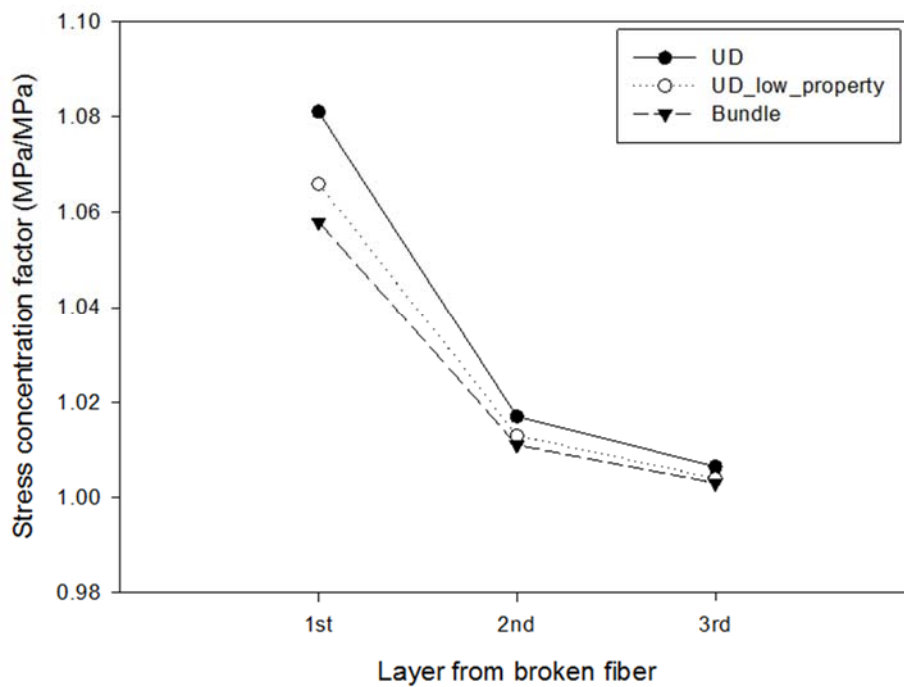


Fig. 4.4. SCF of HFBCs and comparison to homogeneous composite

The composite strength and fracture toughness of HFBCs was also determined via same statistical model in chapter 2 and 3. The prediction results are shown in Fig. 4.5. The results can be compared with the analysis result of 30 % volume fraction of CFRP. The results show a clear difference in two models. First the critical multiple fracture number of HFBCs are much lower than that of homogeneous UD composite. Only two fibers (actually bundles) are broken until the composite failure. Note that it means actually over 200 fibers are broken in the bundle model. The result of excessive multiple fracture makes the meaningful degradation of composite tensile strength to the level of 700 MPa, which is much lower than the rule of mixture. In fact the effect of multiple fracture and degradation of properties are already reflected in decreased fiber property in chapter 4.2. The value of this hierarchical model, however, is the highly enhanced fracture toughness. The fracture toughness of hierarchical model reaches about two times of the fracture toughness of homogeneous UD composite. The isolation of the multiple fracture between bundles are effectively operated in here. And it means also, if the whole fiber bundle consists of 100 fibers in certain level, the hierarchical structure can sustain the whole composite structure by thick buffer layers of polymer. Note that the split and debonding inside the bundles are not considered in this model, so if we can consider the properties of each bundle and reflect them even the expected toughness can be a larger value. The relative property, i.e. the product of toughness and strength is much larger in the hierarchical structure.

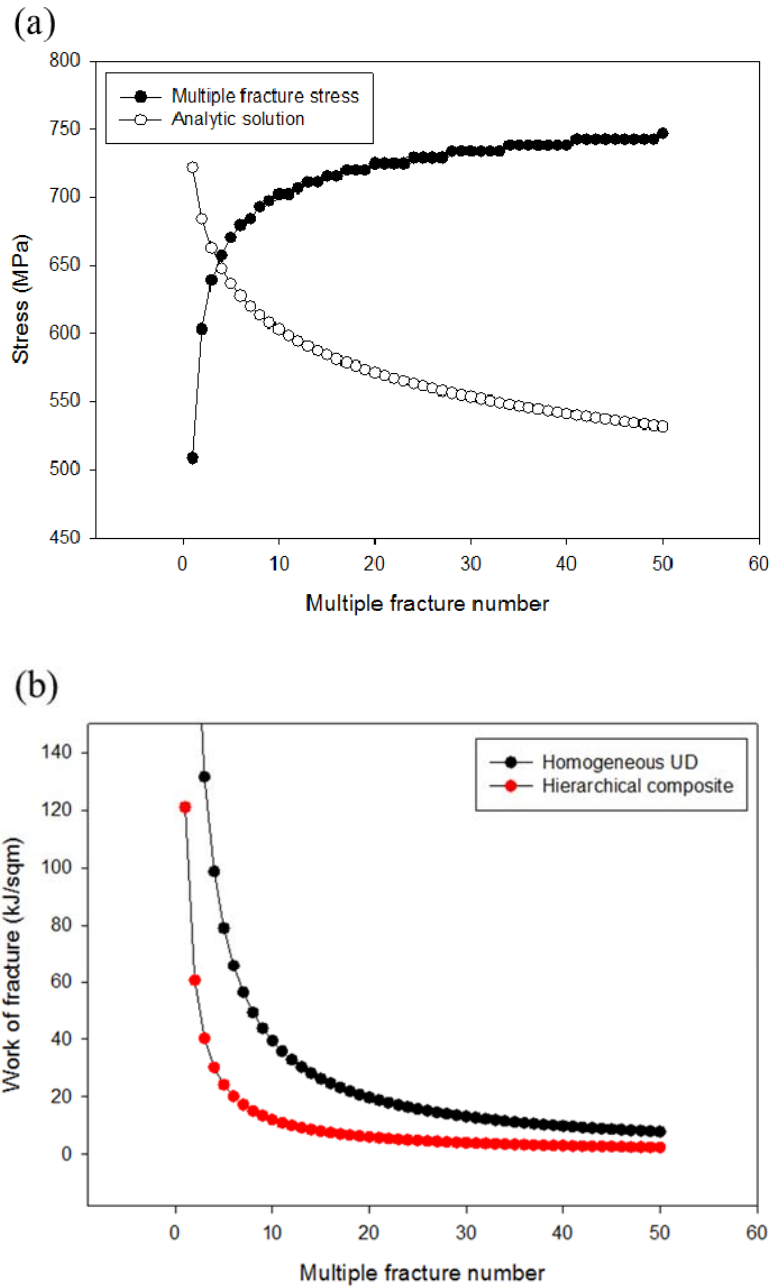


Fig. 4.5. Composite properties of HFBCs (a) composite strength determination (b) fracture toughness prediction

This HFBCs structure shows a possibility for the conquest of strength-toughness dilemma, making high toughness in relatively less degraded strength. Strictly speaking, further validation with the manufactured HFBCs is demanded to this and it is hard to control the local structure possessing maldistribution. In some researches the trial of making hierarchical structure inducing hierarchical fracture using some structural pre-crack and other methods [2]. And the researches shows much higher toughness than the expected CFRP shown in Table 4.2. Especially the toughness is treated importantly in industrial fields when it considers the safety of product. The most proper example is the automotive part. In the automotive part, the impact and fracture is the catastrophic situation that the supplier always should take account. Leaving some special example out of the discussion such as a high-class car or racing machine, the high strength steel which is applied to the automotive demands still fracture toughness (see Table 4.2 [3, 10]). Unfortunately the fracture toughness of CFRP currently used is less than that to a level of half. If we can control the toughness in extreme and satisfy the demanded strength, the applications would be promoted and this model would be utilized to that [86].

Table 4.2. Fracture energy of various materials

Material	Fracture energy (kJ/m ²)	Fracture toughness (MPa m ^{1/2})
<i>Polymer</i>		
Epoxy resin	0.1-0.3	0.3-0.5
Nylon 6.6	2-4	3
Polypropylene	8	3
<i>Metals</i>		
Pure Al	100-1000	100-350
Al alloy	8-30	23-45
Mild steel	100	140
High strength steel	50-125	100-200
<i>Ceramics</i>		
Soda glass	0.01	0.7
SiC	0.05	3
<i>Composites</i>		
GFRP	40-100	42-60
Al based MMC	2-10	15-30
SiC laminate	5-8	45-55
CFRP	25-60	70-110

4.4. Summary

In this chapter an application was considered, which explore the possibility for the overcome of strength-toughness dilemma. As a result a hierarchical fiber bundle composites (HFBCs), which have a localized dense fiber bundle and isolating thick zone, is suggested in this chapter. A hierarchical structure was simplified to UD composite following assumptions controlling the geometry and properties. Stress concentration analysis and strength prediction via statistical model were carried out in the same manner with the chapter 2 and 3. The analysis results shows that, the composite strength degraded somewhat, but the toughness was enhanced largely, more than compensating the strength degradation. This possibility would be applied to optimum structural design, with target fracture properties.

5. Concluding remarks

A prediction method for the strength and toughness of unidirectional fiber-reinforced composite was developed in this thesis. The important point of this approach was the linkage of IFSS between load transfer and multiple fracture phenomenon, considering the IFSS. Differently from previous researches, the multiple fracture stress was calculated from the statistical model which was implemented by MATLAB code and the determination of composite strength was completely determined by the multiple fracture stress and analytic solution considering the multiple fracture number. Other important configurations was the stress analysis via finite element method, evaluating the stress concentration factor. The accuracy of stress concentration analysis, up to 8~10 % of addition of stress in this material system, was definitely the key point.

Significance of this model is that it satisfied some requirement that unidirectional fiber composites have to solve. First, suggested model can predict the tensile strength and toughness in the same time, so it can be applied to the design of composite for specific application. Second, suggested model can predict the strength and toughness without additional fracture criterion based on the propagated crack size. The strength is determined completely by the information of constituents and interface and based on the strength (exactly the multiple fracture number at composite failure) the toughness is also determined. The stress concentration factor and multiple fracture number are the only thing to consider. These things were validated through experiments using CFRP and the results showed the consistency of experimental and modeling results.

A prediction of composite strength and toughness for hierarchical fiber bundle composites was also developed according to the assumption estimating the property of fiber bundles. The modeling results showed that the toughness could be enhanced drastically with less degradation of composite strength by hierarchical structure making the inter-bundle distance larger. The modeling of hierarchical fiber bundle composite itself also has meaning in composite mechanics field. In previous studies the composites have homogeneous structure and the failure is only the progressive and unpredictable thing. However based on some previous studies trying to predict the strength and toughness in bundle fracture and pull-out, this study also can contribute to the design of hierarchical composite.

Consequently, these analysis showed the advantages of this model. Because the model was developed for unidirectional composite and tensile situation, it can be adopted into not only various loading situation such as compression and cyclic loading, but also various structured composite such as laminated and woven composite. These also showed in some applications. Whether it is UD or hierarchical, the strength and toughness prediction considering the relative dilemma can be used in various applications.

References

1. Kim, J.-K. and Y.-w. Mai, *High strength, high fracture toughness fibre composites with interface control—A review*. Composites Science and Technology, 1991. **41**(4): p. 333-378.
2. Pimenta, S. and S.T. Pinho, *An analytical model for the translaminar fracture toughness of fibre composites with stochastic quasi-fractal fracture surfaces*. Journal of the Mechanics and Physics of Solids, 2014. **66**: p. 78-102.
3. Laffan, M.J., et al., *Translaminar fracture toughness testing of composites: A review*. Polymer Testing, 2012. **31**(3): p. 481-489.
4. Arai, M., et al., *Mode I and mode II interlaminar fracture toughness of CFRP laminates toughened by carbon nanofiber interlayer*. Composites Science and Technology, 2008. **68**(2): p. 516-525.
5. Pinho, S.T., P. Robinson, and L. Iannucci, *Fracture toughness of the tensile and compressive fibre failure modes in laminated composites*. Composites Science and Technology, 2006. **66**(13): p. 2069-2079.
6. Zweben, C. and B.W. Rosen, *A statistical theory of material strength with application to composite materials*. Journal of the Mechanics and Physics of Solids, 1970. **18**(3): p. 189-206.
7. Zweben, C., *Tensile failure of fiber composites*. AIAA Journal, 1968. **6**(12): p. 2325-2331.
8. Rosen, B.W., *Tensile failure of fibrous composites*. AIAA Journal, 1964. **2**(11): p. 1985-1991.
9. Cox, H.L., *The elasticity and strength of paper and other fibrous materials*. British Journal of Applied Physics, 1952. **3**(3): p. 72-79.
10. Hull, D. and T.W. Clyne., *An Introduction to Composite Materials*. 1996: Cambridge University Press.
11. Hedgepeth, J.M. and P. Van Dyke, *Local Stress Concentrations in Imperfect Filamentary Composite Materials*. Journal of Composite Materials, 1967. **1**(3): p. 294-309.
12. Beyerlein, I.J. and S.L. Phoenix, *Stress concentrations around multiple fiber breaks in an elastic matrix with local yielding or debonding using quadratic influence superposition*. Journal of the Mechanics and Physics of Solids, 1996. **44**(12): p. 1997-2039.
13. Hironobu, N. and N. Nao-Aki, *Stress concentration of a strip with double edge notches under tension or in-plane bending*. Engineering Fracture Mechanics, 1986. **23**(6): p. 1051-1065.
14. Pimenta, S. and S.T. Pinho, *Hierarchical scaling law for the strength of composite fibre bundles*. Journal of the Mechanics and Physics of Solids, 2013. **61**(6): p. 1337-1356.
15. Suo, Z. and J.W. Hutchinson, *Interface crack between two elastic layers*. International Journal of Fracture, 1990. **43**(1): p. 1-18.

16. Budiansky, B., J.W. Hutchinson, and A.G. Evans, *Matrix fracture in fiber-reinforced ceramics*. Journal of the Mechanics and Physics of Solids, 1986. **34**(2): p. 167-189.
17. Hsu, C.-Y., et al., *A study of stress concentration effect around penetrations on curved shell and failure modes for deep-diving submersible vehicle*. Ocean Engineering, 2005. **32**(8–9): p. 1098-1121.
18. Nedele, M.R. and M.R. Wisnom, *Stress concentration factors around a broken fibre in a unidirectional carbon fibre-reinforced epoxy*. Composites, 1994. **25**(7): p. 549-557.
19. Swolfs, Y., et al., *Stress concentrations in an impregnated fibre bundle with random fibre packing*. Composites Science and Technology, 2013. **74**: p. 113-120.
20. Bisanda, E.T.N. and M.P. Ansell, *The effect of silane treatment on the mechanical and physical properties of sisal-epoxy composites*. Composites Science and Technology, 1991. **41**(2): p. 165-178.
21. Li, X., L. Tabil, and S. Panigrahi, *Chemical Treatments of Natural Fiber for Use in Natural Fiber-Reinforced Composites: A Review*. Journal of Polymers and the Environment, 2007. **15**(1): p. 25-33.
22. Li, Y., J. Yu, and Z.-X. Guo, *The influence of silane treatment on nylon 6/nano-SiO₂ in situ polymerization*. Journal of Applied Polymer Science, 2002. **84**(4): p. 827-834.
23. Bader, M.G., *Tensile Strength of Uniaxial Composites*, in *Science and Engineering of Composite Materials*. 1988. p. 1.
24. Madhukar, M.S. and L.T. Drzal, *Fiber-Matrix Adhesion and Its Effect on Composite Mechanical Properties: II. Longitudinal (0°) and Transverse (90°) Tensile and Flexure Behavior of Graphite/Epoxy Composites*. Journal of Composite Materials, 1991. **25**(8): p. 958-991.
25. Hatta, H., K. Goto, and T. Aoki, *Strengths of C/C composites under tensile, shear, and compressive loading: Role of interfacial shear strength*. Composites Science and Technology, 2005. **65**(15–16): p. 2550-2562.
26. Hatta, H., et al., *Damage detection of C/C composites using ESPI and SQUID techniques*. Composites Science and Technology, 2005. **65**(7–8): p. 1098-1106.
27. Kim, B.W. and J.A. Nairn, *Observations of Fiber Fracture and Interfacial Debonding Phenomena Using the Fragmentation Test in Single Fiber Composites*. Journal of Composite Materials, 2002. **36**(15): p. 1825-1858.
28. Zhou, X.F., J.A. Nairn, and H.D. Wagner, *Fiber-matrix adhesion from the single-fiber composite test: nucleation of interfacial debonding*. Composites Part A: Applied Science and Manufacturing, 1999. **30**(12): p. 1387-1400.
29. Drzal, L.T., et al., *Adhesion of Graphite Fibers to Epoxy Matrices: II. The Effect of Fiber Finish*. The Journal of Adhesion, 1983. **16**(2): p. 133-152.
30. Zhao, F.M. and N. Takeda, *Effect of interfacial adhesion and statistical fiber strength on tensile strength of unidirectional glass fiber/epoxy composites*.

- Part I: experiment results.* Composites Part A: Applied Science and Manufacturing, 2000. **31**(11): p. 1203-1214.
31. Shioya, M., S. Yasui, and A. Takaku, *Relation between interfacial shear strength and tensile strength of carbon fiber/resin composite strands.* Composite Interfaces, 1998. **6**(4): p. 305-323.
 32. Nairn, J.A., *Fracture Mechanics of Unidirectional Composites Using the Shear-Lag Model I: Theory.* Journal of Composite Materials, 1988. **22**(6): p. 561-588.
 33. Nairn, J.A., *Fracture Mechanics of Unidirectional Composites.* Journal of Reinforced Plastics and Composites, 1990. **9**(1): p. 91-101.
 34. Okabe, T., et al., *A 3D shear-lag model considering micro-damage and statistical strength prediction of unidirectional fiber-reinforced composites.* Composites Science and Technology, 2001. **61**(12): p. 1773-1787.
 35. Beyerlein, I.J. and C.M. Landis, *Shear-lag model for failure simulations of unidirectional fiber composites including matrix stiffness.* Mechanics of Materials, 1999. **31**(5): p. 331-350.
 36. de Moraes, A.B., *Prediction of the longitudinal tensile strength of polymer matrix composites.* Composites Science and Technology, 2006. **66**(15): p. 2990-2996.
 37. Hollister, S.J. and N. Kikuchi, *A comparison of homogenization and standard mechanics analyses for periodic porous composites.* Computational Mechanics, 1992. **10**(2): p. 73-95.
 38. Xia, Z., Y. Zhang, and F. Ellyin, *A unified periodical boundary conditions for representative volume elements of composites and applications.* International Journal of Solids and Structures, 2003. **40**(8): p. 1907-1921.
 39. Nedele, M.R. and M.R. Wisnom, *Three-dimensional finite element analysis of the stress concentration at a single fibre break.* Composites Science and Technology, 1994. **51**(4): p. 517-524.
 40. Van Den Heuvel, P.W.J., et al., *Failure phenomena in two-dimensional multi-fibre model composites: 5. a finite element study.* Composites Part A: Applied Science and Manufacturing, 1998. **29**(9-10): p. 1121-1135.
 41. Xia, Z., T. Okabe, and W.A. Curtin, *Shear-lag versus finite element models for stress transfer in fiber-reinforced composites.* Composites Science and Technology, 2002. **62**(9): p. 1141-1149.
 42. Batdorf, S.B. and R. Ghaffarian, *Size effect and strength variability of unidirectional composites.* International Journal of Fracture, 1984. **26**(2): p. 113-123.
 43. Smith, R.L., *The random variation of stress concentration factors in fibrous composites.* Journal of Materials Science Letters, 1983. **2**(8): p. 385-387.
 44. Oh, J.H., K.K. Jin, and S.K. Ha, *Interfacial Strain Distribution of a Unidirectional Composite with Randomly Distributed Fibers under Transverse Loading.* Journal of Composite Materials, 2006. **40**(9): p. 759-778.

45. Wongsto, A. and S. Li, *Micromechanical FE analysis of UD fibre-reinforced composites with fibres distributed at random over the transverse cross-section*. Composites Part A: Applied Science and Manufacturing, 2005. **36**(9): p. 1246-1266.
46. Fukuda, H., *Stress concentration factors in unidirectional composites with random fiber spacing*. Composites Science and Technology, 1985. **22**(2): p. 153-163.
47. Manders, P.W., M.G. Bader, and T.W. Chou, *Monte Carlo simulation of the strength of composite fibre bundles*. Fibre Science and Technology, 1982. **17**(3): p. 183-204.
48. Goda, K., *The role of interfacial debonding in increasing the strength and reliability of unidirectional fibrous composites*. Composites Science and Technology, 1999. **59**(12): p. 1871-1879.
49. Goda, K. and H. Fukunaga, *The evaluation of the strength distribution of silicon carbide and alumina fibres by a multi-modal Weibull distribution*. Journal of Materials Science, 1986. **21**(12): p. 4475-4480.
50. Ochiai, S., K. Schulte, and P.W.M. Peters, *Strain concentration factors for fibers and matrix in unidirectional composites*. Composites Science and Technology, 1991. **41**(3): p. 237-256.
51. Honjo, K., *Fracture toughness of PAN-based carbon fibers estimated from strength-mirror size relation*. Carbon, 2003. **41**(5): p. 979-984.
52. Pinho, S.T., P. Robinson, and L. Iannucci, *Developing a four point bend specimen to measure the mode I intralaminar fracture toughness of unidirectional laminated composites*. Composites Science and Technology, 2009. **69**(7-8): p. 1303-1309.
53. Morris, C.E.H.a.D.H., *Fracture mechanics: Seventeenth Volume, ASTM STP905*. 1986: p. 124-135.
54. Tattersall, H.G. and G. Tappin, *The work of fracture and its measurement in metals, ceramics and other materials*. Journal of Materials Science, 1966. **1**(3): p. 296-301.
55. Cantwell, W.J. and J. Morton, *The impact resistance of composite materials — a review*. Composites, 1991. **22**(5): p. 347-362.
56. Marston, T.U., A.G. Atkins, and D.K. Felbeck, *Interfacial fracture energy and the toughness of composites*. Journal of Materials Science, 1974. **9**(3): p. 447-455.
57. Atkins, A.G., *Intermittent bonding for high toughness/ high strength composites*. Journal of Materials Science, 1975. **10**(5): p. 819-832.
58. Piggott, M.R., *Theoretical estimation of fracture toughness of fibrous composites*. Journal of Materials Science, 1970. **5**(8): p. 669-675.
59. Fitz-Randolph, J., et al., *The fracture energy and acoustic emission of a boron-epoxy composite*. Journal of Materials Science, 1972. **7**(3): p. 289-294.
60. Kelly, A. and W.R. Tyson, *Tensile properties of fibre-reinforced metals:*

- Copper/tungsten and copper/molybdenum*. Journal of the Mechanics and Physics of Solids, 1965. **13**(6): p. 329-350.
61. Cooper, G.A., *The fracture toughness of composites reinforced with weakened fibres*. Journal of Materials Science, 1970. **5**(8): p. 645-654.
 62. Allix, O., P. Ladev  ze, and A. Corigliano, *Damage analysis of interlaminar fracture specimens*. Composite Structures, 1995. **31**(1): p. 61-74.
 63. Allix, O. and A. Corigliano, *Modeling and simulation of crack propagation in mixed-modes interlaminar fracture specimens*. International Journal of Fracture, 1996. **77**(2): p. 111-140.
 64. Segurado, J. and J. Llorca, *A new three-dimensional interface finite element to simulate fracture in composites*. International Journal of Solids and Structures, 2004. **41**(11-12): p. 2977-2993.
 65. Tvergaard, V. and J.W. Hutchinson, *The relation between crack growth resistance and fracture process parameters in elastic-plastic solids*. Journal of the Mechanics and Physics of Solids, 1992. **40**(6): p. 1377-1397.
 66. Gullerud, A.S., et al., *Simulation of ductile crack growth using computational cells: numerical aspects*. Engineering Fracture Mechanics, 2000. **66**(1): p. 65-92.
 67. Lin, Y., *Role of matrix resin in delamination onset and growth in composite laminates*. Composites Science and Technology, 1988. **33**(4): p. 257-277.
 68. Al-Ostaz, A. and I. Jasiuk, *Crack initiation and propagation in materials with randomly distributed holes*. Engineering Fracture Mechanics, 1997. **58**(5-6): p. 395-420.
 69. Al-Ostaz, A., A. Diwakar, and K. Alzebdeh, *Statistical model for characterizing random microstructure of inclusion-matrix composites*. Journal of Materials Science, 2007. **42**(16): p. 7016-7030.
 70. Jiang, M., et al., *Scale and boundary conditions effects in elastic properties of random composites*. Acta Mechanica, 2001. **148**(1-4): p. 63-78.
 71. Garrett, K.W. and J.E. Bailey, *Multiple transverse fracture in 90  cross-ply laminates of a glass fibre-reinforced polyester*. Journal of Materials Science, 1977. **12**(1): p. 157-168.
 72. Manders, P., et al., *Statistical analysis of multiple fracture in 0 /90 /0  glass fibre/epoxy resin laminates*. Journal of Materials Science, 1983. **18**(10): p. 2876-2889.
 73. Aveston, J. and A. Kelly, *Theory of multiple fracture of fibrous composites*. Journal of Materials Science, 1973. **8**(3): p. 352-362.
 74. Cooper, G.A. and J.M. Sillwood, *Multiple fracture in a steel reinforced epoxy resin composite*. Journal of Materials Science, 1972. **7**(3): p. 325-333.
 75. Scott, A.E., et al., *Damage accumulation in a carbon/epoxy composite: Comparison between a multiscale model and computed tomography experimental results*. Composites Part A: Applied Science and Manufacturing, 2012. **43**(9): p. 1514-1522.
 76. Scott, A.E., et al., *In situ fibre fracture measurement in carbon-epoxy*

- laminates using high resolution computed tomography*. Composites Science and Technology, 2011. **71**(12): p. 1471-1477.
77. Marston, C., et al., *Failure characteristics in carbon/epoxy composite tows*. Composites Part A: Applied Science and Manufacturing, 1996. **27**(12 PART A): p. 1183-1194.
 78. Frenkel, D., *Perspective on "The effect of shape on the interaction of colloidal particles"*. Theoretical Chemistry Accounts, 2000. **103**(3-4): p. 212-213.
 79. Garcia, E., D.C. Williamson, and A. Martinez-Richa, *Effects of molecular geometry on liquid crystalline phase behaviour: isotropic-nematic transition*. Molecular Physics, 2000. **98**(3): p. 179-192.
 80. Michael Levitt, et al., *PROTEIN FOLDING: The Endgame*. Annual Review of Biochemistry, 1997. **66**(1): p. 549-579.
 81. Gao, H., *Application of Fracture Mechanics Concepts to Hierarchical Biomechanics of Bone and Bone-like Materials*. International Journal of Fracture, 2006. **138**(1-4): p. 101-137.
 82. Miserez, A., et al., *The Transition from Stiff to Compliant Materials in Squid Beaks*. Science, 2008. **319**(5871): p. 1816-1819.
 83. Krauss, S., et al., *Mechanical Function of a Complex Three-Dimensional Suture Joining the Bony Elements in the Shell of the Red-Eared Slider Turtle*. Advanced Materials, 2009. **21**(4): p. 407-412.
 84. West, G.B., J.H. Brown, and B.J. Enquist, *A General Model for the Origin of Allometric Scaling Laws in Biology*. Science, 1997. **276**(5309): p. 122-126.
 85. Meyers, M.A., et al., *Biological materials: Structure and mechanical properties*. Progress in Materials Science, 2008. **53**(1): p. 1-206.
 86. Abd-Allah, N.M., et al., *Fracture toughness properties of high-strength martensitic steel within a wide hardness range*. Journal of Materials Engineering and Performance, 2001. **10**(5): p. 576-585.

Korean abstract

이 논문은 일축 복합재 (Unidirectional fiber reinforced composite, UD FRCs) 의 계면 현상을 고려한 인장강도 예측 모델을 제시하고, 그에 따른 인성 (fracture toughness) 예측 모델을 제시한다. 또한 해당 모델의 응용으로 일축 섬유다발 복합재 (Hierarchical fiber bundle composites, HFBCs) 에 대한 강도 예측 가능성을 제시한다.

기존 연구에서, 섬유복합재의 인장강도는 일반적으로 계면전단강력이 향상됨에 따라 향상되는 것으로 알려져 있는데, 이는 복합재 수지의 전단변형 및 그에 의한 응력 회복에 의한 영향으로 알려져 있다. 이에 따라 계면전단강력이 향상될수록 인장강도 또한 이론강도에 가까워질 것으로 기대되었으나 시험적인 결과를 통해 실제로 계면전단강력의 증가에 따라 일방적으로 복합재 강도가 증가하지는 않는 것으로 나타나며, 나아가 최적의 계면전단강력이 존재함이 확인되었다. 이러한 현상은 바로 섬유의 다중파괴, 그리고 그에 의한 취성의 증가에 의한 것으로 해석될 수 있다.

이 논문에서 제시하고자 하는 새로운 복합재료 강력 예측 방법은 재료의 인장거동 시 발생하는 두 가지 계면 현상에 기반하고 있으며, 특히 계면전단강력 (Interfacial shear strength, IFSS) 의 영향을 주요하게 고려한다. 계면전단강력에 의한 섬유응력의 회복 및 그에 의한

인장강도의 증가, 그리고 섬유응력의 회복을 위한 전단변형이 주위 섬유에 미치는 응력집중, 최종적으로 그에 의한 섬유의 다중파괴 (multiple fracture) 간의 연구를 수행하여 일축 복합재의 인장 상황에 대한 예측이 가능하도록 하였다.

이 논문에서는 이러한 다중파괴 현상의 발생 예측 모델을 정립하고 이를 바탕으로 복합재의 인장강도를 예측하였으며, 탄소섬유/에폭시 복합소재를 대상으로 해당 모델을 검증하였다. 또한 해당 모델을 통하여 최적의 계면전단강력이 존재하는지 여부를 탐색하였다. 최종적으로 해당 계면전단강력 및 인장강도에서의 인성을 예측하고, 이에 따라 일축 복합소재의 최적 설계에 활용할 수 있는 통합적인 모델을 제작하는 것을 목표로 하였다. 구체적으로 2장에서 해당 모델에 대한 상세한 유도 및 기존 방법과의 비교 및 검증을 수행하고 3장에서는 이를 탄소섬유 복합재료에 적용하여 구체적인 분석 및 검증을 수행하였다. 마지막 4장에서는 이를 일축 섬유다발 구조 (hierarchical fiber bundle composites, HFBCs) 에 확장하여 해당 모델의 응용 가능성을 제시하였다. 상기 결과를 통하여 파괴에 대한 별도의 시험정보 없이 일축 복합재료의 인장강도를 예측할 수 있는 모델을 개발하였으며, 이 모델을 재료설계 및 최적화 연구에 활용할 수 있음을 확인하였다. 특히 복합재료 설계를 위한 최적 계면전단강력이 존재하며 제시한 모델을 통해 이를 탐색할 수 있음을 확인하였다.

핵심어: 탄소섬유 복합재료, 일축 섬유강화 복합재료, 계면전단강력,
섬유 다중파괴, 인장강도, 파괴인성

학번: 2010-20598